IAEA RADIOISOTOPES AND RADIOPHARMACEUTICALS SERIES No. 7

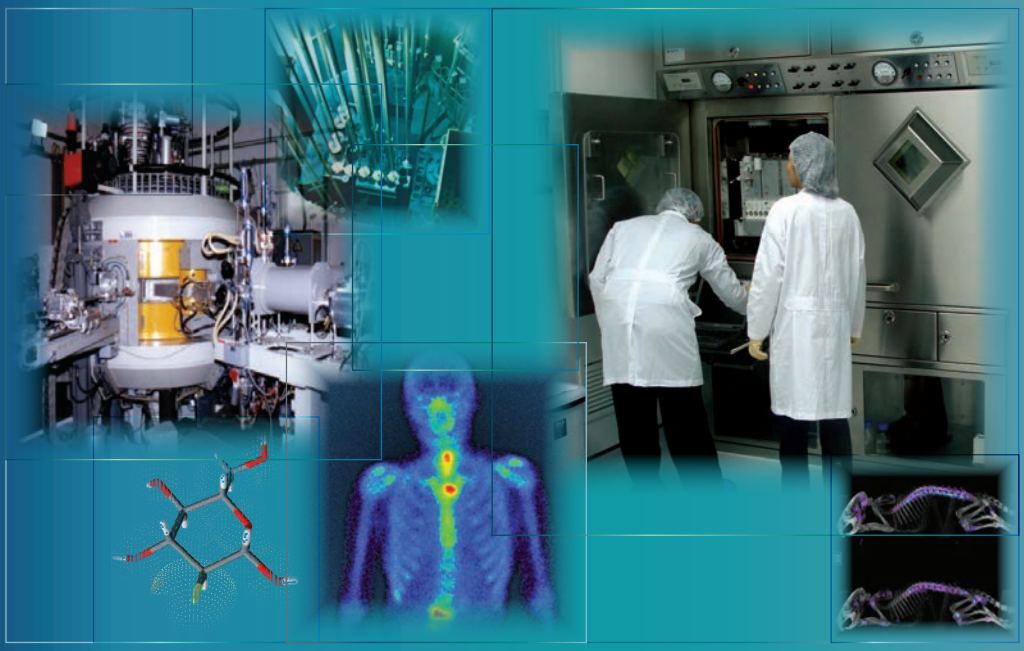

Copper-64 Radiopharmaceuticals: Production, Quality Control and Clinical Applications

IAEA
International Atomic Energy Agency

IAEA RADIOISOTOPES AND RADIOPHARMACEUTICALS SERIES PUBLICATIONS

One of the main objectives of the IAEA Radioisotope Production and Radiation Technology programme is to enhance the expertise and capability of IAEA Member States in deploying emerging radioisotope products and generators for medical and industrial applications in order to meet national needs as well as to assimilate new developments in radiopharmaceuticals for diagnostic and therapeutic applications. This will ensure local availability of these applications within a framework of quality assurance.

Publications in the IAEA Radioisotopes and Radiopharmaceuticals Series provide information in the areas of: reactor and accelerator produced radioisotopes, generators and sealed sources development/production for medical and industrial uses; radiopharmaceutical sciences, including radiochemistry, radiotracer development, production methods and quality assurance/quality control (QA/QC). The publications have a broad readership and are aimed at meeting the needs of scientists, engineers, researchers, teachers and students, laboratory professionals, and instructors. International experts assist the IAEA Secretariat in drafting and reviewing these publications. Some of the publications in this series may also be endorsed or co-sponsored by international organizations and professional societies active in the relevant fields.

There are two categories of publications: the **IAEA Radioisotopes and Radiopharmaceuticals Series** and **IAEA Radioisotopes and Radiopharmaceuticals Reports**.

IAEA RADIOISOTOPES AND RADIOPHARMACEUTICALS SERIES

Publications in this category present guidance information or methodologies and analyses of long term validity, for example protocols, guidelines, codes, standards, quality assurance manuals, best practices and high level technological and educational material.

IAEA RADIOISOTOPES AND RADIOPHARMACEUTICALS REPORTS

In this category, publications complement information published in the IAEA Radioisotopes and Radiopharmaceuticals Series in areas of the: development and production of radioisotopes and generators for medical and industrial applications; and development, production and QA/QC of diagnostic and therapeutic radiopharmaceuticals. These publications include reports on current issues and activities such as technical meetings, the results of IAEA coordinated research projects, interim reports on IAEA projects, and educational material compiled for IAEA training courses dealing with radioisotope and radiopharmaceutical related subjects. In some cases, these reports may provide supporting material relating to publications issued in the IAEA Radioisotopes and Radiopharmaceuticals Series.

All of these publications can be downloaded cost free from the IAEA web site:

www.iaea.org/Publications/index.html

Further information is available from:

Marketing and Sales Unit
International Atomic Energy Agency
Vienna International Centre
PO Box 100
1400 Vienna, Austria

Readers are invited to provide feedback to the IAEA on these publications. Information may be provided through the IAEA web site, by mail at the address given above, or by email to:

Official.Mail@iaea.org

COPPER-64 RADIOPHARMACEUTICALS: PRODUCTION, QUALITY CONTROL AND CLINICAL APPLICATIONS

The following States are Members of the International Atomic Energy Agency:

AFGHANISTAN
ALBANIA
ALGERIA
ANGOLA
ANTIGUA AND BARBUDA
ARGENTINA
ARMENIA
AUSTRALIA
AUSTRIA
AZERBAIJAN
BAHAMAS
BAHRAIN
BANGLADESH
BARBADOS
BELARUS
BELGIUM
BELIZE
BENIN
BOLIVIA, PLURINATIONAL STATE OF
BOSNIA AND HERZEGOVINA
BOTSWANA
BRAZIL
BRUNEI DARUSSALAM
BULGARIA
BURKINA FASO
BURUNDI
CAMBODIA
CAMEROON
CANADA
CENTRAL AFRICAN REPUBLIC
CHAD
CHILE
CHINA
COLOMBIA
COMOROS
CONGO
COSTA RICA
CÔTE D'IVOIRE
CROATIA
CUBA
CYPRUS
CZECH REPUBLIC
DEMOCRATIC REPUBLIC OF THE CONGO
DENMARK
DJIBOUTI
DOMINICA
DOMINICAN REPUBLIC
ECUADOR
EGYPT
EL SALVADOR
ERITREA
ESTONIA
ESWATINI
ETHIOPIA
FIJI
FINLAND
FRANCE
GABON
GEORGIA
GERMANY
GHANA
GREECE
GRENADA
GUATEMALA
GUYANA
HAITI
HOLY SEE
HONDURAS
HUNGARY
ICELAND
INDIA
INDONESIA
IRAN, ISLAMIC REPUBLIC OF
IRAQ
IRELAND
ISRAEL
ITALY
JAMAICA
JAPAN
JORDAN
KAZAKHSTAN
KENYA
KOREA, REPUBLIC OF
KUWAIT
KYRGYZSTAN
LAO PEOPLE'S DEMOCRATIC REPUBLIC
LATVIA
LEBANON
LESOTHO
LIBERIA
LIBYA
LIECHTENSTEIN
LITHUANIA
LUXEMBOURG
MADAGASCAR
MALAWI
MALAYSIA
MALI
MALTA
MARSHALL ISLANDS
MAURITANIA
MAURITIUS
MEXICO
MONACO
MONGOLIA
MONTENEGRO
MOROCCO
MOZAMBIQUE
MYANMAR
NAMIBIA
NEPAL
NETHERLANDS
NEW ZEALAND
NICARAGUA
NIGER
NIGERIA
NORTH MACEDONIA
NORWAY
OMAN
PAKISTAN
PALAU
PANAMA
PAPUA NEW GUINEA
PARAGUAY
PERU
PHILIPPINES
POLAND
PORTUGAL
QATAR
REPUBLIC OF MOLDOVA
ROMANIA
RUSSIAN FEDERATION
RWANDA
SAINT KITTS AND NEVIS
SAINT LUCIA
SAINT VINCENT AND THE GRENADINES
SAMOA
SAN MARINO
SAUDI ARABIA
SENEGAL
SERBIA
SEYCHELLES
SIERRA LEONE
SINGAPORE
SLOVAKIA
SLOVENIA
SOUTH AFRICA
SPAIN
SRI LANKA
SUDAN
SWEDEN
SWITZERLAND
SYRIAN ARAB REPUBLIC
TAJIKISTAN
THAILAND
TOGO
TONGA
TRINIDAD AND TOBAGO
TUNISIA
TÜRKİYE
TURKMENISTAN
UGANDA
UKRAINE
UNITED ARAB EMIRATES
UNITED KINGDOM OF GREAT BRITAIN AND NORTHERN IRELAND
UNITED REPUBLIC OF TANZANIA
UNITED STATES OF AMERICA
URUGUAY
UZBEKISTAN
VANUATU
VENEZUELA, BOLIVARIAN REPUBLIC OF
VIET NAM
YEMEN
ZAMBIA
ZIMBABWE

The Agency's Statute was approved on 23 October 1956 by the Conference on the Statute of the IAEA held at United Nations Headquarters, New York; it entered into force on 29 July 1957. The Headquarters of the Agency are situated in Vienna. Its principal objective is "to accelerate and enlarge the contribution of atomic energy to peace, health and prosperity throughout the world".

IAEA RADIOISOTOPES AND RADIOPHARMACEUTICALS SERIES No. 7

COPPER-64 RADIOPHARMACEUTICALS: PRODUCTION, QUALITY CONTROL AND CLINICAL APPLICATIONS

INTERNATIONAL ATOMIC ENERGY AGENCY
VIENNA, 2022

COPYRIGHT NOTICE

Marketing and Sales Unit, Publishing Section
International Atomic Energy Agency
Vienna International Centre
PO Box 100
1400 Vienna, Austria
fax: +43 1 26007 22529
tel.: +43 1 2600 22417
email: sales.publications@iaea.org
www.iaea.org/publications

Printed by the IAEA in Austria
November 2022
STI/PUB/1961

IAEA Library Cataloguing in Publication Data

Names: International Atomic Energy Agency.
Title: Copper-64 radiopharmaceuticals : production, quality control and clinical applications / International Atomic Energy Agency.
Description: Vienna : International Atomic Energy Agency, 2022. | Series: IAEA radioisotopes and radiopharmaceuticals series, ISSN 2077–6462 ; no. 7 | Includes bibliographical references.
Identifiers: IAEAL 22-01490 | ISBN 978–92–0–129621–4 (paperback : alk. paper) | ISBN 978–92–0–129321–3 (pdf) | ISBN 978–92–0–129421–0 (epub)
Subjects: LCSH: Copper — Isotopes — Therapeutic use. | Copper — Isotopes — Quality control. | Radiopharmaceuticals.
Classification: UDC 615.849:546.56 | STI/PUB/1961

FOREWORD

Positron emission tomography (PET) has attracted interest from both clinicians and radiopharmaceutical scientists in recent decades. Metal based radionuclides such as ^{68}Ga have become increasingly important in the field of nuclear medicine owing to the facile radiochemistry, production automation and development of cold kits. However, ^{68}Ga has limitations owing to its short half-life (67.1 min), even when produced using a ^{68}Ga generator. Research on the applications of other metallic PET radionuclides with longer half-lives has led to the introduction of alternative radionuclides, such as the copper series (^{60}Cu, ^{61}Cu, ^{62}Cu and ^{64}Cu). Among copper radionuclides, ^{64}Cu has advantageous characteristics given its rather longer half-life and decay via positron and beta particle emission. Additionally, copper as a trace element plays a pivotal role in several human metabolic processes and is involved in malignant cell biochemistry pathways. This has opened an opportunity for scientists to explore the theranostic capabilities of ^{64}Cu. ^{64}Cu in chloride form has already been applied as a radiopharmaceutical, while ^{64}Cu conjugated radiopharmaceuticals, such as peptides and monoclonal antibodies, are the subject of intense radiopharmacy research and development.

Drawing on a recent IAEA coordinated research project entitled Copper-64 Radiopharmaceuticals for Theranostic Applications and on the interesting collaborative work of scientists from 13 Member States between 2016 and 2020, this publication describes recent advances in the production and application of ^{64}Cu theranostic radiopharmaceuticals. This publication is the outcome of the continuous efforts of a selected team of international experts from the coordinated research project during 2019 and 2020. It is aimed at all professionals involved in the field and specifies ideal production, formulation and quality control of various ^{64}Cu radiopharmaceuticals for theranostic applications, along with clinical aspects.

The IAEA wishes to thank the contributing experts for their valuable work and scientific contributions, especially M.A. Avila-Rodriguez and C.S. Cutler. The IAEA technical officers responsible for this publication were A. Jalilian of the Division of Physical and Chemical Sciences and F. Giammarile of the Division of Human Health.

EDITORIAL NOTE

Although great care has been taken to maintain the accuracy of information contained in this publication, neither the IAEA nor its Member States assume any responsibility for consequences which may arise from its use.

This publication does not address questions of responsibility, legal or otherwise, for acts or omissions on the part of any person.

Guidance provided here, describing good practices, represents expert opinion but does not constitute recommendations made on the basis of a consensus of Member States.

The use of particular designations of countries or territories does not imply any judgement by the publisher, the IAEA, as to the legal status of such countries or territories, of their authorities and institutions or of the delimitation of their boundaries.

The mention of names of specific companies or products (whether or not indicated as registered) does not imply any intention to infringe proprietary rights, nor should it be construed as an endorsement or recommendation on the part of the IAEA.

The IAEA has no responsibility for the persistence or accuracy of URLs for external or third party Internet web sites referred to in this book and does not guarantee that any content on such web sites is, or will remain, accurate or appropriate.

CONTENTS

1. INTRODUCTION

1.1. BACKGROUND

Copper-64 has several unique attributes that make it a multipurpose radionuclide with many potential applications. It has a complex decay scheme, with electron capture, beta emission and positron emission branches. The positron emission (17.5%) has a low energy, allowing high resolution images, and there are none of the abundant gamma emissions that impair the imaging properties of several other positron emitters. The combination of positron and beta emission (38.5%) imparts a high local radiation dose at the cellular level, making it suitable (at least in principle) for targeted radionuclide therapy (TRT), while the electron capture decay (44%) is accompanied by the emission of high linear energy transfer Auger electrons, which add to the cytotoxic potency if the radionuclide is located inside cells, particularly if it is within or close to cell nuclei. Thus, ^{64}Cu may be described as an archetypal theranostic radionuclide, producing excellent positron emission tomography (PET) molecular images at low administered activities without major dosimetry or radiobiological concerns and offering potential for radionuclide therapy at high activities, with the possibility of using PET imaging for accurate radionuclide distribution and dosimetry during therapy.

Its half-life of 12.7 h is short enough to be useful for tracers with rapid pharmacokinetics, such as small molecules and peptides, yet long enough to be useful for tracers with slow pharmacokinetics; for example, for those associated with monoclonal antibodies (mAbs) and for the tracking of cell migration. The 12.7 h half-life also makes it useful as a laboratory tool for the development of new tracers in the context of other copper radionuclides with longer and shorter half-lives (^{60}Cu, ^{61}Cu and ^{62}Cu for PET and ^{67}Cu for therapy).

Its chemistry offers several advantages: although it is less substitutionally inert than other transition metals, with well designed macrocyclic chelators it can be stably attached to targeting molecules such as antibodies, peptides and antibody fragments, among others. Many years of design and optimization of these chelators have generated a wide selection of useful bifunctional chelators for this purpose, and the radiolabelling process is simple and straightforward. It is redox active, and the reduction of Cu(II) to Cu(I) in a biological milieu can be used as a basis for molecular imaging with very simple complexes, allowing blood flow and hypoxia imaging.

Copper is an essential, naturally occurring metal and its trafficking, accumulation and clearance are tightly controlled in normal health states but often disturbed in disease states such as dementia, cancer, inflammation, nutritional

abnormalities and inherited diseases of copper metabolism. This creates additional unique potential for ^{64}Cu in imaging these processes, and perhaps in therapy. This potential is almost entirely untapped at present.

The production of ^{64}Cu using a low/medium energy cyclotron is well established and straightforward, and most centres apply protons of 11–15 MeV energy for the irradiation of isotopically enriched ^{64}Ni. Some other routes are also practical, although difficulties and limitations in quality and/or quantity may arise. Preparation of the solid target requires careful consideration and design for applications in different systems. Basically, most groups use an underlying gold layer, electroplated over the backing, followed by a ^{64}Ni electroplated layer. This approach has been widely used in many centres with a medical cyclotron capable of product transport within two hours of production. Recently, some groups have developed methods using liquid targets in cyclotrons and other groups have used research reactors; however, results have shown limitations in liquid target production, as well as in the research reactor method, compared with low/medium energy cyclotron irradiation of solid ^{64}Ni.

1.2. OBJECTIVE

Because of the interest in ^{64}Cu for the existing and potential applications of its radiopharmaceuticals, an IAEA coordinated research project was initiated in 2016. It became apparent early on that an IAEA publication would be useful for Member States trying to apply these agents in clinics. This publication covers the characteristics of ^{64}Cu radiopharmaceuticals, the latest developed agents in the field, and recommendations and suggestions for production, quality control and quality assurance procedures for Member State laboratories in charge of radiopharmaceutical production. This publication aims to offer, from an international perspective, an overview for newcomers to the field who need guidance, and to establish comparable levels of guidelines for current users to enable successful practice across the globe.

Only a limited number of companies worldwide produce ^{64}Cu and its agents. A combination of the short shelf life (i.e. half-life) of ^{64}Cu radiopharmaceuticals, which affects the feasibility of long distance transportation for distribution, and high prices has led to limited commercial availability, so some Member States have opted to produce their own products according to their local capacities and regulations. This has presented challenges for several reasons, including a lack of international guidelines on the use of these radiopharmaceuticals, their production and quality control, and a lack of resources on practical experience to meet local needs.

1.3. SCOPE

The purpose of this publication is to provide a general overview of the following:

— The nature and chemistry of copper;
— The biological aspects of copper in living systems, especially humans;
— The latest techniques for producing the ^{64}Cu radionuclide;
— Appropriate chelation techniques and available ligands for copper labelling;
— The design and application of ^{64}Cu peptide radiopharmaceuticals;
— The preparation and evaluation of ^{64}Cu immunoconjugates;
— The formulation and quality control of [^{64}Cu]$CuCl_2$ radiopharmaceuticals;
— An introduction to the most important ^{64}Cu radiopharmaceuticals in clinical applications;
— Examples of experiences in the production of important ^{64}Cu radiopharmaceuticals.

Although suitable for many applications, ^{64}Cu is ideal for very few; for each potential application, an alternative radionuclide or radiopharmaceutical may be found that is superior. For example, ^{68}Ga is a powerful competitor for PET imaging of fast tracers, while ^{89}Zr has advantages for slow tracers such as antibodies. However, these radioisotopes are not without limitations of their own (in terms of production, distribution, etc.). For purely diagnostic PET imaging, radiation doses associated with ^{64}Cu are higher than ^{18}F and ^{68}Ga.

Despite its relatively simple and straightforward production, the availability of ^{64}Cu remains limited. As mentioned earlier, the main production route is based on ^{64}Ni as the target material, which has low natural abundance and high cost. Intense cyclotron beam proton flux or irradiation time would place a large burden on most biomedical cyclotrons to produce high scale batches of ^{64}Cu for several human studies or possibly a single radionuclide therapy dose. Solid targetry considerations for a wide range of commercial cyclotron designs would be costly and require special engineering designs. Chemical processing is laborious and exposes personnel to radiation, requiring intensive and costly automated equipment. Thus, ^{64}Cu remains an expensive radionuclide both for producers and their customers, and making it available on a daily basis in centres would be challenging. Usually, ^{64}Cu is produced once a week or twice a month.

Its half-life of 12.7 h places some restrictions on ^{64}Cu availability to centres that are not close to a suitable cyclotron. Even when supplying several hospitals within a few hours' travelling time of a production facility, capacity remains an issue because of the long irradiation times required to produce a relatively small number of doses. This limitation may be quantified as 'doses per beam hour', and ^{64}Cu will score

badly on this measure compared with mainstream PET radionuclides such as ^{18}F. While other radionuclides, especially ^{99m}Tc and ^{68}Ga, are available via a generator, having a suitable generator does not solve the distribution problems of ^{64}Cu.

1.4. STRUCTURE

This publication aims to provide radiopharmaceutical production centres and nuclear medicine units with the knowledge necessary to understand the background and standard operation procedures for the production, quality control and clinical application of ^{64}Cu radiopharmaceuticals. It is divided into seven sections, the first of which covers the background, objective, scope and structure of the book. Section 2 reviews recent advances in the production of ^{64}Cu, with an overview of existing methods. Section 3 discusses copper chelation chemistry, as well as known chelates important for the development of ^{64}Cu radiopharmaceuticals. Section 4 describes the history of the development of ^{64}Cu peptides, including biological targets, ligands and preclinical evaluation. The development and biological evaluation of immunomolecules labelled with ^{64}Cu, including the required quality control and preclinical evaluation procedures, is the subject of Section 5. Section 6 focuses on the formulation and use of [^{64}Cu]$CuCl_2$ radiopharmaceuticals. Finally, Section 7 discusses the situation of existing ^{64}Cu radiopharmaceutical applications in the clinic, with a look towards the future. General conclusions are outlined in Section 7. Annex I describes the importance and role of copper in biological systems at a molecular and cellular level. Owing to the importance of critical new findings on the applications of [^{64}Cu]$CuCl_2$ radiopharmaceuticals in various malignant and physiological diseases, Annex II has been added to this publication to review the chemistry and biochemistry of copper. Annex III provides a detailed step-by-step procedure for the preparation of a standard [^{64}Cu]Cu labelled monoclonal antibody used in clinical trials.

2. COPPER-64 PRODUCTION

2.1. DECAY SCHEME

Copper is relatively abundant (68 ppm) in Earth's crust, where it is mainly found in the form of chalcocite (Cu_2S), chalcopyrite ($CuFeS_2$) and malachite ($CuCO_3 \cdot Cu(OH)_2$), and sometimes as a free metal [1]. In the human body copper

occurs at 1 ppm level, mostly in the protein bound state. Copper ($Z = 29$) has two stable isotopes, ^{63}Cu (69.15%) and ^{65}Cu (30.85%), and 27 radioisotopes. Among them, there are four positron emitters, ^{60}Cu ($T_{1/2}$ = 23.7 min, 93% β^+), ^{61}Cu ($T_{1/2}$ = 3.33 h, 61% β^+), ^{62}Cu ($T_{1/2}$ = 9.7 min, 98% β^+) and ^{64}Cu ($T_{1/2}$ = 12.7 h, 19% β^+, 38% β^-), and an electron emitter, ^{67}Cu ($T_{1/2}$ = 61.83 h, 100% β^-). These are of particular importance for nuclear medicine. Placed at the beginning of the 'coinage' metal group 11 of the periodic table and followed by silver and gold, copper has a $3d^{10}4s^1$ electronic configuration. It is the d → sp band transition that causes the reddish-brown colour of the metal. Copper has the best electrical conductivity of any metal except silver and excellent thermal conductivity. Situated below hydrogen in the electromotive series, copper does not react with non-oxidizing acids, such as HCl, but dissolves in nitric acid and in hot concentrated sulphuric acid.

Copper-64 possesses unique decay characteristics that make it a multipurpose radionuclide with many potential applications. It decays with a half-life of 12.7 h via three modes: positron emission (17.5% β^+), beta emission (38.5% β^-) and electron capture (44.0% EC), as schematically shown in Fig. 1. Electron capture, in addition to characteristic X rays, is accompanied by the emission of high linear energy transfer Auger electrons, which add to its cytotoxic potency if the radionuclide is located inside cells, particularly within or close to cell nuclei, given the short range of these low energy electrons. Figure 2 shows the spectra of gamma and positron emissions experimentally measured and the spectra of Auger electrons obtained by Monte Carlo simulation.

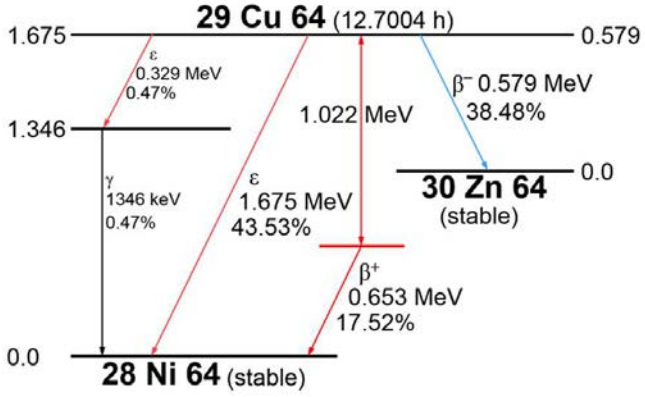

FIG. 1. Decay scheme for the decay of ^{64}Cu (courtesy of F. Alves, University of Coimbra).

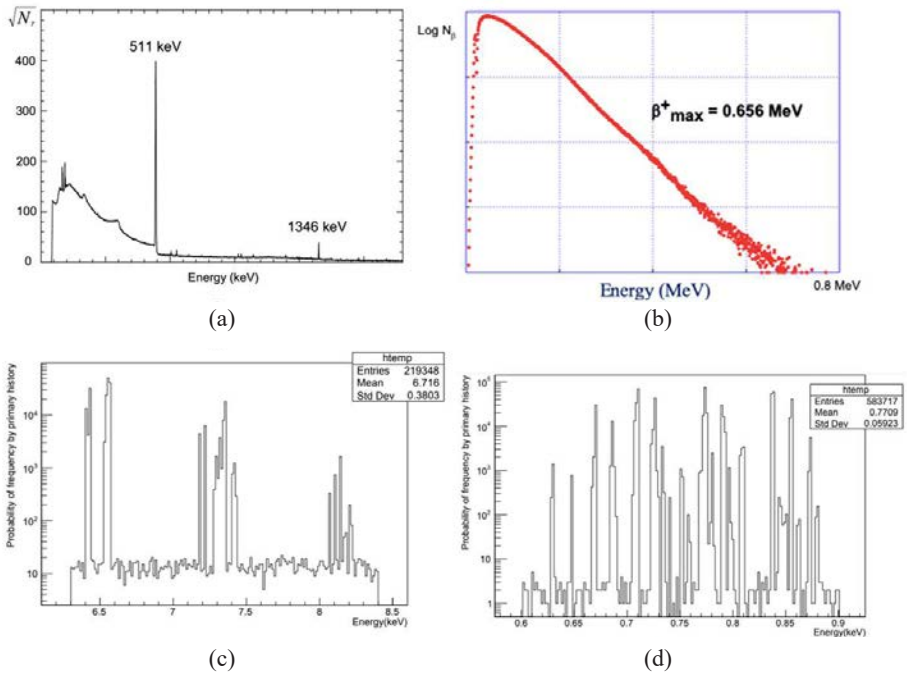

FIG. 2. Spectra of the different types of radiation emitted during the decay of ^{64}Cu: (a) gamma emission, showing the characteristic photopeaks of ^{64}Cu; (b) positron emission; (c) Auger electrons from the K shell; and (d) Auger electrons from the L shell (courtesy of M.A. Avila-Rodriguez, National Autonomous University of Mexico).

2.2. ROUTES OF PRODUCTION

Several routes to producing ^{64}Cu have been reported in the last five decades, while methods to produce no-carrier-added ^{64}Cu feasible for medical applications have been developed more recently. Copper-64 can be produced using a reactor or a cyclotron. The different methods of production lead to products of varying quality in terms of radionuclide, radiochemical and chemical purities, in addition to yield and specific activity. Reactor production can lead to high or low specific activity, depending on whether production is by direct activation, (n, γ), or indirect, through the (n, p) reaction on a Zn target. The highest specific activity is, however, achieved by cyclotron irradiation of enriched ^{64}Ni targets. Table 1 [2–26] summarizes the different routes of production, including their experimental yields.

TABLE 1. DISTINCT PRODUCTION PROCESSES LEADING TO THE PRODUCTION OF ^{64}Cu WITH SOLID TARGETS

	Nuclear reaction	Projectile energy (MeV)	^{64}Cu production yield	Ref.
Neutrons	^{nat}Cu(n, γ)		176 MBq · g^{-1} · h^{-1}	[2]
			32 MBq · g^{-1} · h^{-1}	[3]
	^{64}Zn(n, p)		19 MBq · m · g^{-1}	[4]
			572 MBq · g^{-1} · h^{-1}	[5]
			201 MBq · g^{-1} · h^{-1}	[2]
Charged particles (deuterons)	^{64}Ni(d, x)	19	>300 MBq · μA^{-1} · h^{-1}	[6]
	^{nat}Zn(d, x)	45	>200 MBq · μA^{-1} · h^{-1}	[7]
		<20	≤30 MBq · μA^{-1} · h^{-1}	[8, 9]
				[10]
				[11]
				[12]
				[13]
	^{64}Zn(d, 2p)	20	≤30 MBq · μA^{-1} · h^{-1}	[14]
				[15]
	^{66}Zn(d, α)	13 → 7	>5 MBq · μA^{-1} · h^{-1}	[13]

TABLE 1. DISTINCT PRODUCTION PROCESSES LEADING TO THE PRODUCTION OF ^{64}Cu WITH SOLID TARGETS (cont.)

	Nuclear reaction	Projectile energy (MeV)	^{64}Cu production yield	Ref.
Charged particles (protons)	^{64}Ni(p, n)	20	≤100 MBq · μA^{-1} · h^{-1}	[12]
				[16, 17]
				[18]
				[19]
				[20]
				[21]
				[22]
				[23]
	^{66}Zn(p, 2pn)	70 → 35	>750 MBq · μA^{-1} · h^{-1}	[24]
	^{68}Zn(p, αn)	30 → 20	≤65 MBq · μA^{-1} · h^{-1}	[25]
				[26]
				[13]
				[24]
		37 → 20	>150 MBq · μA^{-1} · h^{-1}	[24]

As can be seen from Table 1, the reactor production method leads to low yields. On the other hand, the production of ^{64}Cu via the (d, 2n) and (p, n) reactions leads to high yields, and the (p, n) reaction has the advantage that a low energy cyclotron is adequate to produce ^{64}Cu in sufficient quantity and quality for clinical applications. This is very important because the medical cyclotrons most commonly used for the production of PET radionuclides are low energy single particle machines that produce a proton beam with a kinetic energy in the range of 11–18 MeV, most of which are idle when not making ^{18}F for ^{18}F-fluorodeoxyglucose (FDG) labelling.

2.2.1. Reactor production

Copper-64 is producible in a nuclear reactor by thermal neutron capture, $^{63}Cu(n, \gamma)^{64}Cu$, or by fast neutron capture, $^{64}Zn(n, p)^{64}Cu$ [2–5]. Although the latter route results in the production of ^{64}Cu in a no-carrier-added form, it requires access to a reactor with reasonably high fast neutron flux positions, which are limited around the world. On the other hand, the majority of radioisotopes produced in research reactors worldwide are products of thermal neutron induced nuclear reactions, mainly by (n, γ) reactions, and of the available options for production of ^{64}Cu, the (n, γ) reaction presents the least intricate route. As already stated, while the $^{63}Cu(n, \gamma)^{64}Cu$ production route is quite promising, this approach provides ^{64}Cu of low specific activity, which is unsuitable for labelling receptor targeted ligands with limited expression. However, the use of neutron activated ^{64}Cu in the form of $^{64}CuCl_2$ as a radiopharmaceutical for the non-invasive assessment of various types of cancer is deemed worthy of consideration.

This strategy of direct utilization of neutron activated $^{64}CuCl_2$ as a PET radiotracer would be especially advantageous for countries with limited cyclotron facilities for radioisotope production. The IAEA database provides a summary of approximately 251 research reactors currently operating worldwide. Fifty of these research reactors have thermal neutron flux of $>1 \times 10^{14}$ n · cm^{-2} · s^{-1} and the thermal flux of an additional 85 reactors ranges from 1×10^{12} to 1×10^{14} n · cm^{-2} · s^{-1}. Seventy-eight of the above reactors are involved in radioisotope production and these reactors have a good geographic distribution. Many of these research reactors could be used for the production of neutron activated ^{64}Cu, which in turn would increase the global availability of this radioisotope [27].

There is a scope and need to probe the feasibility of using low specific activity $^{64}CuCl_2$ produced by the (n, γ) route as a cost effective radiotracer for non-invasive visualization of tumours by PET scan. Seeking a viable strategy for large scale production of ^{64}Cu with high radionuclidic purity and acceptable specific activity for use as a PET radiotracer by careful optimization of irradiation parameters is worthy of the utmost attention.

2.2.2. Cyclotron

2.2.2.1. Solid targets

There are several routes for the cyclotron production of ^{64}Cu using solid targets; however, high specific activity ^{64}Cu in high yields is best achieved by $^{64}Ni(p, n)^{64}Cu$ using isotopically enriched ^{64}Ni on a suitable backing substrate [22, 23, 28]. Proton irradiation of enriched ^{64}Ni at energies greater than

5 MeV produces, in addition to ^{64}Cu, ^{61}Co ($T_{1/2}$ = 1.65 h, 100% β^-, γ = 67 keV, $E_{\beta max}$ = 1.3 MeV) via the ^{64}Ni(p, α) reaction. The (p, α) reaction yield is modest when compared with the (p, n) reaction; however, useful quantities of ^{61}Co for small animal studies can be produced concurrently with ^{64}Cu. In addition, a single column ion exchange chromatography process separates the ^{64}Cu and ^{61}Co products at high specific activities while preserving the ^{64}Ni substrate [23].

Solid targets to produce medical radionuclides require careful design for adaptation to different cyclotrons. A variety of backing materials and protocols for the electroplating and dissolution of the irradiated target are currently in use. The specifics of the protocols have important ramifications for the time that it takes to prepare the target, the end of bombardment yield, resin based purification and quality control.

2.2.2.2. Liquid targets

In recent years, the irradiation of aqueous salts of target isotopes was established as a reliable and sustainable method for the production of radiometals in cyclotrons [29–32]. This method intends to overcome the practical difficulties associated with the use of solid targets — such as time consuming preparation [33–35], issues with the quality of the electroplating technique, loss of the expensive target material by evaporation during irradiation or the complex procedure of recovering and recycling the enriched material [17, 36] — that have prevented the widespread use of this technique, although high production yields have been reported and extensive descriptions are available in the literature [37–39].

The so called ‘liquid target approach’ allows the use of simplified and automated procedures throughout the process, including target loading, fully automated remotely controlled transfer of the irradiated target solution and post-processing of the irradiated solution, finally providing a metal chloride solution ready to be used for radiolabelling in compliance with current good manufacturing practice (GMP) [32]. The process thus eliminates the need for pre- and post-irradiation target preparation and simplifies the transfer of irradiated material to an automated chemistry module located inside a shielded hot cell, with substantial enhancement of radiological protection conditions and significant reduction in both processing time and cost when compared with the solid target approach.

Moreover, the target loading, irradiation and transfer of irradiated target material, as well as the required targetry and associated infrastructure, are very similar to those used in the production of ^{18}F from ^{18}O enriched water and so can be easily adapted and adopted in the more than 1000 cyclotrons [40, 41] used worldwide for the production of this isotope.

Systematically, the production of ^{64}Cu from liquid targets, in the chemical form of $^{64}CuCl_2$, comprises three different steps: preparation of the target solution, target irradiation and separation (Fig. 3).

2.2.3. Target solution

Chemically stable 'ready to use' target solutions of nickel nitrate ($^{64}Ni(NO_3)_2{\cdot}6H_2O$) at different concentrations are available from many suppliers providing GMP compliant certificates of analysis. Alternatively, the target solution can be prepared from commercially available ^{64}Ni in metallic or oxide form, ensuring that all raw materials (e.g. water, nitric acid) are of metal basis quality.

To avoid isotopic contamination, highly isotopically enriched ^{64}Ni (>95%) is ideally used. The remaining nickel isotopes contribute to the production of undesired ^{60}Cu, ^{61}Cu and ^{62}Cu. Fortunately, the half-lives of these isotopic contaminants are shorter than that of ^{64}Cu, so their relative amount can be reduced by using long irradiation times and/or after irradiation decay. Other metal contamination, in all raw materials, is ideally carefully avoided.

2.2.4. Target irradiation

Although the target body geometry and design do not differ from other liquid targets, namely those used for ^{18}F, metal contamination is ideally prevented in all steps of the solution's preparation and handling, including control of the materials to which the solution is exposed. A dedicated target is therefore absolutely recommended, and will also prevent cross-contaminations from other isotopes produced. Niobium, because of its chemical inertness, has been reported to have been successfully used as the target and target window (in contact with the solution) material for ^{64}Cu production [32].

The irradiation procedure and the behaviour of the target material under beam irradiation have also been described in the literature, where a production

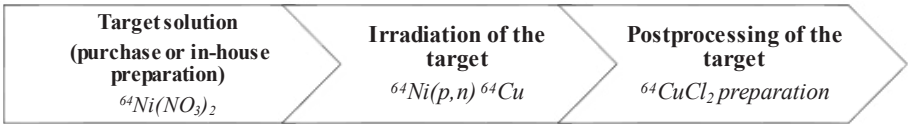

FIG. 3. Flow chart showing the preparation of ^{64}Cu chloride solution from liquid target production (courtesy of F. Alves, University of Coimbra).

yield of 0.14 MBq · μA^{-1} · h^{-1} · mg^{-1}, leading to 5 GBq after 5 h irradiation of a solution containing 100 mg of ^{64}Ni, has been reported [32].

Regarding transfer lines, ethylene tetrafluoroethylene is recommended (although not exclusively) owing to its excellent physicochemical properties, such as high resistance to corrosion and very low friction coefficient. The latter is an important factor, since the viscosity of the solution can lead to long transfer times or, ultimately, to failure in the transfer process when using conventional liquid target helium pressure (2–6 bar).

2.2.5. Separation of produced copper-64

The methods used to separate the produced ^{64}Cu from the target material and other side products and contaminants are based on the same processes used for solid targets, although the solid target dissolution step is avoided. Solid phase extraction is often preferred because of its amenability to automation. Strong cation exchange using a strong cation resin containing divinylbenzene [42] is the most commonly used method. A second purification step is frequently used to reduce the quantity of metallic contaminants. A secondary resin is also often used to reduce the hydrochloric acid concentration of the final solution. Table 2 [43–45] provides a summary of the different separation methods described in the literature that result in a chloride solution ($^{64}CuCl_2$) suitable for radiolabelling.

The selected separation/purification method will ideally be included in a robust, reliable and cost effective process, avoiding sensitive and manual steps, reducing operator variability, minimizing errors and avoiding radiation exposure. A fully automated process ensures these properties and is critical to achieving

TABLE 2. COMMON METHODS FOR SEPARATION OF CYCLOTRON PRODUCED ^{64}Cu

Radionuclide	First resin	Eluent	Second resin	Ref.
^{64}Cu	Cu resin	HCl 3M; 7 ml	SAX	[43]
	AG50W–X4	8M HCl	AG1–X4	[44]
	2.5 g of BioRad AG1–X8 resin	8M HCl	n.a.	[45]

Note: n.a.: not applicable; SAX: strong anionic exchange.

GMP compliance. Such an automated process has been recently described in the literature [46]. It uses a commercially available module and dedicated disposable cassettes. Separation of ^{64}Cu from ^{64}Ni is achieved using a highly selective Cu resin, complemented with a second exchanger column to reduce HCl concentration and to provide additional decontamination from other metals. A schematic diagram of the process is shown in Fig. 4.

As a first step, the irradiated solution is diluted to achieve a pH equal to or greater than 3 because this is necessary to ensure quantitative trapping of the produced ^{64}Cu on the resin, which is preconditioned by water [43]. Removal of the remaining Ni from the resin is performed by washing with a 1 mM nitric acid wash before the cartridge is finally dried by inert gas. The trapped ^{64}Cu is then transferred onto the strong anionic exchange (SAX) cartridge (preconditioned consecutively with water and 8M HCl) by elution of the trapping resin with

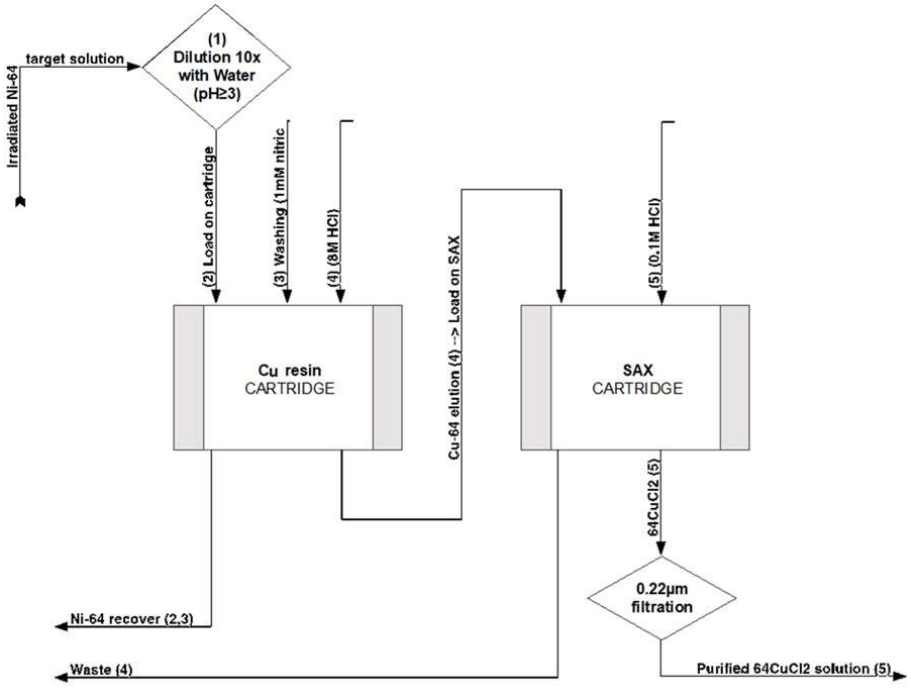

FIG. 4. Schematic of automated separation method of liquid target produced ^{64}Cu (courtesy of F. Alves, University of Coimbra).

8M HCl. Finally, the SAX cartridge is dried using an inert gas and eluted with 0.1M HCl. A $^{64}CuCl_2$ suitable to be used as a precursor for radiolabelling is obtained after a 1 h process.

2.2.6. Quality control

2.2.6.1. Chemical purity

Considering that the production of ^{64}Cu (as of radiometals in general) for incorporation into radiopharmaceuticals relies heavily on ensuring trace level concentrations of any possible contaminant, analytical techniques with the highest sensitivity possible (parts per trillion level) are required. Inductively coupled plasma mass spectrometry (ICP-MS) meets that need, coupling versatility with the capability to provide accurate information on species identification and quantitative concentration values.

2.2.6.2. Radiochemical purity

In order to evaluate the presence of the ionic forms of the radiometal isotopes and the absence of colloidal complexes, radio thin layer chromatography (TLC) analysis of the purified $^{64}CuCl_2$ is strongly recommended. Tables 3 and 4 and Fig. 5 illustrate experimental data obtained from quality control data for the automated process described above [46]. Excellent chemical purity (98%) and decay corrected yields above 80% are reported.

TABLE 3. ICP-MS DETERMINED QUANTITIES OF Cu AND OTHER TRACE METALS IN 4 ml $^{64}CuCl_2$ PRODUCT (μg, n = 10). Co, Ag AND In WERE IN THE NANOGRAM RANGE

Al	Mn	Fe	Ni	^{64}Ni	Cu	Zn	Ga	Pb
0.534 ±0.790	0.018 ±0.030	0.184 ±0.220	0.084 ±0.100	0.069 ±0.090	0.051 ±0.060	0.111 ±0.150	0.008 ±0.010	0.032 ±0.030

TABLE 4. PERCENTAGE OF TOTAL ACTIVITY MEASURED (LOST) IN EACH STEP OF THE PURIFICATION PROCESS

Cu resin cartridge	Recovery vial (^{64}Ni)	SAX cartridge	Waste of SAX	Filter	$^{64}CuCl_2$ vial
0.65 ± 0.72	4.53 ± 6.79	3.48 ± 4.74	8.23 ± 8.47	0.18 ± 0.60	82.93 ± 9.12

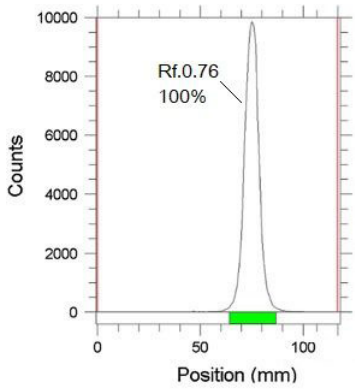

FIG. 5. Instant TLC (iTLC) chromatogram obtained using a scanner. Stationary phase: iTLC silica gel strips; mobile phase: 0.1M sodium citrate (pH adjusted to 4–4.5). Retention factor (Rf) values were Rf = 0.1–0.2 for the colloidal form and Rf = 1.0 for the free radioisotope.

2.2.7. Target material recovery

Highly enriched ^{64}Ni is very expensive (approximately US $35–40 per milligram) and therefore target material recovery and recycling for further use is mandatory for process cost efficiency. In the automated process described in Section 2.2.5, target material is collected in a specific waste vial, allowing the recovery of the expensive ^{64}Ni. The recovery process is based on a redissolution and evaporation method schematically presented in Fig. 6. After final isolation of the ^{64}Ni fraction, enriched material (estimated to 99% of the original ^{64}Ni target mass) is obtained in diluted nitric acid solution (<0.01M). ICP-MS analysis of recovered ^{64}Ni nitrate to evaluate for metal impurities is strongly recommended.

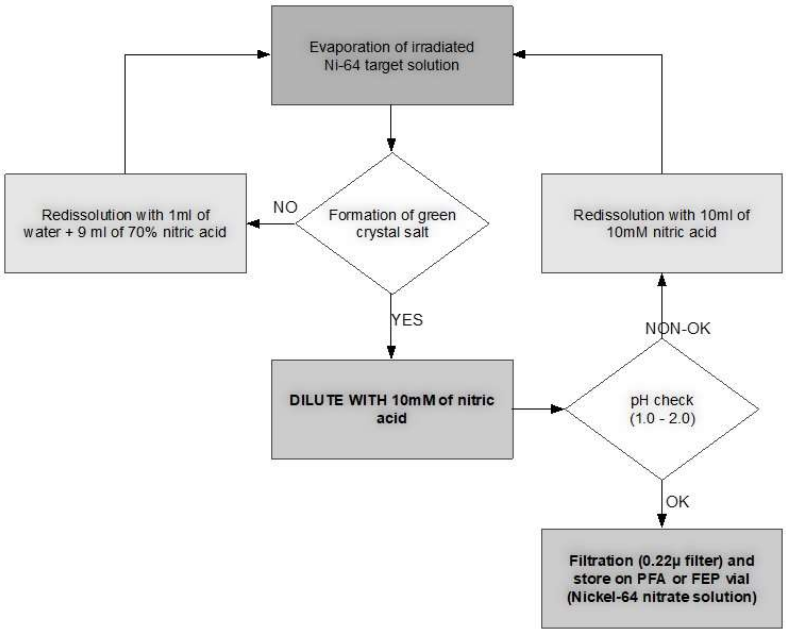

FIG. 6. Recovery process for ^{64}Ni target material (courtesy of F. Alves, University of Coimbra). PFA: perfluoroalkoxy alkanes; FEP: fluorinated ethylene propylene.

3. CHELATING LIGANDS FOR COPPER

Although ^{64}Cu is a very attractive radionuclide for radiopharmaceutical development, most radiopharmaceuticals are composed of chelators already developed for other radiometals, such as ^{68}Ga and ^{177}Lu, among others. The stability of the copper conjugated form via these chelators sometimes limits the application of the tracers in human clinical trials owing to coupled disassociation and unwanted normal tissue radiation doses. Therefore, the development of new specific copper chelators for dedicated radiopharmaceuticals is of great interest. Although many naturally existing copper chelators have been used in medicine and biology for the metabolic copper disorders, as well as for research activities, not all of these have been applied in radiopharmaceutical chemistry (a concise overview of these ligands is presented at the end of Annex I, Fig. I–1). In this section we discuss various copper chelator agents, including synthetic ones used in existing and future copper radiopharmaceuticals.

Acyclic chelators, such as ethylenediaminetetraacetic acid (EDTA), are known for their fast copper complexation and can often be used at room temperature under titration conditions [47]. Their stability constants, however, are too low to compete with copper proteins, which typically display subfemtomolar or better binding. While 1,4,7-triazacyclononane-1,4,7-triacetic acid (NOTA) based ligands can be radiolabelled at room temperature, the cyclen based ligands require mild heating (40–90°C). The cross-bridged chelators generally need even harsher conditions (95°C for 60 min), which limits their application to heat resistant biovectors, although the use of phosphonate armed analogues can sometimes alleviate the driving radiolabelling conditions [48]. The radiolabelling of porphyrins typically requires not only elevated temperatures, but also the presence of dimethyl sulphoxide (DMSO) and reductive stabilizers [49]. At present, the sarcophagine (SAR) ligands appear to be the most optimal copper chelators, allowing for fast copper incorporation at room temperature in a broad pH range of 4–9 and no copper release [50].

Copper proteins present a significant challenge to radiocopper chelates in vivo. Most of the chelates do release the radiocopper through transchelation to proteins, which often end up in the liver and kidneys. Numerous experimental results point to superoxide dismutase (SOD) and ceruloplasmin as the main copper enzymes responsible for copper transchelation in vivo [49, 51]. An intracellular reduction from Cu^{2+} to Cu^{+} is either required or facilitates this process.

Research and development on the creation and selection of the best copper chelators is ongoing, as many research groups worldwide seek to obtain molecules of tissue chelator conditions and study the chelators' stability and biological properties.

3.1. ACYCLIC CHELATORS

The most important acyclic copper chelators are bis(thiosemicarbazones) (BTSCs), which readily react with Cu^{2+} to produce neutral, stable and relatively lipophilic organocopper complexes (Fig. 7) [52]. The ^{nat}Cu and ^{64}Cu chelated Cu-BTSC compounds have attracted significant interest as potential tracers for perfusion tumour hypoxia and as metallodrugs, owing to their anti-proliferative activities. The simple chemical structure of the ligand lends itself to easy functionalization, allowing the systematic study of the Cu-BTSC structure–activity relationship. Numerous studies have revealed that the properties and biodistribution of Cu-BTSC appear to be sensitive to backbone substitution (R_1 and R_2) and only marginally sensitive to terminal substitution. The alkyl substitution in the backbone governs (a) the Cu^{2+}/Cu^{+} redox potential, (b) the release of copper from the complex inside the cell, (c) the ability to penetrate

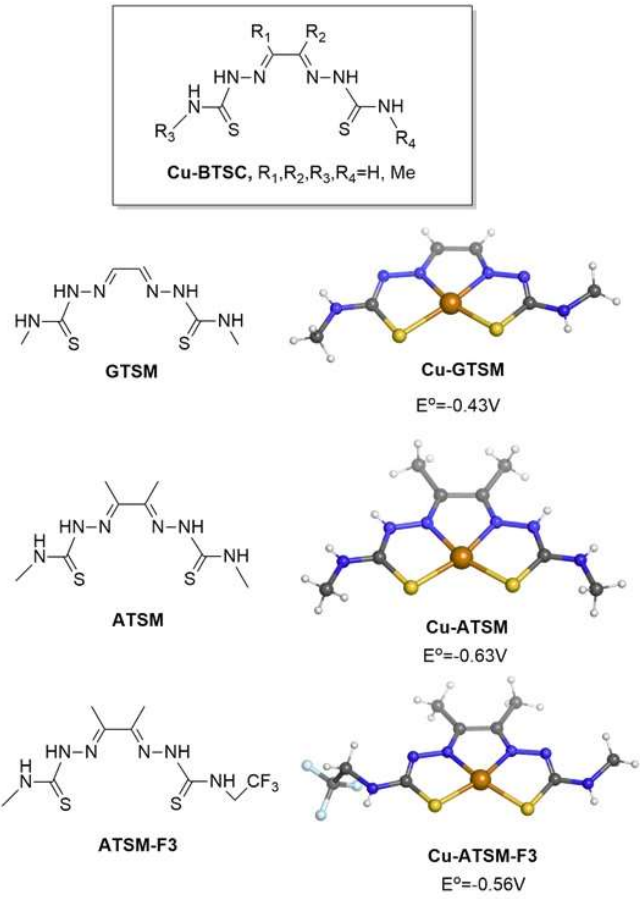

FIG. 7. Bis(thiosemicarbazones) (BTSCs) and the crystal structures of the corresponding copper complexes (courtesy of F. Zhuravlev, Technical University of Denmark).

the cellular membrane and (d) anti-neoplastic activity [53–55]. A case in point is the pair of copper complexes Cu-GTSM and Cu-ATSM. They differ only in two methyl groups attached to the imine backbone of Cu-ATSM. Cu-ATSM is a successful tumour hypoxia tracer and Cu-GTSM is hypoxically inactive. The rationale is that the dimethyl substitution donates more electron density onto the metal centre, which makes Cu-ATSM more difficult to reduce than Cu-GTSM (in other words, Cu-ATSM is a poorer oxidant). As a result, Cu-ATSM is not reduced inside normal cells. However, hypoxic tumours are stronger reductants, allowing the weaker oxidant to be reduced (the hypoxic window of selectivity for the Cu^{2+}/Cu^{+} redox potential is below –0.5 V). Accordingly, with a potential of

E_0 = –0.63 V at 1 M and 1 bar, Cu^{2+}/Cu^{+} is efficiently reduced in hypoxic cells. How the cells retain the reduced Cu^{+} is not known exactly, but it is conceivable that Cu^{+} eventually decomplexes from the ligand and is picked up by one of the copper chaperones. The Cu^{2+}/Cu^{+} hypoxia driven reduction has been elegantly demonstrated by the observation of ^{19}F nuclear magnetic resonance (NMR) from a hypoxic cell treated with Cu(I)-ATSM-F3 (diamagnetic, well resolved NMR), while no ^{19}F NMR was observed in normoxic cell cultures as Cu(II)-ATSM-F3 owing to the paramagnetic relaxation enhancement of the ^{19}F NMR quench [52].

3.2. MACROCYCLIC CHELATORS

3.2.1. Ring size effect

Macrocyclic chelators are strongly preferred to their acyclic counterparts because of their higher stability. N-macrocycles favour Cu^{2+} chelation, while the S-donors tend to stabilize the Cu^{+} state. Two main effects govern the stability of Cu^{2+} inside the N-containing macrocycles: the chelate ring size and the cavity size. The Cu^{2+} ion, being a relatively small ion (0.57 Å) has C–N bond lengths of 2.03 Å. This indicates a borderline case between six and five membered chelate rings, with a slight preference for a six membered ring. In 12-aneN_4 (cyclen family), the cavity is too small for in-plane copper, which is reflected in its stability constant ($\log K_{ML}$ = 24.8) [56]. As a result, the metal is pushed above the macrocyclic ring, adopting pseudotetrahedral geometry (Fig. 8) [56]. The cavity of 13-aneN_4 is large enough to accommodate in-plane copper and the metal enjoys a six membered ring stabilization. 14-aneN_4 adds another six membered ring stabilization, lowering bond angle strain and making it the most stable macrocycle in the series ($\log K_{ML}$ = 28.9) [56].

3.2.2. Polyaza carboxylate, phosphonate and sarcophagine chelators

The functionalization of the nitrogen atoms of the N-macrocycles with -CH_2-X (X = CO_2H, PO_3H_2, etc.) moieties leads to a family of polyaza chelators (Table 5) [57–67]. The methylene carboxylate or methylene phosphonate arms allow the copper to increase its coordination number to 6. The small cavity size of NOTA [68] (Table 5, entry 1) leads to a distorted trigonal prismatic geometry around Cu^{2+} and weak interactions with the axial substituents. This facilitates protonation of the complex, which still retains its high copper affinity in the protonated state. However, the great flexibility of the NOTA ligand allows for remarkably fast complexation (milliseconds) and the formation of thermodynamically stable complexes ($\log K_{ML}$ = 23.33), even at low pH [69]. As such, NOTA remains a

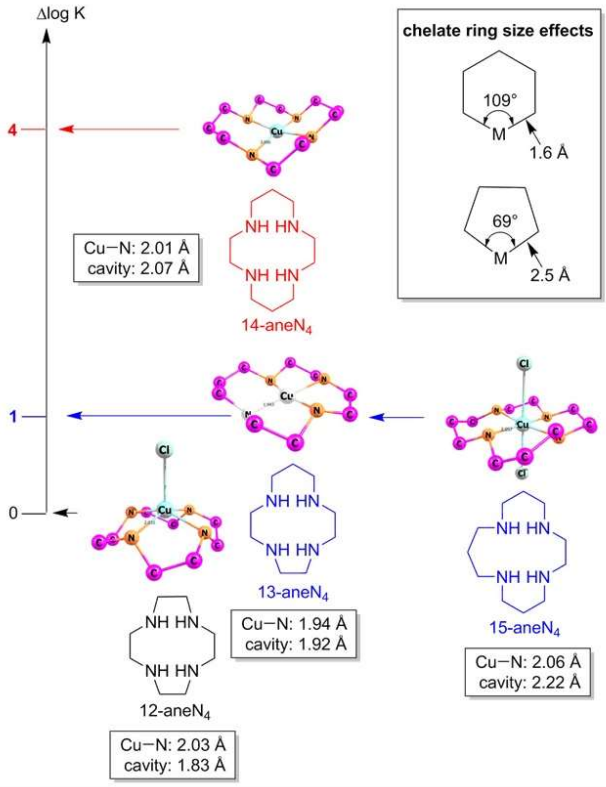

FIG. 8. Ring size effect in the N-macrocycles (courtesy of F. Zhuravlev, Technical University of Denmark).

popular choice as a chelator for radiocopper because of its room temperature complexation and adequate in vivo stability (see Section 3.2.1). A member of the cyclen family, 1,4,7,10-tetraazacyclododecane-1,4,7,10-tetraacetic acid (DOTA) is arguably the most popular chelator for radiometals in general, and for radiocopper in particular. Upon complexation, DOTA imposes distorted octahedral coordination on Cu^{2+}. DOTA complexes copper much more slowly than NOTA (~1 s) [69] and requires heating to complete the complexation. On the timescale of most ^{64}Cu applications, DOTA demonstrates good thermodynamic stability ($\log K_{ML}$ = 22.3) [70] and adequate, for most parts, in vivo stability. Removing one carboxylate arm (DO3A) barely changes the stability ($\log K_{ML}$ = 22.9), but DO2A is appreciably less stable ($\log K_{ML}$ = 18.9). In contrast, the phosphonate analogues are significantly more stable: DO2P ($\log K_{ML}$ = 28.7), DO3P ($\log K_{ML}$ = 26.9) and DOTP ($\log K_{ML}$ = 26.2). The first member of the cyclam

family, 1,4,8,11-tetraazacyclotetradecane-1,4,8,11-tetraacetic acid (TETA), is also characterized by a high stability constant ($\log K_{ML} = 21.9$) but suffers from copper dissociation in vivo. A large number of N-functionalized mono- and bifunctional chelators of the cyclen and cyclam families have been synthesized, and a growing number are becoming commercially available (Table 5, entries 3–14).

TABLE 5. THE FAMILY OF THE POLYAZA CHELATORS

No.	Structure	R1	R2	R3	R4	Name
1		CH_2CO_2H	CH_2CO_2H	CH_2CO_2H		NOTA [68]
2		CH_2CO_2H	CH_2CO_2H			NODAGA-NHS
	Cyclen based	R1	R2	R3	R4	
3		H	H	H	H	Cyclen [71]
4		H	CH_2CO_2H	H	CH_2CO_2H	DO2A [70]
		H	H	$CH_2PO_3H_2$	$CH_2PO_3H_2$	DO2P [70]
5		H	CH_2CO_2H	CH_2CO_2H	CH_2CO_2H	DO3A [70]
		H	$CH_2PO_3H_2$	$CH_2PO_3H_2$	$CH_2PO_3H_2$	DO3P [70]
6		CH_2CO_2H	CH_2CO_2H	CH_2CO_2H	CH_2CO_2H	DOTA [72]
7		$CH_2PO_3H_2$	$CH_2PO_3H_2$	$CH_2PO_3H_2$	$CH_2PO_3H_2$	DOTP [70]
8		CH(Me) CO_2Na	CH(Me) CO_2Na	CH(Me) CO_2Na	CH(Me) CO_2Na	DOTMA
9		CH_2CO_2H	CH_2CO_2H	CH_2CO_2H		DOTA-NHS ester
10		$CH_2CO_2{}^tBu$	$CH_2CO_2{}^tBu$	$CH_2CO_2{}^tBu$		2-aminoethyl-monoamide-DOTA^{t}Bu ester

TABLE 5. THE FAMILY OF THE POLYAZA CHELATORS (cont.)

No.	Structure	R1	R2	R3	R4	Name
	CB-cyclen based	R1	R2			
11		H	H		CB-cyclen	CB-cyclen
12		CH_2CO_2H	CH_2CO_2H			CB-DO2A [51]
	Cyclam based	R1	R2			
13		H	H	H	H	Cyclam [73]
14		CH_2CO_2H	CH_2CO_2H	CH_2CO_2H	CH_2CO_2H	TETA
	CB-cyclam based	R1	R1			
15		H	H			CB-cyclam
16		CH_2CO_2H	CH_2CO_2H			CB-TE2A [74]
17		$CH_2PO_3H_2$	$CH_2PO_3H_2$			CB-TE2P [74]
18		CH_2CO_2H	$CH_2PO_3H_2$			CB-TE1A1P
	SAR based					
19		H	H			SAR [75]
20		NH_2	NH_2			diamSAR [75]
21			NH_2			SarAr [76]
22			NH_2			SarAr-NCS [77]
23			NH_2			AmBaSar [78]

Note: CB: closed bridge; SAR: sarcophagine.

Connecting two nitrogen atoms in the cyclen or cyclam ligands by a methylene chain yields the corresponding cross-bridging structures presented in Table 5, entries 15–18. Although providing little additional thermodynamic stability to the complex, the bridge significantly boosts the kinetic inertness [48].

Synthesized by Sargeson [75], the capsule shaped hexamine-macrobicyclic cage amine ligands known as SARs confer outstanding kinetic stability to the resulting copper complexes. The SAR-bound Cu^{2+} also resists reduction to Cu^{+} up to a potential of –1 V, which also suggests its resistance to in vivo reduction and subsequent transchelation to copper proteins [50]. Both electrophilic and nucleophilic bifunctional chelators have been reported (Table 5, entries 21–23). The crystal structures provide insight into the geometry of the cross-bridged and SAR ligands and the degree of steric shielding that they provide.

3.2.3. Porphyrins

Porphyrins are gaining popularity as a multimodality family of copper chelators [79]. Sharing its basic tetrapyrrole structure with many natural pigments, such as hemin, chlorophyll and bacteriochlorophyll, porphyrin provides stable tetradentate coordination to copper while retaining its photosensitizing capacity for use in photodynamic therapy and optical imaging. Copper-64 incorporates well into a series of meso-functionalized porphyrins (Fig. 9, left) [49]. Similarly, the biologically important protophorphyrin IX based scaffold and its PEG6-BBN bioconjugate (Fig. 9, centre) can be radiolabelled with ^{64}Cu. A photosensitive porphyrine (pyropheophorbide) was synthesized (Fig. 9, right) and radiolabelled with ^{64}Cu as a promising PET imaging and photodynamic tumour therapy agent by linking it to a prostate-specific membrane antigen (PSMA) [80].

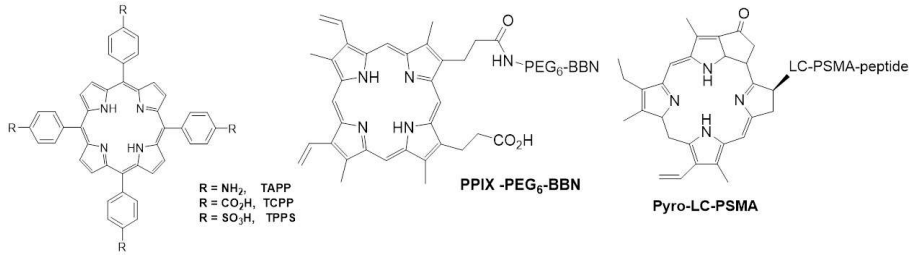

FIG. 9. Meso-functionalized porphyrins (left) [49], protoporphyrin IX (PPIX) based PPIX-PEG6-BBN (centre) and pyropheophorbide-a core based pyro-LC-PSMA bioconjugates (right) [80] (reproduced from Refs [49, 80] with permission).

4. COPPER-64 RADIOLABELLED PEPTIDES

4.1. INTRODUCTION

Molecular imaging is defined as the visualization, characterization and measurement of biological processes at the molecular and cellular levels in humans and other living systems. Molecular imaging is a non-invasive procedure that involves clinical in vivo administration of a biologically active, receptor specific, targeting vector (i.e. peptides, small proteins, antibody fragments or intact antibodies) conjugated to a radioligand, nanoparticle and/or fluorescent/magnetic resonance imaging (MRI) probe, followed by acquisition and quantification of the signal by PET, single photon emission computed tomography (SPECT), MRI, fluorescence imaging or ultrasound [81].

Radiolabelled antibodies have demonstrated the potential to be used as site-directed compounds for the development of new and successful diagnostic and therapeutic radiopharmaceuticals for human cancers. However, antibodies suffer from very slow clearance from blood serum/non-target tissue and often less than desirable tumour uptake. Peptides, on the other hand, offer distinct advantages over higher molecular weight compounds (i.e. antibodies or antibody fragments), including rapid clearance from whole blood, ease of penetration into the tumour vascular endothelium, more rapid excretion from the body and relatively low immunogenicity. Furthermore, radiolabelled peptides can be chemically tuned to target cell surface receptors that tend to be expressed in very high numbers on human cancer cells, offering the advantage of identifying and treating diseased human tissue with minimal collateral damage to neighbouring normal tissues [82]. High affinity receptors selectively overexpressed on a variety of neoplastic cells have been identified for several small peptides, making them ideal candidates for use as new diagnostic and/or therapeutic targeting vectors. Peptide based targeting vectors for molecular imaging or therapy comprise a targeting vector (the peptide construct), a pharmacokinetic modifier (hydrophilic aliphatic or amino acid tethering molecule), a bifunctional chelating agent (BFCA, a complexing agent capable of producing a kinetically inert, in vivo radiometal–ligand complex while linking it to the regulatory peptide) and a radiometal (a gamma or positron (γ or β^+) emitting diagnostic or a beta or alpha (β^- or α) emitting therapeutic radionuclide) [83].

Herein we report investigations that describe advances and new targeting strategies using ^{64}Cu radiolabelled peptides in the molecular imaging of specific human diseases. Specifically, we discuss somatostatin (SST), gastrin releasing peptide (GRP), melanocortin and other receptor targeting peptides and highlight recent advances in the use of radiolabelled, multimeric/multivalent regulatory

peptides for targeting and molecular imaging of multiple cell surface receptors via the ^{64}Cu radionuclide.

4.2. RADIOCHEMISTRY OF COPPER-64

Copper-64 labelled radiopharmaceuticals are of primary interest because of the ideal nuclear characteristics of ^{64}Cu (see Section 4.1), which make it useful for in vivo molecular imaging [84]. 'Matched pairs' offer the unique opportunity to use information derived from routine patient diagnostic SPECT or PET studies to determine the degree of receptor density on primary and metastatic tissues prior to administration of the corresponding therapeutic analogue. In this way, treatment is only administered to patients previously demonstrating expression of the target receptor. Furthermore, the diagnostic radiopharmaceutical can be invaluable in prescreening receptor positive patients for therapy with respect to drug pharmacokinetics, receptor density and patient dosimetry, potentially reducing or eliminating unsuccessful radiotherapeutic regimens. The ^{64}Cu radionuclide is considered to be its own 'matched pair', in that it is useful for PET molecular imaging and therapy of human cancers [85].

4.3. PEPTIDES

4.3.1. Somatostatin receptor targeting peptides

To date, radiolabelled analogues of SST have been the gold standard for peptide receptor imaging and therapeutic agents. For example, the clinical success of Octreoscan® for visualizing primary and metastatic SST receptor positive tumours has paved the way for the exploration and radiolabelling of other biologically active peptides described herein. SST, a peptide hormone expressed in the central and peripheral nervous systems, exists naturally in two forms: SST-14 and SST-28. SST-14 and SST-28 have a cyclic structure because of the presence of a single disulphide bond. Five known G protein coupled SST receptor (SSTR) subtypes exist, SSTR1–SSTR5. These are expressed in very high quantities on tumours of neuroendocrine origin, with SSTR2 being the most prolific. Therefore, radiolabelled agents based on SSTR targeting peptides are viable candidates for site directed molecular imaging of neuroendocrine receptor expressing tumours [86–91].

SSTR targeting peptides have proved their diagnostic and therapeutic efficacy in the clinic and are the benchmark to which all other radiolabelled peptides will ideally be compared. For example, targeted therapy of

primary and metastatic tumours of neuroendocrine origin has focused on DOTA conjugated SSTR targeting peptides radiolabelled with β^- emitting ^{90}Y or ^{177}Lu. Until now, much of the focus for targeting SSTR2 with radiolabelled SST derivatives has centred on octreotide (D-Phe-Cys-Phe-D-Trp-Lys-Thr-Cys-Thr(ol)), [Tyr^3]octreotide [D-Phe-Cys-Tyr-D-Trp-Lys-Thr-Cys-Thr(ol)] and [Tyr^3]octreotate (D-Phe-Cys-Tyr-D-Trp-Lys-Thr-Cys-Thr). These studies and others have shown that molecular imaging and treatment of neuroendocrine tumours (NETs) via radiolabelled SSTR targeting peptides is clearly a success and will ideally be considered as a model for future treatment strategies for tumours of this general type [90–93].

Many pioneering investigations involving SSTR targeting peptides radiolabelled with ^{64}Cu (after intravenous injection) have been described by Anderson et al. In 2001 they described the development of [^{64}Cu]Cu-TETA-OC [94]. This novel PET tracer was compared directly with Octreoscan® in a pilot study involving eight patients bearing NETs. Their findings showed that [^{64}Cu]Cu-TETA-OC demonstrated increased sensitivity for imaging NETs, presumably owing to the enhanced sensitivity of PET when compared directly with SPECT. Their second generation agent, [^{64}Cu]Cu-TETA-Y3-TATE, showed even more promise as a true theranostic radiopharmaceutical [94]. When compared directly with [^{64}Cu]Cu-TETA-OC [95], [^{64}Cu]Cu-TETA-Y3-TATE showed improved uptake in rodents bearing SSTR positive, AR42J rat pancreas tumours. A third generation agent demonstrated the superiority of the cross-bridged TE2A complexing agent for ^{64}Cu over DOTA or TETA [96–98]. In Refs [86, 87] they evaluated [^{64}Cu]Cu-CB-TE2A-Y3-TATE in male Lewis rats bearing AR42J tumours. High labelling efficiency and radiochemical purity of the tracer were observed. In addition, uptake and retention of the tracer in SSTR positive AR42J tumours was found to be superior to [^{64}Cu]Cu-TETA-Y3-TATE [98].

In 2014, Nedrow et al. reported investigations in which they conjugated *p*-SCN-Bn-NOTA and 1,4,7-triazacyclononane, 1-glutaric acid-4,7-acetic acid (NODAGA) to the SSTR2 targeting agonist Y3-TATE through β-alanine and PEG8 linking substituents (Fig. 10) [99]. In that study the authors report uptake values in HCT116-SSTR2 tumours of 15 ± 4.8 and 13 ± 3.1 per cent injected dose per gram (% ID/g) at 4 h post-injection (p.i.) for [^{64}Cu]Cu-NODAGA-Y3-TATE and [^{64}Cu]Cu-CB-TE2A-Y3-TATE, respectively. These values were superior to those containing β-alanine and PEG8 linkers, which showed ~5% ID/g in the tumour. High quality, high contrast micro-positron emission tomography (microPET) images in mice bearing SSTR2 positive tumours were obtained for all of the new tracers. The authors concluded that [^{64}Cu]Cu-NODAGA-Y3-TATE and [^{64}Cu]Cu-CB-TE2A-Y3-TATE behave similarly in vitro and in vivo, and are ideal for molecular imaging investigations via PET. However, superiority arises for [NODAGA-Y3-TATE] in that it can be used to produce both ^{68}Ga and ^{64}Cu

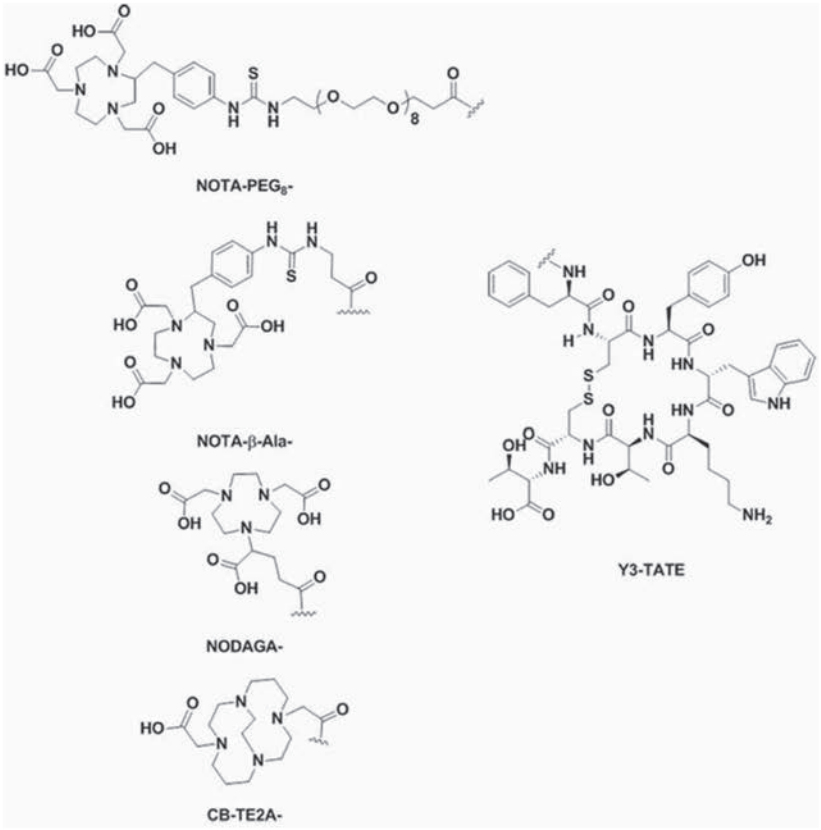

FIG. 10. Structural representation of [^{64}Cu]Cu-X-Y3-TATE (where X = NOTA-PEG, NOTA-β-Ala, NODAGA- or CB-TE2A) radiopharmaceuticals (reproduced from Ref. [99] with permission).

tracers. Furthermore, NODAGA-Y3-TATE can be radiolabelled under milder conditions than CB-TE2A-Y3-TATE [99].

Perhaps some of the more exciting ^{64}Cu work discussed in recent years has come from research groups in Denmark. Clinical investigations of [^{64}Cu]Cu-DOTATATE when directly compared with [^{111}In]In-DTPA-OC in patients bearing NETs showed the diagnostic sensitivity and accuracy of [^{64}Cu]Cu-DOTATATE to be clearly superior to [^{111}In]In-DTPA-OC (Octreoscan®) (Fig. 11) [100]. The high quality, high contrast PET images with minimal tracer accumulation in liver tissue have somewhat dispelled the 'myth' of in vivo demetallation of the ^{64}Cu from the DOTA complexing agent, and prove that this phenomenon could be species dependent. The diagnostic performance and PET images obtained using [^{64}Cu]Cu-DOTATATE in human

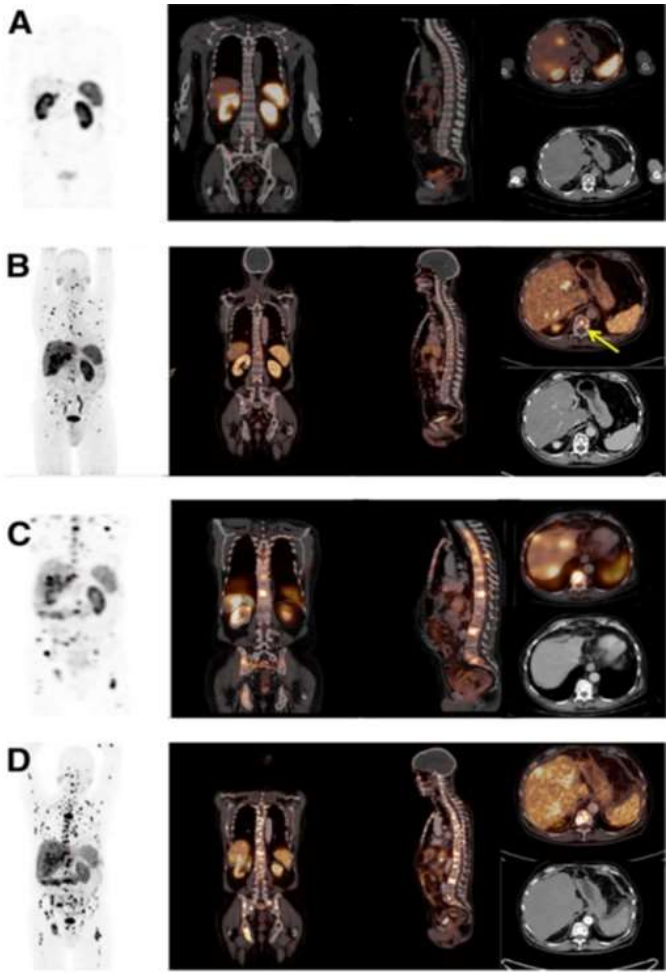

FIG. 11. Patient identified with metastatic bone lesions when administered [^{64}Cu]Cu-DOTATATE via PET. Only a single lesion was identified when administered Octreoscan® via SPECT. (a) Octreoscan®, 2010; (b) [^{64}Cu]DOTATATE, 2010; (c) Octreoscan®, 2012; (d) [^{64}Cu]DOTATATE, 2012 (reproduced from Ref. [100] with permission).

patients have catalysed investigations by many companies to pursue development of [^{64}Cu]Cu-DOTATATE for routine clinical use for the diagnosis of NETs.

Researchers in Australia have obtained exciting results regarding the usage of ^{64}Cu-MeCOSar-octreotate ([^{64}Cu]Cu-SARTATE) in a prospective study involving ten patients that had previously been identified with neuroendocrine neoplasia and positive uptake of [^{68}Ga]DOTATATE (Netspot) [101] (see Fig. 12).

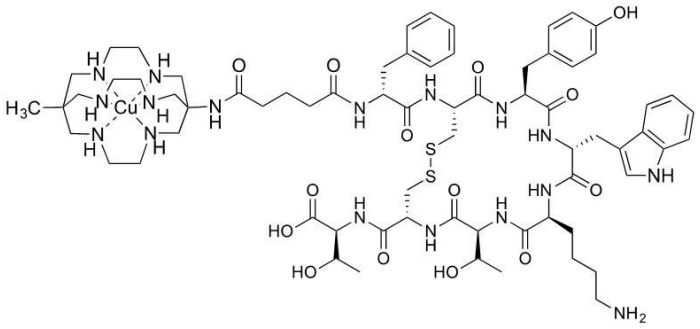

FIG. 12. Structural representation of [^{64}Cu]Cu-SARTATE radiopharmaceutical (reproduced from Ref. [102] with permission).

In this study, PET–computed tomography (CT) imaging was performed 0.5, 1, 4 and 24 h after administration of the tracer. The authors concluded that [^{64}Cu]Cu-SARTATE was well tolerated and that PET–CT images obtained at 4 h p.i. were comparable to [^{68}Ga] DOTATATE PET–CT images obtained at 1 h. Overall, [^{64}Cu]Cu-SARTATE appears to be a viable theranostic tool for NETs. In addition, the longer physical half-life of ^{64}Cu when compared with ^{68}Ga may allow for widespread distribution of the drug [101].

Until recently, clinical evaluation in human patients has been limited to SSTR-targeting agonist ligands. Agonist ligands elicit a biological response from the cell and are effectively endocytosed and internalized upon binding to the receptor. Antagonist ligands, on the other hand, are not internalized and have previously been deemed inappropriate for targeted molecular imaging and peptide receptor TRT. Recent studies with SSTR targeting antagonist ligands, however, have indicated that the preferable use of agonist ligands for in vivo molecular imaging and therapy clearly bears reconsideration [96, 103]. Wadas et al. have reported the synthesis of CB-TE2A-sst$_2$-ANT radiolabelled with ^{64}Cu [92]. This conjugate is a potentially useful SSTR antagonist for PET imaging of SSTR positive tumours. In that study, they determined that [^{64}Cu]Cu-CB-TE2A-sst$_2$-ANT showed higher ‘tumour to blood’ and ‘tumour to muscle’ ratios compared with [^{64}Cu]Cu-CB-TE2A-Y3-TATE, a SSTR2 positive agonist. MicroPET–CT imaging of male Lewis rats bearing AR42J tumours showed high quality diagnostic images with excellent tumour to background contrast at 4 h after injection [103].

4.3.2. Gastrin releasing peptide receptor targeting peptides

GRP receptors are present in high concentrations on human cancers such as prostate, breast, pancreatic and small cell lung carcinoma [57, 82]. Mammalian bombesin peptide (BBN) receptors are G protein coupled, 7-transmembrane receptors with the capacity to be endocytosed upon binding by an effective agonist ligand. There are four known receptor subtypes of BBN, including the neuromedin B receptor (subtype 1), the GRP receptor (GRPR, subtype 2), the orphan receptor (subtype 3) and the BBN receptor (subtype 4) [58]. The driving force for development of site directed, theranostic agents has been GRPR. To date, design and development of radiolabelled agents for GRPRs have focused on the highly prolific BB2 receptor subtype targeted by BBN- or BBN-like analogues. BBN is the 14 amino acid amphibian peptide analogue of the 27 amino acid mammalian regulatory peptide GRP. BBN and GRP share a homologous seven amino acid amidated C-terminus, -WAVGHLM-NH_2, which is essential for high affinity receptor binding to GRPR.

The BBN(7–14)NH_2 agonist has been the primary focus of many research groups and has been evaluated in great detail. For example, ^{64}Cu-BBN(7–14)NH_2 radiopharmaceuticals have been of interest because of the ideal nuclear characteristics of ^{64}Cu, which make it useful for in vivo molecular imaging and therapy. Parry et al. reported the first structure–activity studies using a host of aliphatic/amino acid linkers to form constructs of the general type [DOTA-X-BBN(7–14)NH_2] [59]. When radiolabelled with ^{64}Cu, the new tracers exhibited very high affinity for GRPR. However, some accumulation and retention of tracer in hepatic tissue was observed, presumably due to dissociation of the metal centre from the DOTA complexing agent. Garrison and co-workers performed a side by side comparison of the CB-TE2A and DOTA complexing agents when conjugated to the DOTA-8-Aoc-BBN(7–14) NH_2 agonist construct [60]. The results showed improved stability in vivo for the CB-TE2A derivative. For example, accumulation of tracer in hepatic tissue was reduced from 9.56% ID/g to 2.15% ID/g at the 1 h time point. Accumulation of tracer in PC-3 xenografted tumours was 4.95% ID/g and 6.95% ID/g for the DOTA and CB-TE2A derivatives, respectively [60]. MicroPET images obtained in mice bearing PC-3 xenografted tumours demonstrated site-directed uptake in tissue with high background radiation.

Prasanphanich and co-workers radiolabelled [NO2A-8-Aoc-BBN(7–14)NH_2] conjugate with ^{64}Cu and reported improved in vivo stability compared with the DOTA complexing agent. Furthermore, radiolabelling conditions were vastly improved compared with CB-TE2A derivatives previously reported. These studies resulted in tumour uptakes of 3.59 ± 0.70% ID/g at 1 h p.i. in PC-3 tumour-bearing severe combined immunodeficient (SCID) mice [61, 62] and 2.27 ± 0.08% ID/g at 1 h p.i. in T-47D tumour-bearing SCID mice [63]. High quality, high contrast microPET images were obtained in both mouse models. A series of [^{64}Cu]Cu-NO2A-(X)-BBN(7–14)

NH_2 conjugates using an X pharmacokinetic modifier (beta-alanine, 5-aminovaleric acid, 6-aminohexanoic acid, 8-aminooctanoic acid, 9-aminonanoic acid or para-aminobenzoic acid) and NO2A 1,4,7-triazacyclononane-1,4-diacetic acid [62, 64] were investigated for prostate cancer (PCa) imaging. Competitive binding assays in PC-3 cells indicated high receptor binding affinity for the NO2A-(X)-BBN(7–14)NH_2 and [^{nat}Cu]Cu-NO2A-(X)-BBN(7–14)NH_2 conjugates. In vivo biodistribution studies of the [^{64}Cu]Cu-NO2A-(X)-BBN(7–14)NH_2 conjugates at 1, 4 and 24 h p.i. showed very high uptake of tracer in GRPR positive tissue with little accumulation and retention in non-target tissues, including the liver. For example, uptake in GRPR positive PC-3 tumours ranged from 3.59% ID/g to 6.05% ID/g. In Ref. [100], the microPET–CT images obtained at 18 h p.i. in PC-3 tumour-bearing SCID mice agree with data obtained from the biodistribution studies. These images clearly demonstrate the effect of size and hydrophilicity X has on the in vivo pharmacokinetics of the [^{64}Cu]Cu-NO2A-(X)-BBN(7–14)NH_2 conjugates (Fig. 13). The shorter, more hydrophilic pharmacokinetic modifier, AMBA, produced superior microPET images, with minimal accumulation in collateral tissue. The [^{64}Cu]Cu-NO2A-(X)-BBN(7–14)NH_2 conjugates (where X = 6-Ahx or 8-Aoc) also showed clear tumour contrast from surrounding tissues, with minimal uptake and retention in the renal tissue. The longer, more lipophilic pharmacokinetic modifier (X = 9-Anc) for [^{64}Cu]Cu-NO2A-(9-Anc)-BBN(7–14)NH_2, reported with high accumulation of radioactivity in the liver and abdominal region, produced less than optimal whole body image contrast.

Nanda and co-workers showed vast improvement in excretion pharmacokinetics and microPET molecular imaging investigations by only changing the complexing agent in the development of new radiotracers [65]. For

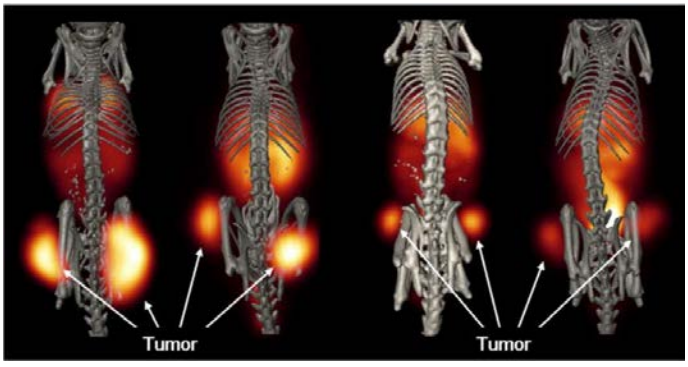

FIG. 13. Maximum intensity microPET tumour and microCT skeletal fusion coronal images of PC-3 tumour-bearing SCID mice 24 h after tail vein injection of [^{64}Cu]Cu-NO2A-(X)-BBN(7–14)NH_2. Left to right: X = AMBA, 6-Ahx, 8-Aoc and 9-Anc (reproduced from Ref. [64] with permission).

example, [^{64}Cu]Cu-NODAGA-(6-Ahx)-BBN(7–14)NH_2 was a markedly improved radiopharmaceutical in preclinical investigations compared with the corresponding NOTA derivatives, [^{64}Cu]Cu-NO2A-(X)-BBN(7–14)NH_2 conjugates (Fig. 14). The NODAGA derivative coupled with the pharmacokinetic modifier 6-Ahx produced superior microPET images, with minimal accumulation in collateral tissue. The [^{64}Cu]Cu-NODAGA-(6-Ahx)-BBN(7–14)NH_2 conjugate also showed clear tumour contrast from surrounding tissues, with minimal uptake and retention in the hepatic or renal tissue (Fig. 15) [65].

The ability of GRPR agonists to be rapidly internalized, coupled with a high incidence of GRPR expression on various neoplasias, has been a driving force for the design and development of new diagnostic and therapeutic agents targeting GRP receptor positive tumours [66]. However, much like the case of molecular targeting of SSTR positive tumours, the use of BBN antagonists has begun the latest trend in GRPR targeting with BBN. In fact, Reubi and others suggest that GRPR antagonists might be the future of BBN radiopharmaceuticals [82]. Nanda and co-workers have developed [^{64}Cu]Cu-(NO2A-X-D-Phe^6-BBN(6–13)NHEt) antagonist radiotracers for potential PET imaging of GRPR expressing tumours [101]. In these studies, competitive displacement binding assays displayed nanomolar binding affinities towards human GRPR for all the newly

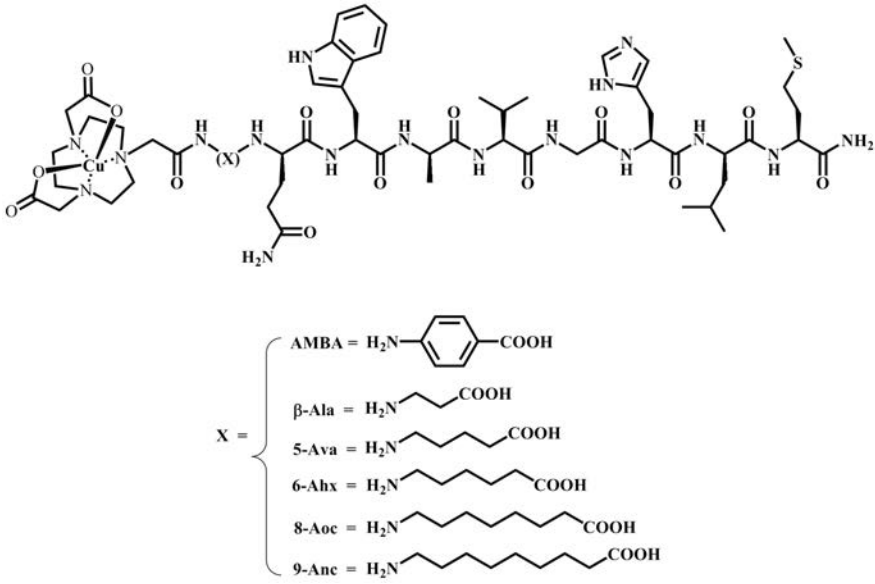

FIG. 14. Structural representation of [^{64}Cu]Cu-NO2A-(X)-BBN(7–14)NH_2 radiopharmaceutical (reproduced from Ref. [64] with permission).

FIG. 15. Maximum intensity microPET tumour and microCT skeletal fusion coronal images of PC-3 tumour-bearing SCID mouse 24 h after tail vein injection of [^{64}Cu]Cu-NODAGA-(6-Ahx)-BBN(7–14)NH$_2$] (reproduced from Ref. [65] with permission).

formed peptide analogues (4–6 nM). Biodistribution studies showed very high uptake and retention of tumour associated radioactivity in PC-3 tumour-bearing rodent models (6–9% ID/g). The radiolabelled conjugates also exhibited rapid urinary excretion and very high tumour to background ratios. MicroPET imaging investigations showed clear visualization of tumours in female PC-3 tumour-bearing mice at 15 h p.i. [65].

Recent studies have shown significant improvement of antagonist based [^{64}Cu]Cu tracers for effective GRPR targeting and molecular imaging. For example, Gourni and co-workers have directly compared [^{64}Cu]Cu radiolabelled NOTA and NODAGA conjugates of the GRPR antagonist MJ9 (Pip-D-Phe-Gln-Trp-Ala-Val-Gly-His-Sta-Leu-NH$_2$) [67]. Biodistribution studies showed very high uptake and retention of tumour associated radioactivity in PC-3 tumour-bearing rodent models (~20% ID/g). The radiolabelled conjugates also exhibited rapid urinary excretion and very high tumour to background ratios. MicroPET imaging investigations showed clear visualization of tumours in PC-3 tumour-bearing mice at 1 h p.i. [67]. Some receptor mediated pancreatic accumulation was observed at the 1 h time point. However, by 4 h p.i., radiotracer activity in the pancreas was essentially eliminated. From these studies, it appeared that the NOTA conjugate was superior to the corresponding NODAGA agent, especially at later time points [67].

Guillou and co-workers have recently reported the development of a novel chelating ligand for Cu^{2+} based on a 1,4,7-triazacyclononane backbone that has been functionalized with two to three methyl thiazolyl pendant arms [104]. In these investigations, they conjugated new copper complexing agents to Ahx-[D-Phe^{6},Statine^{13}]bombesin(6–14) (backbone based on RM2 BBN antagonist) and evaluated the binding affinity of the new complexes for GRPR in human prostate PC-3 cells. The new complexing agents, defined as Hno2th1tha and no2thEtBzNCS, were conjugated to the free peptide using standard techniques and prepared in very high yield. The inhibitory concentration IC_{50} values for the copper complexes of [no2th1th1tha-Ahx-RM2] and [no2thEtBzNCS-Ahx-RM2] were 3.0 ± 0.4 and 46.5 ± 0.3 nM, respectively. Free RM2 antagonist showed an IC_{50} value of 12.5 ± 0.2 nM. The authors concluded that detailed radiochemical investigations with [^{64}Cu]Cu radiometal are warranted for further development of novel PET agents based on their new copper complexing agents [104].

Gourni and co-workers have also reported the design and development of [^{64}Cu]Cu radiolabelled SAR based (Me-COSar) conjugates of the GRPR antagonist D-Phe-Gln-Trp-Ala-Val-Gly-His-Sta-Leu-NH_2 [105]. In these studies, they directly compared PEG4 and PEG2 pharmacokinetic modifiers/linkers in the GRPR expressing PC-3 human PCa cell line. For the PEG4 modifier, tumour uptake at the 1 h time point was 19.6 ± 4.7% ID/g. MicroPET imaging investigations at 1, 4 and 24 h p.i. showed clear visualization of tumours in PC-3 tumour-bearing mice [105]. Some receptor mediated pancreatic accumulation was observed at the 1 h time point. However, as with the NOTA and NODAGA tracers described by the same research group, radiotracer activity in the pancreas was essentially eliminated at 4 h p.i. [105]. The authors concluded that the novel SAR based tracers are well suited for translation into the clinic.

4.3.3. Melanocortin receptor targeting peptides

The α-melanocyte stimulating hormone (α-MSH) is a tridecapeptide of the general structure Ac-S^{1}YSMEHFRWGKPV^{13}-NH_2 that regulates skin pigmentation in most vertebrates [106, 107]. The biological activity of α-MSH in vivo is mediated by virtue of interactions with the G protein coupled melanocortin 1 receptor (MC1R), one of five known subtypes of melanocortin receptor. α-MSH receptors have been identified to be present on melanoma cell lines and on human melanoma tissue samples, catalysing efforts to identify radiolabelled α-MSH peptide analogues for targeted imaging and therapy of melanocortin receptor expressing tumours [108–112].

Studies on the specific targeting of MC1R have been reported in Refs [106–108, 110, 111, 113–115]. Much of that work focused on the cyclic

regulatory peptide CCMSH, (Cys^{3,4,10},D-Phe^{7},Arg^{11}) α-MSH$_{3–13}$. The presence of a non-radioactive rhenium metal centre coordinated to sulphydryl functional groups on the cysteine residues affords cyclization of the peptide, making it highly resistant to chemical and proteolytic degradation without compromising the biological integrity of the molecule [108].

As an alternative to the CCMSH targeting vector, Guo and co-workers have reported lactam bridge-cyclized α-MSH peptide analogues for diagnostic molecular imaging of melanoma [116]. They described the development of [^{64}Cu]Cu-NOTA-GGNle-CycMSH$_{hex}$ and [^{64}Cu]Cu-DOTA-GGNle-CycMSH$_{hex}$ (Fig. 16). The binding affinities in B16/F1 melanoma cells for the NOTA and DOTA conjugates were 1.6 and 2.1 nM, respectively. Each of the new PET tracers were evaluated in B16/F1 melanoma-bearing C57 mice (Fig. 17). Replacing the DOTA complexing agent with NOTA dramatically reduced uptake in the liver (11.6% ID/g to 1.1% ID/g) and increased tumour accumulation to ~12% ID/g (DOTA = 5.6% ID/g). High quality, high contrast microPET images were obtained

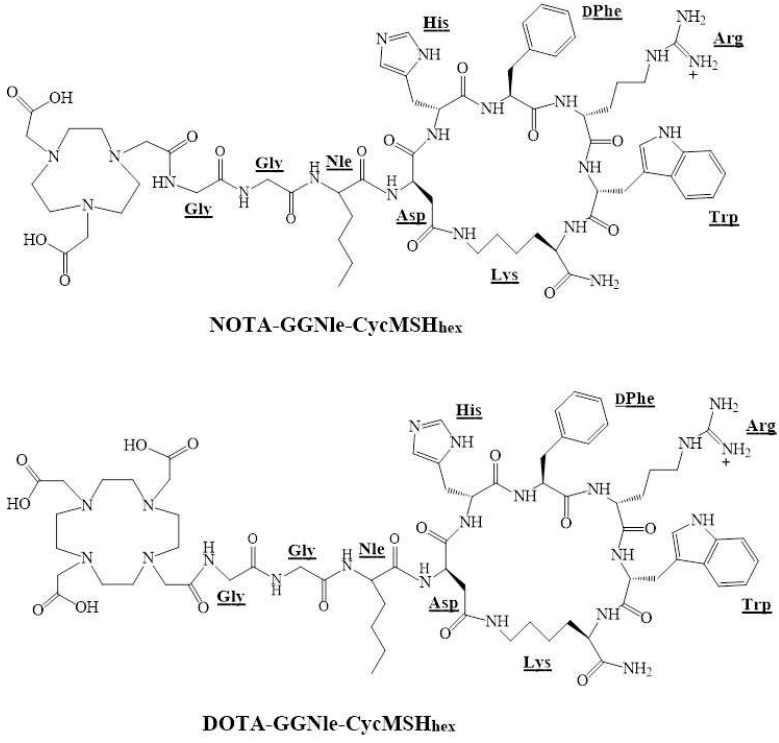

FIG. 16. Structural representation of NOTA-GGNle-CycMSH$_{hex}$ and DOTA-GGNle-CycMSH$_{hex}$ targeting agents for radiolabelling with ^{64}Cu (reproduced from Ref. [116] with permission).

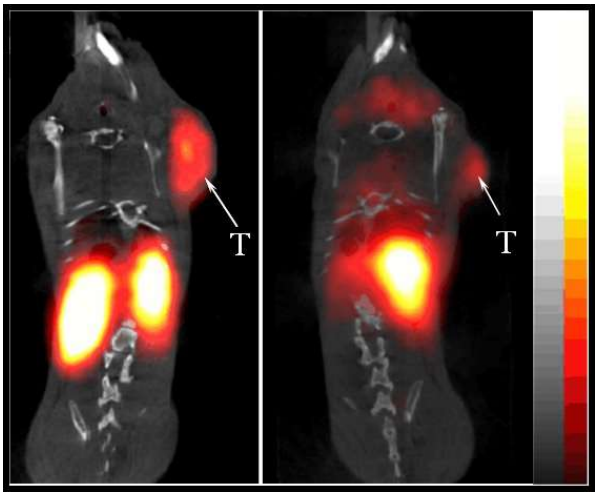

FIG. 17. Whole body microPET imaging investigations in mice using [^{64}Cu]Cu-NOTA-GGNle-CycMSH$_{hex}$ (left) and [^{64}Cu]Cu-DOTA-GGNle-CycMSH$_{hex}$ (right) radiopharmaceuticals (reproduced from Ref. [116] with permission).

in tumour-bearing C57 mouse models for [^{64}Cu]Cu-NOTA-GGNle-CycMSH$_{hex}$. The authors concluded that the new PET tracer was an ideal candidate for melanoma imaging and potential radiotherapy [116].

4.3.4. Integrin receptor targeting peptides

Angiogenesis is the physiological process for the growth of new blood vessels and is a regulatory mechanism for the transition of tumour tissue from a dormant to a malignant or metastatic state [117–121]. Integrins are cell surface transmembrane glycoproteins existing as αβ heterodimers. $\alpha_v\beta_3$ and $\alpha_v\beta_5$ integrin subtypes are expressed on the endothelial cells of tumour neovasculature during angiogenesis and form the basis of investigations for molecular imaging and therapy of angiogenesis and tumour formation in vivo. The $\alpha_v\beta_3$ integrin is known to be expressed in very high numbers in many tumour cell types, including lung carcinomas, osteosarcomas, breast cancer and glioblastomas [81]. Radiolabelled peptides containing the amino acid sequence Arg–Gly–Asp (RGD) are non-regulatory peptides that have been used extensively to target $\alpha_v\beta_3$ receptors upregulated on tumour cells and neovasculature, therefore providing a molecular vehicle for early detection of rapidly growing tumours and metastatic disease [109, 118, 122, 123].

Cyclic RGD containing peptide analogues are not considered to be members of the regulatory peptide family. Nonetheless, radiolabelled dimeric or tetrameric cyclic RGD peptides have shown significant improvements to the $\alpha_v\beta_3$ integrin binding domain compared with radiolabelled monomeric RGD targeting vectors, and their use does bear some discussion. For example, the [^{68}Ga]Ga-NOTA conjugated dimer, E[c(RGDyK)]$_2$, and tetramer, E{E[c(RGDyK)]$_2$}$_2$, have been shown to have improved tumour uptake in U87MG glioblastoma xenografts compared with the ^{68}Ga NOTA labelled monomer, c(RGDyK) [121, 124–127].

These studies were corroborated by the work of Chen et al. ^{64}Cu-DOTA-c(RGDyK) monomer showed only minor accumulation in $\alpha_v\beta_3$-expressing U87MG human glioblastoma tumours in mice at 4 h p.i. (1.44% ID/g) [128]. Usage of dimeric RGD derivatives increased tumour uptake and retention, and improved overall molecular imaging investigations [129]. Both tracers suffered from high retention in the liver and kidneys and precluded further preclinical/clinical investigations. PEGylation of the monomer did improve liver and kidney accumulation/retention [130].

Sprague and co-workers evaluated CB-TE2A [^{64}Cu]Cu complexing agent coupled to the c(RGDyK) monomer (Fig. 18), showing uptake of tracer in osteoclasts and opening the possibility of targeting the $\alpha_v\beta_3$ integrin on diseases such as osteoarthritis, osteoporosis or metastatic bone cancer for molecular imaging and potential therapy [131]. Wei and co-workers evaluated CB-TE2A-RGD peptides labelled with ^{64}Cu. They showed improved targeting of $\alpha_v\beta_3$ using the [^{64}Cu]Cu-CB-TE2A-c(RGDyK) monomer over the corresponding [^{64}Cu]Cu-diamsar-c(RGDyK) in mice bearing M21 and M21L human melanoma tumour xenografts [132]. Cai et al. have also evaluated the SAR complexing agent conjugated to c(RGDyK) for ^{64}Cu radiolabelling investigations [133]. They evaluated [^{64}Cu]Cu-AmBaSar-c(RGDyK) and [^{64}Cu]-DOTA-c(RGDyK) directly in nude mice bearing U87MG xenografted tumours. Each of the two conjugates exhibited uptake in tumour (~2% ID/g) at 1 h p.i. However, as expected, significant uptake (3.7%) of tracer in the liver was exhibited by the [^{64}Cu]Cu-DOTA-c(RGDyK) monomer [133]. Finally, Jiang and co-workers evaluated a cross-bridged complexing agent containing a pendant methyl phosphonic acid arm (TE1A1P) for [^{64}Cu]Cu radiometal when conjugated to LLP2A for targeting $\alpha_4\beta_1$ integrin (very late antigen 4, VLA-4) [134]. A direct comparison of [^{64}Cu]Cu-TE1A1P-LLP2A and [^{64}Cu]Cu-CB-TE2A-LLP2A conjugates in mice bearing B16F10 melanoma tumours showed high accumulation of [^{64}Cu]Cu-TE1A1P-LLP2A (11.4% ID/g at 2 h p.i.). [^{64}Cu]Cu-CB-TE2A-LLP2A, on the other hand, showed accumulation of less than 5% ID/g at the same time point. In addition, the usage of TE1A1P chelator for [^{64}Cu]Cu radiolabelling showed an improved strategy for labelling under mild conditions compared with CB-TE2A constructs [134]. MicroPET imaging in

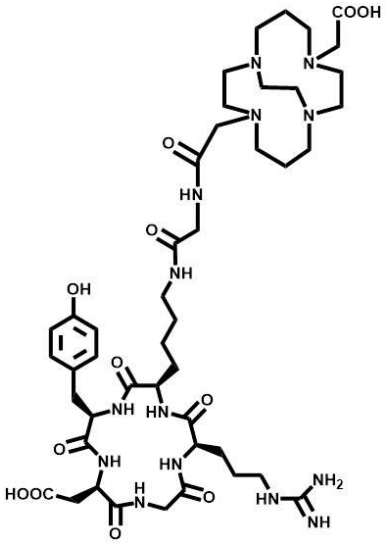

FIG. 18. Structural representation of [^{64}Cu]Cu-CB-TE2A-c(RGDyK) radiopharmaceutical (courtesy of J. Smith, University of Missouri).

B16F10 tumour-bearing mice showed very high quality, high contrast images for [^{64}Cu]Cu-TE1A1P-LLP2A compared with [^{64}Cu]Cu-CB-TE2A-LLP2A [134].

In closing, it appears that the usage of multimeric, integrin targeting agents improves tumour uptake and retention of tracer. However, this is often at the cost of higher kidney and liver accumulation/retention and might limit consideration of tracers of this type for use in clinical investigations. Furthermore, the choice of chelating ligand for the [^{64}Cu]Cu radionuclide is very important in developing new tracers for targeting cell surface integrins that might be expressed in human diseases.

4.3.5. Multivalent receptor targeting peptides

The clinical utility of monomeric radiolabelled peptides can be limited by several factors, including receptor density, binding affinity and pharmacokinetics. For example, high quality, high tumour to background PET or SPECT images require a high degree of receptor expression on tumour cells compared with normal, collateral tissue. Furthermore, the number of effective receptors may differ significantly during tumour development, resulting in significantly reduced uptake and retention of targeting vector, limiting the quality of the diagnostic image. Finally, the binding affinity of monomeric peptides can be relatively low

compared with multimeric targeting vectors [109, 135, 136]. The advantages of using a bivalent multitarget approach are as follows:

— Usage of a single agent for targeting biomarkers that are differentially expressed during tumour development could result in an enhancement of accumulation and retention of targeting vector.
— Agents targeting multiple biomarkers can potentially increase the sensitivity of detection through improvement in binding affinity [137].
— Improved targeting specificity and diagnostic utility of multivalent probes.
— The potential of advance in the therapeutic utility of multivalent probes [138].

Much of the research on multimeric regulatory peptide probes performed by Liu and co-workers has focused on RGD/BBN multimeric peptide conjugates for integrin/GRPR dual receptor imaging, since many GRPR positive tumours are also $\alpha_v\beta_3$ integrin positive [124, 137, 139–141]. The group's work focused on PC-3 tumour uptake in nude mice with ^{68}Ga or ^{64}Cu [NOTA-RGD-BBN(7–14)NH_2] (NOTA = *p*-NCS-Bz-NOTA), where the RGD and BBN targeting motifs are linked by a glutamic acid. Their studies showed that [^{68}Ga]Ga-NOTA-RGD-BBN(7–14)NH_2 and [^{68}Ga]-NOTA-BBN(7–14)NH_2 have comparable uptake at all time points in xenografted PC-3 tumours. The [^{68}Ga]Ga-NOTA-RGD monomer, on the other hand, showed much lower accumulation. At 2 h p.i., PC-3 tumour uptake was shown to be approximately 4.0, 3.2 and 0.80% ID/g for [^{68}Ga]Ga-NOTA-RGD-BBN(7–14)NH_2, [^{68}Ga]Ga-NOTA-BBN(7–14)NH_2 and [^{68}Ga]Ga-NOTA-RGD, respectively. Clearance of the peptide heterodimer was primarily via the renal/urinary excretion pathway (about 5.0% ID/g, 2 h p.i.). Furthermore, uptake and retention of the conjugate in hepatic tissue for [^{68}Ga]Ga-NOTA-RGD-BBN(7–14)NH_2 was significantly improved compared with [^{68}Ga]Ga-NOTA-BBN(7–14)NH_2 [137]. Some degree of improvement in retention was seen by radiolabelling these conjugates with [^{64}Cu]Cu radionuclide. For example, at 20 h p.i., PC-3 tumour retention was 2.04 ± 0.35, 0.44 ± 0.39 and 0.55 ± 0.32% ID/g for [^{64}Cu]Cu-NOTA-RGD-BBN(7–14)NH_2, [^{64}Cu]Cu-NOTA-BBN(7–14)NH_2 and [^{64}Cu]Cu-NOTA-RGD, respectively. Once again, clearance of the peptide [^{64}Cu]Cu heterodimer was primarily through the kidneys (1.87 ± 0.41% ID/g, 20 h p.i.). This new conjugate also exhibited lower liver retention (0.98 ± 0.40% ID/g, 20 h p.i.) than BBN (4.20 ± 0.53% ID/g, 20 h p.i.) and RGD (1.67 ± 0.69% ID/g, 20 h p.i.) monomeric conjugates. All tracers cleared quickly from the blood, with less than 0.75% ID/g remaining at 30 min p.i. [139].

Jackson and co-workers designed a heterodimeric RGD/BBN agonist peptide ligand for dual receptor targeting of the form [^{64}Cu]Cu-NO2A-RGD-Glu-6-Ahx-BBN(7–14)NH_2 [142]. The results showed that competitive

displacement binding assays were in the single digit nanomolar range, showing very high binding affinities towards GRPR for the new heterodimeric peptide analogues. In vivo biodistribution studies showed high uptake and retention of tumour associated radioactivity in PC-3 tumour-bearing rodent models with little accumulation and retention in non-target tissues. The radiolabelled conjugate also exhibited rapid urinary excretion and high tumour to background ratios. MicroPET molecular imaging investigations produced high quality, high contrast images in PC-3 tumour-bearing mice at 15 h p.i. [142].

Durkan and co-workers evaluated an RGD/BBN multimeric probe that was of antagonist nature [109]. The dual $\alpha_v\beta_3$/GRPR targeting agent of the form RGD-Glu-[^{64}Cu]Cu-NO2A]-6-Ahx-RM2 (Fig. 19) was produced in high radiochemical yield (≥95%). The in vivo behaviour of the radiolabelled peptide conjugate was investigated in normal CF-1 mice and in a PC-3 human PCa experimental model. A competitive displacement receptor binding assay in human prostate PC-3 cells using ^{125}I-[Tyr^4]BBN as the radioligand showed high binding affinity of RGD-Glu-[^{nat}Cu]Cu-NO2A]-6-Ahx-RM2 conjugate for the GRPR (3.09 ± 0.34 nM). A similar assay in human glioblastoma U87-MG cells using [^{125}I] I-echistatin as the radioligand indicated a moderate receptor binding affinity for the $\alpha v\beta_3$ integrin (518 ± 37.5 nM). In vivo studies of RGD-Glu-[^{64}Cu]Cu-NO2A]-6-Ahx-RM2 showed high accumulation (4.86 ± 1.01% ID/g, 1 h p.i.) and prolonged retention (4.26 ± 1.23% ID/g, 24 h p.i.) of tracer in PC-3 tumour-bearing mice. MicroPET molecular imaging studies produced high quality, high contrast images in PC-3 tumour-bearing mice at 4 h p.i. (Fig. 20) [109].

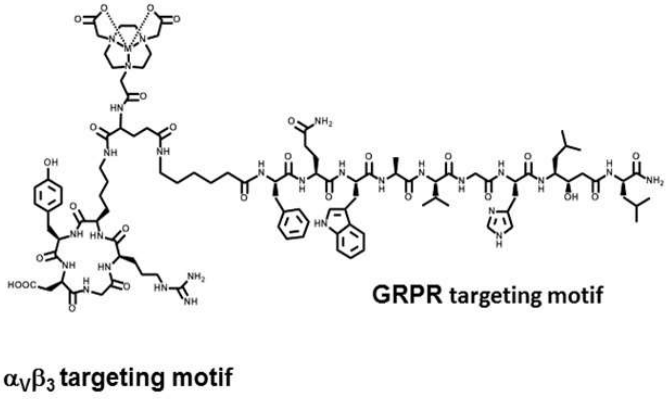

FIG. 19. Structural representation of RGD-Glu-[[64Cu]Cu-NO2A]-6-Ahx-RM2 radiopharmaceutical (reproduced from Ref. [109] with permission).

FIG. 20. Maximum intensity microPET tumour and microCT skeletal fusion coronal whole body image of a PC-3 tumour-bearing SCID mouse at 4 h after tail vein injection of RGD-Glu-[[^{64}Cu]Cu-NO2A]-6-Ahx-RM2 (reproduced from Ref. [109] with permission).

4.3.6. Prostate specific membrane antigen

Prostate specific membrane antigen (PSMA), also known as folate hydrolase I or glutamate carboxypeptidase II, is a 750 amino acid integral membrane protein that is present in the neovasculature of most solid tumours, including renal carcinoma, colorectal carcinoma, glioblastoma multiforme, pancreatic duct carcinoma and breast carcinoma, and yet is absent in normal vascular endothelium of non-cancer-bearing tissues [143, 144]. PSMA is expressed in prostate tumour epithelium, yet not in the vasculature of PCa itself [145–147]. However, while PSMA is largely limited to the epithelium of PCa cells, upregulation and translocation from internal organelles to the cell surface generally occurs as androgen independent, metastatic disease progresses [145–147]. This is a particularly important issue as nearly all PCas progress to the androgen independent, metastatic stage [145–147]. For example, homogeneous receptor expression has been found in metastatic lesions localized in the lymphatic tissue, bone and lungs [144]. PSMA is highly expressed on the majority of all prostate cancers and is expressed in very low numbers or not at all on surrounding collateral tissues. For example, the density per cancer cell is ~10^6 [146], ~1000 times higher than normal PSMA expressing tissues such as the kidney, brain or small intestine [148]. PSMA undergoes internalization via clathrin coated pits and has a tendency to be recycled on the surface of PCa cells

for additional internalization events [149, 150]. The ability of PSMA to be rapidly internalized coupled with a high incidence of expression on various neoplasias, including prostate cancer, has recently led to the design and development of new diagnostic and therapeutic agents targeting PSMA as a clinical biomarker for early detection, staging and potential treatment of human disease.

GRPR and PSMA are two identifying biomarkers expressed in very high numbers on PCa cells and could serve as a useful tool for molecular targeting and diagnosis of disease via PET. Bandari and co-workers produced the multipurpose, bivalent DUPA-6-Ahx-([^{64}Cu]Cu-NODAGA)-5-Ava-BBN(7–14)NH_2 radioligand (Fig. 21) [135] for PCa imaging, where DUPA 2-[3-(1,3-bis-tert-butoxycarbonylpropyl)-ureido]pentanedioic acid, a small-molecule, PSMA-targeting probe, 6Ahx 6-aminohexanoic acid, 5-Ava 5-aminovaleric acid, NODAGA [2-(4,7-biscarboxymethyl)-1,4,7-(triazonan-1-yl) pentanedioic acid] (a derivative of NOTA) and BBN(7–14)NH_2 bombesin or BBN, a GRPR specific peptide targeting probe. The PSMA/GRPR dual targeting ligand precursor DUPA-6-Ahx-K-5-Ava-BBN(7–14)NH_2 was synthesized by solid phase and manual peptide synthesis, after which NODAGA was added via manual conjugation to the γ-amine of lysine (K).

The new bivalent GRPR/PSMA targeting vector was purified by reversed phase high performance liquid chromatography, characterized by electrospray ionization mass spectrometry and metallated with $^{64}CuCl_2$ and [^{nat}Cu]$CuCl_2$. The receptor binding affinity was evaluated in human prostate PC-3 (GRPR positive) and lymph node carcinoma of the prostate (LNCaP) (PSMA positive) cells, and the tumour targeting efficacy was determined in

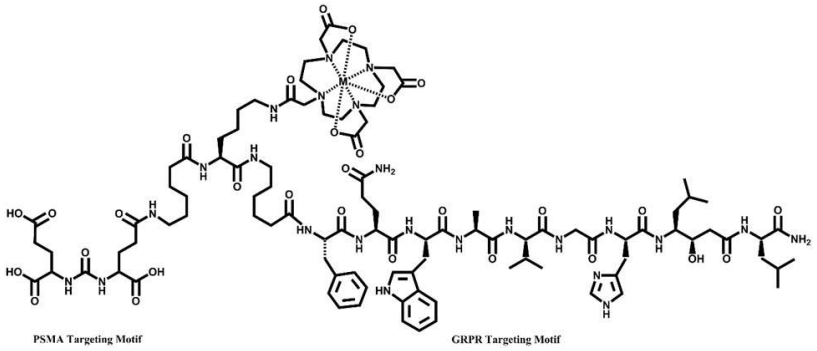

FIG. 21. Structure of DUPA-6-Ahx-([64Cu]Cu-NODAGA)-5-Ava-BBN(7–14)NH_2 radiopharmaceutical (reproduced from Ref. [135] with permission).

SCID and athymic nude mice bearing PC-3 and LNCaP tumours. Whole body maximum intensity microPET–CT images of PC-3/LNCaP tumour-bearing mice were obtained at 18 h p.i. Competitive binding assays in PC-3 and LNCaP cells indicated high receptor binding affinity for the DUPA-6-Ahx-([^{nat}Cu]Cu-NODAGA)-5-Ava-BBN(7–14)NH_2 conjugate. MicroPET scintigraphy in PC-3/LNCaP tumour-bearing mice indicated that xenografted tumours were visible at 18 h p.i., with high collateral background radiation also being observed in non-target tissue. Nonetheless, DUPA-6-Ahx-([^{64}Cu]Cu-NODAGA)-5-Ava-BBN(7–14)NH_2 targeting vector, as described herein, was the first example of a dual GRPR-/PSMA targeting radioligand for molecular imaging of prostate tumours, and pioneering efforts are currently under way to optimize the uptake and retention of tracer in GRPR and PSMA positive tissues [135].

Finally, Ma and co-workers reported on the usage of a SAR based complexing agent used to effectively link two Lys-3-BBN constructs to form a multivalent BBN peptide. Radiolabelling investigations with ^{64}Cu showed very high radiolabelling yields. However, the effectiveness of GRPR targeting has yet to be evaluated [151].

In brief, the development of new ^{64}Cu targeting vectors based on regulatory peptide targeting vectors has resulted in conjugates with biodistribution profiles that are ideal for microPET imaging. MicroPET molecular imaging of xenografted tumour models has revealed focal sites of radioactivity uptake and retention with relatively high resolution and low background contrast. In some cases, necrotic regions of the tumours were able to be discriminated in the microPET images, demonstrating the usability of this radionuclide to image even very fine structure in vivo. The clinical successes of Octreoscan® have paved the way for exploring and radiolabelling other biologically active peptides. Studies have indicated improved imaging characteristics when SSTR targeting peptides are labelled with ^{64}Cu compared with ^{68}Ga or ^{111}In labelled analogues. For example, [^{64}Cu]Cu-DOTATATE has been proved to be far superior to [^{111}In]In-DTPA-OC in patients bearing NETs [100]. These studies have led to the development of [^{64}Cu]Cu-DOTATATE for routine clinical use for diagnosis of NETs [100]. Other cancer types that express regulatory peptide receptors in very high numbers include neuropeptide-Y receptors in breast tumours, glioblastomas and sarcomas; glucagon-like peptide-1 receptors in insulinomas; cholecystokinin-2 receptors in medullary thyroid cancers; and neurotensin receptors in pancreatic cancers. Continued design and development of multimeric or multivalent peptides capable of targeting multiple receptor subtypes highly expressed in human cancers could do much to improve image resolution and contrast.

5. COPPER-64 LABELLED ANTIBODIES

5.1. INTRODUCTION

The overwhelming success of antibody based therapies for various autoimmune, neurological and infectious disorders continues to drive the demand for these agents. The exceptional ability of antibodies to accurately target specific receptors, while avoiding toxicity due to non-specific tissue binding, is one of the key attributes that makes these agents so attractive from a clinical standpoint. Additionally, advancements in antibody engineering over the past several decades have made this class of pharmaceuticals a much more accessible treatment modality with a potentially unlimited number of clinical applications. In the oncology setting, immunotherapy — or the ability to make one's own immune system recognize and fight cancer — is often referred to as the 'fourth pillar' of treating cancer, in addition to surgery, radiation therapy and chemotherapy. This special recognition is based on the unparalleled success of antibody based therapies for diseases that had no effective treatments previously.

As a result of these successes, there is significant interest in developing new antibody based therapies. However, the drug development process is a very costly and resource consuming process. Therefore, there is a dire need for tools that enable the critical determination of potential efficacy in early clinical development. ImmunoPET, or imaging with antibody based PET agents, serves as an unparalleled tool that can be used to make these decisions. In vivo real time imaging with a radiolabelled analogue allows for the elucidation of antibody pharmacodynamics, pharmacokinetics and distribution, appropriate patient selection and patient response monitoring. All these factors are critical contributors to a successful clinical evaluation for an agent of interest.

Another emerging application of radiolabelled antibodies in clinics is in the field of theranostics and personalized medicine. In this setting, patient specific information, obtained from imaging by using diagnostic radiolabelled antibodies or antibody fragments, can be used to further guide the course of therapy. The subsequent therapy may be in the form of a different treatment modality or a targeted radiotherapeutic antibody. In the latter setting, the antibody's primary function is to deliver the radionuclide payload to the tumour site so that radiation can kill the tumour cells.

A unique characteristic of antibody based tumour localization in vivo is the relatively long duration of the time required for the antibody to accumulate at the tumour site, subsequently allowing the unbound circulating antibody to clear from blood. While this accumulation time for small molecules is usually minutes, for larger molecules it ranges from hours to days. Therefore, radionuclides used

to radiolabel macromolecules have to possess sufficiently long radioactive half-lives that correspond to the vector molecule behaviour in vivo as closely as possible. Because of its longer half-life, ^{64}Cu is one of a handful of radionuclides that are currently used as radiolabelling biological molecules for PET imaging in the clinic.

The goal of this section is to provide an overview of the methodology that could be applied for preclinical and clinical preparation of ^{64}Cu radiolabelled antibodies, which will ideally facilitate the clinical use of these agents globally.

5.2. ANTIBODY CONJUGATIONS AND QUALITY CONTROL

The general process of radiolabelling antibodies with ^{64}Cu is depicted in Fig. 22. Since copper does not sufficiently bind to any portion of the antibody molecule, antibodies generally need to be chemically modified with linkers that allow for sufficient radionuclide incorporation and retention without affecting the in vivo behaviour and targeting. These linkers are often referred to as 'chelators' or 'bifunctional chelating agents', and the material that has been modified with a linker is referred to as 'conjugated material'. Since the optimal chemical

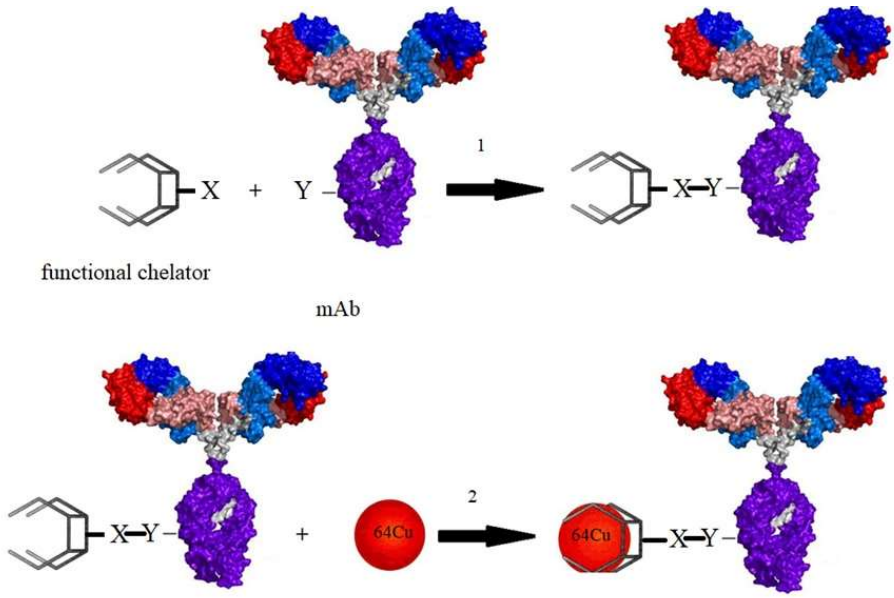

FIG. 22. An overview of the process of conjugation (1) and radiolabelling (2) of antibodies with ^{64}Cu.

conditions for attachment of the bifunctional chelating agent, such as pH or salts content, usually vary from the conditions of the formulation buffer in which the antibody is stored for the long term, the attachment of the chelator requires the protein to be subjected to the buffer exchange process. During this process, the buffer in which the antibody is suspended is changed to another buffer of choice, which allows for the optimal incorporation of the chelator. Once the initial buffer exchange is completed, the chelator is added to the protein in a predetermined quantity and is allowed to incubate under predetermined temperature and time conditions (see Annex III for details). Following incubation, a second buffer exchange has to be performed in order to remove the unincorporated chelator and to suspend the conjugated protein in buffer. That will allow for both long term storage and efficient radiolabelling. Several different techniques exist for the process of buffer exchange and purification during antibody conjugation.

For clinical preparations, size exclusion membranes, either in the form of centrifuge cartridges or single use tangential flow filtration columns, are commonly used. These membranes allow smaller molecular weight species such as buffers, salts and unreacted chelator to be separated from the large antibody molecules that cannot cross the membrane. An image of the tangential flow filtration set-up and an illustration of the principle of filtration are depicted in Fig. 23. Some of the advantages of tangential flow filtration columns over centrifuge cartridges include a less labour intensive process for the operator, better control over the possible stress conditions to which the protein may be subjected during the buffer exchange process and the ability to conjugate antibodies on a larger scale. The disadvantage, however, is an increased cost for both the columns and the peristaltic pump that is used. The final steps of

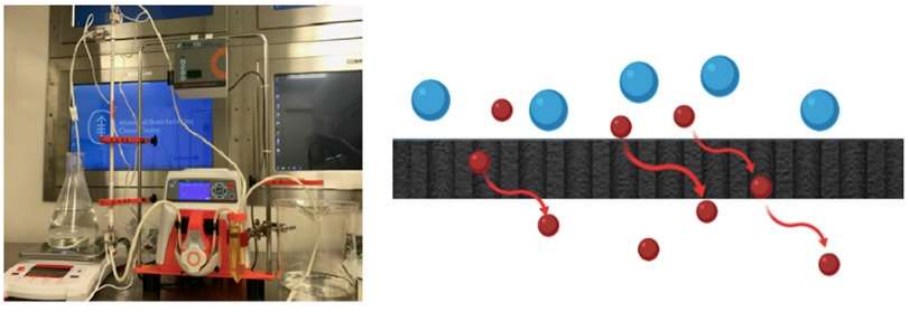

FIG. 23. Tangential flow filtration set-up (left) and illustration of the principle of filtration (right). Red spheres: low molecular weight species; blue spheres: high molecular weight species (here monoclonal antibodies) (courtesy of S.K. Lyashchenko, Memorial Sloan Kettering Cancer Center).

the process involve filtering the obtained bulk material through a 0.22 μm sterilizing grade filter and aseptic aliquoting into smaller containers for long term storage and subsequent radiolabelling.

The process of chemical attachment of the chelator to the antibody subjects the antibody protein to additional stress, which may affect its integrity and affinity, and results in some degree of protein loss. Additionally, not all the chelator that is normally added to the reaction mixture is incorporated into the protein. Therefore, at least the following key characterization parameters need to be evaluated following antibody conjugation: antibody integrity, protein concentration and chelate ratio (i.e. the average number of moles of chelator present in the conjugated material per one mole of antibody). Additional analyses, such as endotoxin content determination, pH determination, sterility testing, potency testing and particulates testing, may be required in situations where conjugated antibodies may need to be administered directly into patients without subsequent modification.

One of the common ways to evaluate protein integrity following conjugation is performing size exclusion high performance liquid chromatography (SEC-HPLC) using an HPLC system equipped with a protein size exclusion column and an ultraviolet (UV) detector. This assay allows for determination of intact protein, as well as both the formation of any aggregated protein or high molecular weight species and the fragmentation and formation of low molecular weight species. According to the principle of size exclusion, any aggregated species produces UV chromatogram peaks with a retention time shorter than the monomer peak retention time, while antibody fragments and low molecular weight species produce peaks with retention times longer than that produced by the monomer.

Protein concentration is normally determined by UV spectrophotometry, using a protein specific absorbance coefficient (also known as extinction coefficient) to convert the absorbance reading to the mass. Generally, the antibody extinction coefficient can be obtained from the mAb manufacturer.

The chelate ratio is an important parameter, since too little chelate may not be adequate for sufficient radionuclide incorporation (i.e. achieving sufficient specific activity), while too much chelator may change the biodistribution and affinity of the compound in vivo. As described below, several different methodologies are commonly used for chelate ratio determination. At this time, however, there is not a single modality that has emerged as the gold standard method for determining the number of moles of chelate per mole of antibody. The most common method used for the determination of the number of chelates is the isotopic dilution method. In this method, the radionuclide solution is intentionally spiked with known increasing molar quantities of the non-radioactive isotope of interest. The molar quantity of the radionuclide in these spiked samples is negligible compared with the molar quantity of the non-radioactive nuclide. These spiked samples react with multiple

samples containing the same predetermined known mass of conjugated antibody. Samples with increased concentrations of the cold isotope yield a decreased degree of radionuclide incorporation. The degree of radionuclide incorporation is measured by TLC using TLC silica gel plates as the stationary phase and radiometal chelating solution as the mobile phase. The obtained incorporation results can then be plotted as a curve. The number of moles of chelate present per one mole of antibody can then be calculated by determining the molar quantity of non-radioactive isotope that results in a 50% decrease of incorporation, as well as doubling that value [152, 153]. This method has been widely used, especially in academic settings, since it is relatively quick, simple and inexpensive, and does not require any additional equipment. An alternative quick method of determining the number of moles of chelate for every mole of antibody is by UV spectrophotometry [154]. The method is based on the differences in UV absorption between the antibody and the chelator at various wavelengths. The method involves measuring a sample at two wavelengths at which the relationship between mass and absorbance of each analyte has been predetermined. The obtained values can then be plugged into a mathematical algorithm where the contributing effect of the chelator on the total UV absorbance at a wavelength normally used to determine the antibody mass (usually 280 nm) is subtracted. This allows for an accurate determination of the antibody amount.

Similarly, the antibody's UV absorbance, which has a contributing effect at a different wavelength, can be subsequently subtracted from the absorbance produced primarily by the chelator to allow for accurate determination of the chelate amount. The chelate ratio is calculated by dividing the obtained molar chelate quantity by the molar antibody quantity. The advantages of this method include simplicity, low cost and reliability. The disadvantage is the labour intensive initial set-up, where correlation between the analyte concentrations and UV spectrophotometer response at two wavelengths needs to be established. An alternative method for determining the chelate ratio is matrix assisted laser desorption ionization (MALDI) time of flight (TOF) analysis. This method relies on the difference in mass between the samples of the unmodified antibody and the chelated antibody. This difference in mass can then be divided by the molecular weight of the antibody in order to determine the molar quantity of the chelator. One practical disadvantage of this method is the additional cost of procuring and maintaining a MALDI-TOF system.

5.3. ANTIBODY RADIOLABELLING AND QUALITY CONTROL

The preparation of radiolabelled antibodies requires the implementation of unique processes designed to preserve antibody integrity and function. A mild radiolabelling environment is a unique requirement specific to radiolabelling

antibodies. Factors such as extreme pH, high reaction temperature and sheer physical stress may all negatively affect the protein. Therefore, the chelator that is normally chosen allows for radionuclide incorporation at physiological pH, as well as at ambient temperature. Following radionuclide incorporation, the drug substance may need to be purified in order to remove the unreacted radiometal and other unwanted small molecular weight impurities (see Annex III for details). The preferred method for purification of radiolabelled antibodies is via the use of desalting gel columns. The desalting columns work via a principle of size exclusion, where the large antibody molecules pass through the gel and are eluted quickly from the column, while small molecular weight species such as salts, including unincorporated radionuclide, are trapped on the gel. The additional benefit of desalting gel purification is that it allows for buffer exchange into a formulation of choice that results in optimal radiolabelled antibody stability. From a clinical use standpoint, the final radiolabelled antibody formulation will ideally be designed to allow for both adequate product stability and compatibility with the intended route of administration. To minimize autoradiolysis, radioprotectants such as gentisic acid, ascorbate or human serum albumin are commonly added to the final formulation and the radioactive concentration is kept to a minimum. In some situations, such as when relying on intrathecal administrations or administrations directly into the central nervous system, the choice of radioprotectants and the formulation volume may be limited. In such circumstances, conducting appropriately designed additional studies in relevant animal species may be required in order to determine whether the intended novel formulation may present an increased risk to patients. Another factor that may affect radiolabelled antibody stability is the storage temperature. Therefore, stability at various temperatures, including freezing, may need to be explored.

The quality control for radiolabelled antibodies is designed to elucidate the key indicators that demonstrate that the final drug product is sufficiently pure, potent and safe to administer to patients. Most of the analytical methods used for quality control testing of radiolabelled antibodies — including pH, appearance, endotoxin content, filter integrity testing, radionuclide purity and identity and sterility testing — are similar methods used for testing other types of radiopharmaceutical, such as radiolabelled peptides or small molecules. There are, however, additional unique characteristics specific to radiolabelled antibodies that need to be evaluated. These antibody specific, unique properties, including the large molecule size, ability to aggregate or fragment, possible loss of potency, deradiometallation and antibody loss during synthesis, may all negatively affect both the safety and efficacy of the drug. Each one of these properties is discussed in more detail below.

The presence of free radiometal may have a negative impact on the efficacy of the drug. Therefore, a determination of the quantity of unincorporated

radiometal may be required. This assay is often referred to as radiochemical purity assessment by instant TLC (iTLC), and a simple and rapid method is using a radio TLC scanner. For ^{64}Cu radiolabelled antibodies, a small product sample is spotted onto iTLC silica gel strips and developed in a metal chelator mobile phase. During development, the radiolabelled antibody remains trapped at the origin while the free radiometal migrates with the solvent front. Once the development step is completed, the strip is scanned in a radio TLC scanner, the area under the curve for the peaks present at the origin and the solvent front is integrated and the percentages of each analyte are calculated using the areas under the curve. Alternatively, in the absence of a scanner, one can use the count method with an appropriate activity meter.

The effect of the total antibody mass on the biodistribution of the systemically administered radiolabelled antibody is well known. The target administered mass will ideally be adequate for both saturating the non-specific binding and elimination mechanisms in vivo and for allowing the radiolabelled antibody to bind to the target receptors. Since some antibody loss occurs during synthesis and purification, the mass of the antibody in the final drug product may need to be determined. Methods based on UV absorbance, such as UV spectrophotometry and SEC-HPLC, may not be practical in some cases owing to radiation safety concerns or interference from the formulation's excipients with the UV signal. In such circumstances, the determination of antibody concentration in the final drug product can be performed via the radiometric method. During this procedure, the total radioactivity of the reaction mixture and the degree of radionuclide incorporation are measured in a dose calibrator and by a radio TLC scanner, respectively, prior to loading the reaction mixture onto the purification column. Multiplying the total activity by the incorporation factor provides a measure of the radiolabelled antibody activity fraction present in the reaction mixture. Once the synthesis of the final drug product is complete, the final drug product radioactivity can be divided by the calculated activity of the radiolabelled antibody fraction to determine the fraction of the radiolabelled antibody lost during purification. This fraction is then multiplied by the initial mass of the antibody that was added to the reaction mixture in order to calculate the final mass of the antibody present in the final drug product.

Another important characteristic unique to antibodies is their propensity for either aggregation or fragmentation when placed under stress. To ensure protein integrity and to determine the amount of the radiolabelled antibody monomer content, SEC-HPLC is commonly utilized. A schematic of the SEC-HPLC system set-up and the principle of separation by size exclusion HPLC column is depicted in Fig. 24. Samples are injected into an HPLC chromatographer equipped with a size exclusion column, a UV detector (usually set at 280 nm wavelength) and a radioactivity detector. The mobile phase and the analysis time

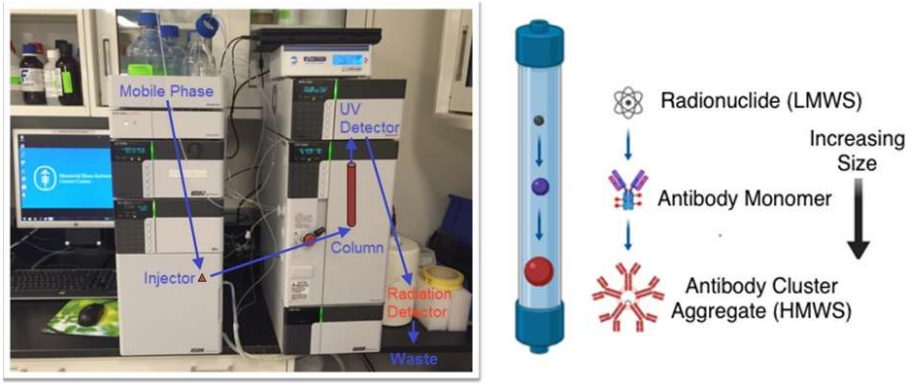

FIG. 24. The principle of size exclusion related to HPLC columns. LMWS: low molecular weight species; HMWS: high molecular weight species (courtesy of S.K. Lyashchenko, Memorial Sloan Kettering Cancer Center).

are normally recommended by the column manufacturer. During analysis, higher molecular weight species interact less with the column and are eluted first by producing a peak with retention time shorter than that of the monomer peak. Any low molecular weight species, if present, produces peaks with a retention time longer than the monomer peak retention time. The percentage of the monomer present in the final drug product can be calculated by dividing the integrated area under the curve for the monomer peak by the total integrated area under the curve for all peaks produced. A representative chromatogram of SEC-HPLC results, showing the radioactive trace (red) and UV trace (green), is depicted in Fig. 25.

One of the most critical characteristics of radiolabelled antibodies is their ability to adequately bind to the target antigen. Suboptimal binding in vivo may result in either decreased image quality in cases of diagnostic use or in increased toxicity in cases of radiotherapeutic application. Factors such as chemical modification by attachment of the chelator, followed by radionuclide incorporation, harsh radiolabelling conditions and autoradiolysis, may all contribute to a decrease in the antibody potency. As a result, an evaluation of the radioimmunoreactive fraction determination of the final drug product is warranted. This assay is also sometimes referred to as immunoreactivity testing. The general overview of the immunoreactive fraction determination process is depicted in Fig. 26 and has been well described in the literature [155]. The method involves the in vitro determination of the percentage of radiolabelled antibody that binds to the present excess antigen. During the process, a known amount of antibody is mixed with an excess known amount of antigen and

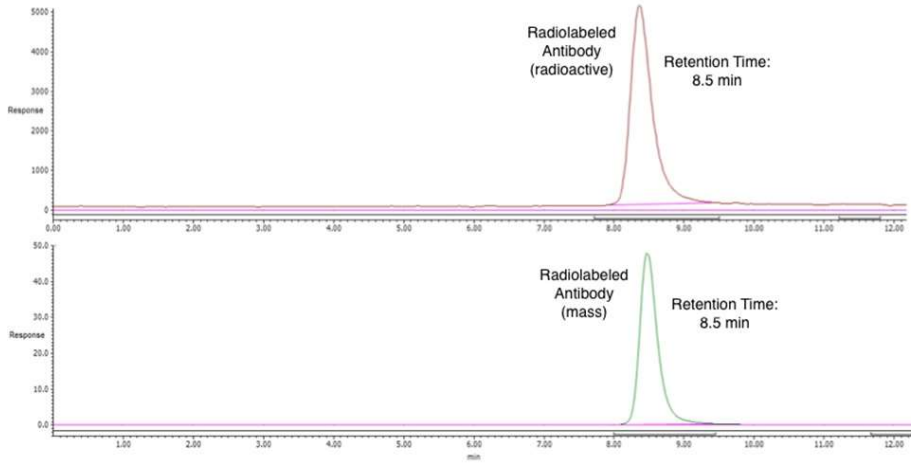

FIG. 25. A representative chromatogram of SEC-HPLC results, with the radioactive trace (red) and UV trace (green) (courtesy of S.K. Lyashchenko, Memorial Sloan Kettering Cancer Center).

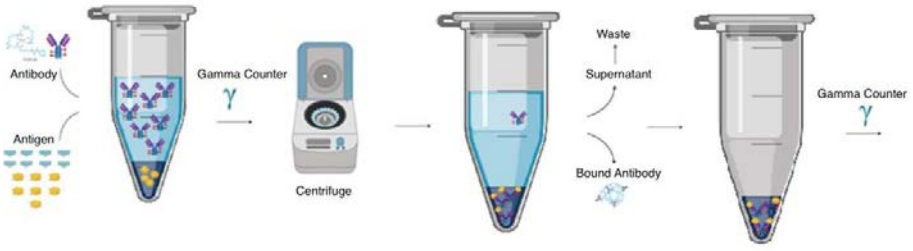

FIG. 26. Overview of radioimmunoreactive fraction determination analysis (courtesy of S.K. Lyashchenko, Memorial Sloan Kettering Cancer Center).

allowed to react. The radioactivity counts in several samples are measured during incubation, and then once again the antigen to which the antibody is binding is physically separated from the rest of the mixture. The separation is normally done via centrifugation, where the antigen settles at the bottom of the sample container while the unbound activity remains in the supernatant, which can be easily removed by pipetting the supernatant out. The radioactivity present on the isolated antigen is then divided by the initial activity in the sample in order to provide a percentage of activity bound to the antigen, which represents the percentage of the immunoreactive fraction. Historically, the method that has been commonly utilized relies on the use of live antigen expressing live cells. However, the limitations of the live antigen expressing cell assay includes a

complex cell growing process and suboptimal accuracy due to the varying and unknown degrees of antigen expression on the cells. These limitations prompted the development of more robust methods based on the presence of a known amount of recombinantly produced antigens.

The main method used currently involves coupling the antigen modified with a linker to magnetic bead particles via either hexahistidine tag or streptavidin binding motif. The antigen bound to the particles is then mixed with a known amount of antibody and allowed to incubate so that the antibody can bind to the antigen. Following incubation, the samples' total radioactivity is measured in a gamma counter, followed by wash–centrifugation cycles in order to separate the unbound activity in the supernatant from the radioactivity produced by the antibody bound to the antigen bead complex that settles at the bottom of the test sample containers. The radioimmunoreactive fraction is calculated by dividing the activity bound to the antigen bead complex against the initial activity in the sample. An alternative, and less labour intensive, method for determining the immunoreactive fraction relies on the SEC-HPLC peak retention time shift. In this process, the antibody is mixed with antigen that has been premodified with a UV absorbing moiety of sufficiently large size to allow for complete baseline separation between the antibody antigen complex and the unbound antibody. Once incubation has been completed, the sample analytes are separated by the size exclusion column, and the areas under the curve for both peaks are integrated. The area under the curve for the peak produced by the antibody antigen complex is then used to calculate the immunoreactive fraction by dividing it by the total area under the curve for all peaks. Both methods require the use of modified antigen, which may have limited availability. The relatively wider availability of hexahistidine tag and streptavidin modified antigens is one of the reasons that the magnetic bead assay is used more widely than the SEC-HPLC peak shift method.

This section has described the generic protocol for the quality control of radiolabelled antibodies for clinical use and its applicability to all-metal based mAbs, with an overview of the methods used in the steps. Further insight and practical information for researchers are provided in Annex III, which includes a detailed, step by step procedure for the preparation of ^{64}Cu labelled mAbs based on the experiences of a Member State laboratory.

6. COPPER-64 DICHLORIDE RADIOPHARMACEUTICAL

6.1. INTRODUCTION

Over the past two decades there has been a growing interest in ^{64}Cu, and important advances have been achieved in preclinical and clinical applications of this emerging radionuclide. Given its favourable physical properties (half-life and decay scheme), ^{64}Cu has the potential to be used for PET molecular imaging and TRT in oncology. The half-life of ^{64}Cu is long enough not only to perform complex radiolabelled processes to match the pharmacokinetics of a broad variety of molecular carriers such as antibodies, but also to allow its transportation over large distances from the site of production. A broad variety of biomolecules conjugated to suitable chelators have been successfully evaluated with this positron emitter [153]. However, in recent years, ^{64}Cu in the chemical form of copper dichloride $[^{64}Cu]CuCl_2$ has been identified as a potential agent for PET molecular imaging and TRT, using the copper transporter protein Ctr1 as the molecular target [156, 157].

It is worthwhile to point out that adaptation of this strategy would obviate the radiolabelling step, preclude the need for expensive target specific ligands such as peptides and antibodies, and would be easy to implement under current GMP compliant conditions because simple target dissolution capabilities would suffice to produce the radiotracer in a form suitable for use in PET imaging.

The widespread use of $[^{64}Cu]CuCl_2$ in PET imaging and theranostic applications in the future will largely depend on showing evidence of the favourable properties of this radiotracer regarding its uptake in cancer cells, biodistribution in normal tissues, obtained image quality and detailed dosimetry assessment — topics that are addressed in this section.

6.2. FORMULATION AND QUALITY CONTROL

Regardless of the method utilized to produce ^{64}Cu, after the separation from the target material (when applicable) the activated product will be in a small volume of acidic solution (usually HCl) with ^{64}Cu in the chemical form of copper chloride. For the preparation and formulation of $^{64}CuCl_2$ solution for injection, after the radiochemical separation, the copper fraction is evaporated to complete dryness. After that, the residue can be treated with 2–5 ml of water and then evaporated to dryness to ensure the evaporation of all acid residues. The activity of ^{64}Cu is recovered with 5 to 10 ml of physiological saline solution and

sterilized by passing it through a 0.22 μm syringe filter (Millex-GV). Given the half-life of ^{64}Cu, the $^{64}CuCl_2$ can also be autoclaved for sterilization.

Quality control of $^{64}CuCl_2$ is necessary to determine the quality of the product. The report of a previous coordinated research project, Cyclotron Produced Radionuclides: Emerging Positron Emitters for Medical Applications: ^{64}Cu and ^{124}I [37], includes a section dedicated to the quality control of $^{64}CuCl_2$ as precursor, including radioactivity, radionuclide purity and chemical purity (metallic impurities). Quality control of $^{64}CuCl_2$ solution as a radiopharmaceutical comprises all the standard quality tests that are performed for PET radiopharmaceuticals, including appearance, pH, radionuclidic identity and purity, chemical purity, membrane filter integrity, bacterial endotoxin and sterility. Suitable methods and acceptance criteria for the quality control of $^{64}CuCl_2$ solution are summarized in Table 6.

TABLE 6. QUALITY CONTROL TESTS AND ACCEPTANCE CRITERIA FOR READY FOR INJECTION ^{64}Cu DICHLORIDE ($^{64}CuCl_2$) RADIOPHARMACEUTICAL

Test	Method	Acceptance criteria
Appearance	Visual inspection	Colourless and free from particles solution
pH	4.5–7.5 (USP)	pH test strips
Radionuclidic identity	Gamma spectroscopy	Two photopeaks at 511 keV and 1345 keV
Radionuclidic purity	Gamma spectroscopy	>99% Cu-64
Chemical purity	Ion exchange HPLC or ICP-OES	Ni, Zn, Fe and Cu <1 μg/GBq
Membrane filter integrity	Bubble point measurement	Membrane has to be integral
Bacterial endotoxin	LAL test (USP)	175 EU/V
Sterility	Incubation in thioglycollate (bacterial) and soybean-casein (fungal) mediums (USP)	Sterile

Note: USP: United States Pharmacopeia; HPLC: high performance liquid chromatography; ICP-OES: inductively coupled plasma optical emission spectrometry; LAL: limulus amebocyte lysate; EU: endotoxin unit.

6.3. BIODISTRIBUTION

Human biodistribution of ^{64}Cu in the chemical form of $CuCl_2$ has been evaluated in PCa patients [158, 159] and in healthy volunteers [160] with whole body PET imaging. Typical biodistribution of $^{64}CuCl_2$ in healthy volunteers is shown in Fig. 27.

$^{64}CuCl_2$ shows rapid uptake in the liver and renal cortex during the first 60 min after injection. At all times after injection, the biodistribution of $^{64}CuCl_2$ is dominated by uptake in the liver, accumulating about 30% of the administered

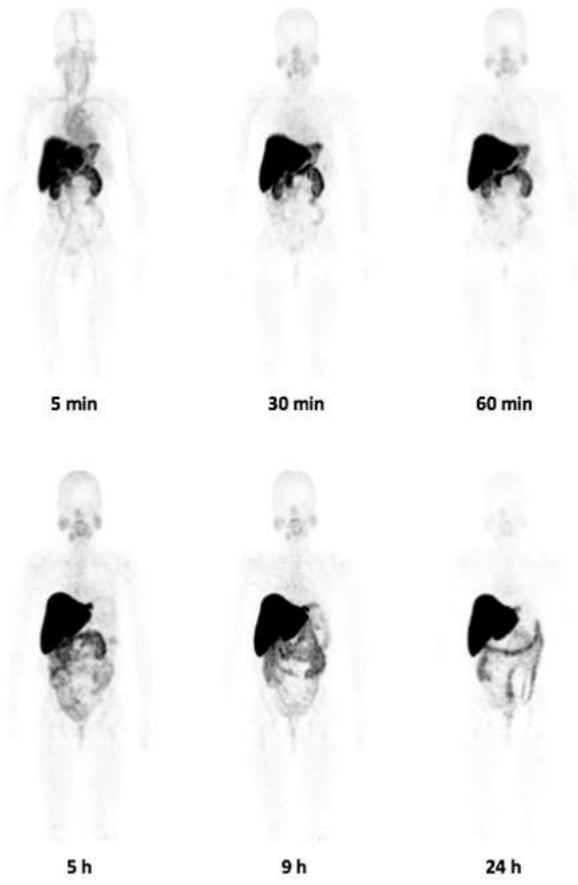

FIG. 27. Typical PET images (maximum intensity projections) showing the normal biodistribution of ^{64}Cu in a healthy volunteer at various times after the injection of a dose of 4 MBq/kg of $^{64}CuCl_2$ (adapted from Ref. [160] with permission).

activity. Uptake is also observed in the salivary glands, biliary tract, pancreas and spleen. The bone marrow and brain show no significant uptake. At later times (24 h p.i.), uptake can be observed at the lower and upper large intestine due to biliary excretion. Elimination by urine is negligible, thus no activity is accumulated in the urinary tract or in the bladder, which facilitates the evaluation of lesions in the abdomen and pelvic area. There are no significant differences in the biodistribution of $^{64}CuCl_2$ between men and women.

6.4. DOSIMETRY

Future clinical applications of ^{64}Cu in the chemical form of $CuCl_2$ will require accurate dosimetric calculations, especially for therapeutic procedures. The most important feature of TRT is to deliver the maximum therapeutic dose to a tumour while causing minimal toxicity to surrounding normal tissues. As dosimetry — in this kind of medical application — uses ionizing radiation, it is very important not only to determine the radiation dose deposited in tumours in order to predict the outcome of TRT, but also to identify dose limiting organs.

6.4.1. Organ dosimetry

Dosimetry of the labelled radiopharmaceutical depends on the pharmacokinetics of the labelled carrier. The medical internal radiation dose (MIRD) is used in the conventional approach of internal dosimetry calculations for the estimation of organ absorbed doses and effective doses of a broad variety of radionuclides used in medical applications for radioprotection purposes. The virtue of this approach is that it systematically reduces complex dosimetric analyses to methods that are relatively simple to use, including software tools, such as the OLINDA/EXM code, for the dose assessment of many radionuclides. In the MIRD formalism, the S-value — the mean absorbed dose of radiation in a target region due to the radioactive decay of a radioisotope in a source region — represents the key physical quantity for converting administered activity to absorbed radiation dose and provides the cumulative activity (total number of disintegrations) in the source region. The S-values depend on the radioisotope and the source target geometry, and the MIRD Committee has calculated these values for most of the radioisotopes used in nuclear medicine applications by using anthropomorphic phantoms representing the standard man, woman and child at different ages.

The above mentioned method has been used to perform dosimetric calculations after the administration of $^{64}CuCl_2$ in humans. The means of absorbed doses to organs and effective doses calculated for $^{64}CuCl_2$ in healthy volunteers

are presented in Fig. 28. Not surprisingly, knowing the biodistribution of $^{64}CuCl_2$, the critical organ is the liver with mean absorbed doses of 310 ± 67 μGy/MBq for men and 421 ± 56 μGy/MBq for women, while the mean effective doses for men and women are 51.2 ± 3.0 μSv/MBq and 61.8 ± 5.2 μSv/MBq, respectively [160]. The differences in the calculated dosimetric values between men and women are mainly due to differences in body and organ sizes, as women generally have smaller body and organ sizes than men. Dosimetric assessment of $^{64}CuCl_2$ has also been performed using biodistribution data obtained from patients suffering PCa [158, 161]. Table 7 shows a comparison of absorbed radiation doses to some specific organs and effective doses obtained to date using biodistribution data from humans. Despite the discrepancies, which could be attributable to the different methodologies in the PET scans for biodistribution and assumptions for dosimetry calculations, what these data show is that the liver is deemed to be the dose limiting organ when considering $^{64}CuCl_2$ for theranostic applications.

Righi et al. [161] studied the biokinetics and performed the dosimetry of PCa lesions for $^{64}CuCl_2$. The absorbed dose per administered activity for each lesion was calculated using the MIRD method. S-values for tumours were obtained by fitting spheres to tumour masses. The radiation dose in the lesions was determined to be 6.00×10^{-2} mGy/MBq, which is too low to have

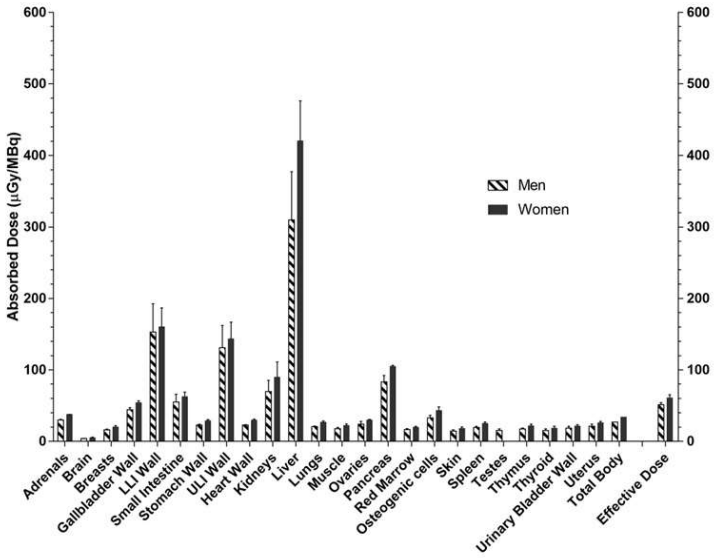

FIG. 28. Organ absorbed doses and effective doses for $^{64}CuCl_2$ in healthy volunteers. Effective dose is given in μSv/MBq (reproduced with permission from Ref. [160]).

TABLE 7. ABSORBED DOSE TO ORGANS (μGy/MBq) AND EFFECTIVE DOSE CALCULATED AFTER THE ADMINISTRATION OF [^{64}Cu]$CuCl_2$ TO PROSTATE CANCER PATIENTS AND HEALTHY VOLUNTEERS

	Male[a] [158]	Male[b] [160]	Male[a] [161]
Liver	294	365 ± 82	271 ± 34
Lower large intestine	19.2	157 ± 28	12.5 ± 4.8
Upper large intestine	23.8	137 ± 24	17.8 ± 5.3
Pancreas	28.8	94.2 ± 13.5	83.9 ± 40.3
Kidneys	33.6	79.9 ± 19.2	139 ± 37.2
Red marrow	25.1	16.7 ± 1.3	22.6 ± 9.0
Total body	26.6	26.9 ± 0.1	20.9 ± 5.6
Effective dose (mSv/MBq)	33.8	56.5 ± 7.0	31.0 ± 8.1

[a] Biodistribution data from prostate cancer patients.
[b] Biodistribution data from healthy volunteers.

a therapeutic effect. However, the therapeutic effect of the Auger electrons was not considered.

The MIRD method has proved to be robust for calculating absorbed doses to organs for radioprotection purposes and the S-values are extremely useful for estimating absorbed doses in nuclear medicine examinations, but the assumptions made in this method limit its applicability for the calculation of doses in radionuclide therapy [162]. The MIRD method assumes that activity is uniformly distributed within the source, ignoring the intracellular distribution of radionuclides emitting short range particles, such as Auger electrons, which results in large errors in the prediction of the biological effects. If we assume that the potential therapeutic effect of $^{64}CuCl_2$ lies mainly in its Auger emissions, microdosimetry with accurate subcellular modelling, including DNA, is required to assess the dosimetry and biological effectiveness when considering therapeutic applications of this tracer. Although this dosimetry may not accurately reflect impact, comparison to other imaging agents and dosimetry would be beneficial. Normally that is done for an imaging agent. Further, there is a large beta component for ^{64}Cu.

6.4.2. Cellular microdosimetry

The complex intracellular and nuclear distribution of copper makes it necessary to perform dosimetry at the cellular and subcellular levels. Microdosimetry takes into account the stochastic nature of the energy deposition

processes in microscopic structures [163], which applies when considering Auger electrons that deposit their energy over subcellular dimensions in the vicinity of the decay site. The Auger spectrum and the single event specific energy distribution are extremely important to calculate the S-values in cellular microdosimetry.

To obtain the S-values for cellular microdosimetry, the standard cellular model consists of two homogeneous concentric spheres of liquid water (density of 1 g/cm^3), with cellular and nuclear radii of 5 and 4 μm, respectively, immersed in an infinite medium of water [164]. The radioactivity is assumed to be uniformly distributed in the cell (C), cytoplasm (Cy), cell surface (Cs) or nucleus (N), and several 'target' ← 'source' combinations are considered, including C ← C, C ← Cs, N ← N, N ← Cy and N ← Cs. A Monte Carlo track structure code with the TOPAS-nBio tool was used to simulate, collision to collision, the complete trajectories in water of electrons generated during the explicit simulation of ^{64}Cu decay in order to calculate the S-values in the five different configurations, taking into account the full spectrum of electrons emitted during the explicit decay of ^{64}Cu. Values are given in Fig. 29 [165]. Note that the dose to the nucleus is far greater when the activity is distributed inside

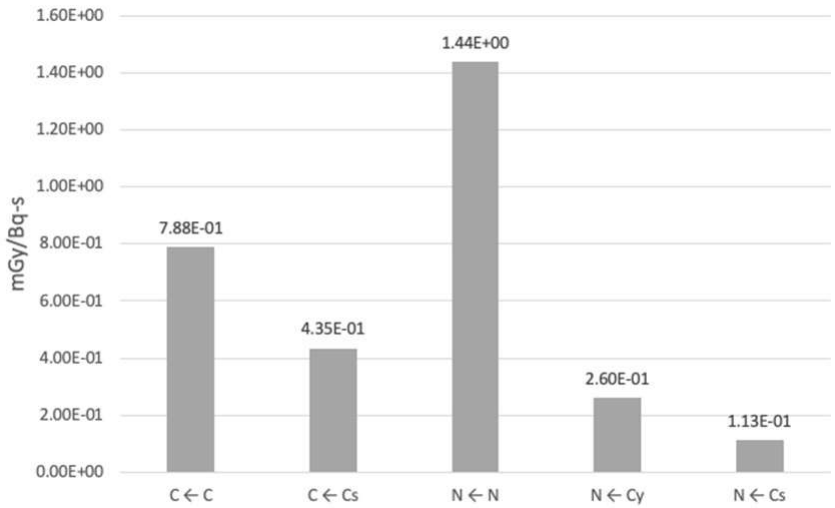

FIG. 29. S-values (mGy · Bq^{-1} · s^{-1}) for ^{64}Cu obtained with TOPAS-nBIO for different configurations (adapted from Ref. [165] with permission). C: cell; Cs: cell surface; N: nucleus; Cy: cytoplasm.

the nucleus itself than when it is distributed in the cytoplasm or the cell surface. This is expected when considering the energy deposition processes of Auger electrons in microscopic structures, which deposit their energy over subcellular dimensions in the vicinity of the decay site.

6.4.3. Nanodosimetry

The evidence of the internalization of copper to the nucleus of cells and the cascade of low energy Auger electrons emitted during the decay of ^{64}Cu suggests that ruptures of the DNA helix can have a lethal therapeutic effect on cells, which requires a study on a nanometric scale. Nanodosimetry is the area of research that aims to link phenomenological dosimetric concepts, such as radiation quality and relative biological effectiveness, to measurable physical quantities related to the track structure of ionizing radiation in nanometric targets such as DNA [166]. The ultimate goal of nanodosimetry is to determine dosimetric quantities that include the initial biological or biophysical action of ionizing radiation. The quantity of interest is the relative frequency distribution of the ionization cluster size, i.e. the number of ionizations produced by a track of particles in a specific target volume, which is a stochastic quantity called the ionization cluster size $P_v(T)$ [167] (T: time). These ionizations can be quantified in terms of statistical moments (M_k) or cumulative probabilities (F_k) that are obtained from frequency distributions of cluster sizes.

Figure 30 shows the frequency distributions determined with TOPAS-nBio for a cylindrical volume of liquid water 2.3 nm in diameter and 3.4 nm in height (corresponding to a DNA segment ten base pairs in length) using a point source of ^{64}Cu placed at different distances from the cylinder axis [165]. The first moment M_1 (the mean number of ionizations in the volume) shows that the cluster size is at its maximum at the centre of the cylinder and monotonically decreases when the source point moves towards the edge of the cylindrical model axis (Fig. 30, solid line). Similar behaviour follows the cumulative probability F_2 (i.e. the distribution of the ionization cluster size), which correlates with the formation of double strand breaks. On the other hand, analysis using density based spatial clustering of applications with noise showed mean numbers of DNA double strand breaks per decay of 0.187 ± 0.001, 0.0317 ± 0.0005 and 0.0125 ± 0.0002 (Bq s)$^{-1}$ for the configurations N ← N, N ← Cs and N ← Cy, respectively [165].

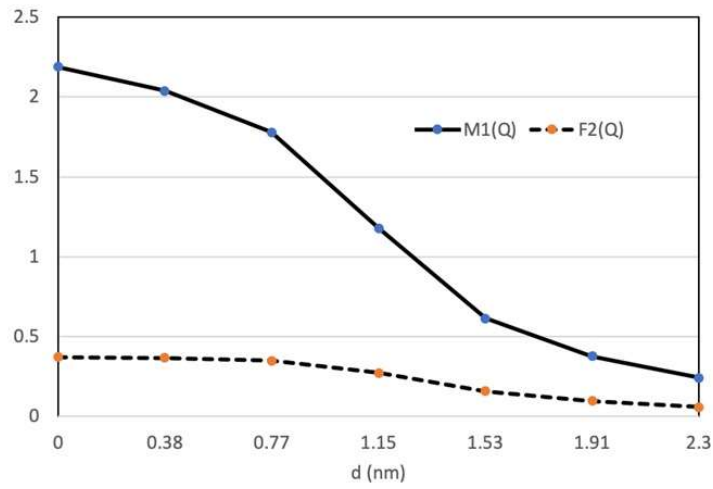

FIG. 30. First moment of the ionization probability distribution $M_1(Q)$ *(solid line) (*Q*: electric charge) and cumulative probability* $F_2(Q)$ *(dashed line) determined in a cylindrical volume of liquid water 2.3 nm in diameter and 3.4 nm in height for a point* ^{64}Cu *source placed at different distances (*d*) from the cylinder axis (adapted from Ref. [165] with permission).*

6.5. [^{64}Cu]$CuCl_2$ FOR PET MOLECULAR IMAGING

PET molecular imaging is a powerful medical imaging technique that can quantitatively map the spatial distribution of positron emitting radionuclides inside the living body at the molecular level. This technique represents the forefront of medical imaging and provides accurate and quantitative information about the physiological processes under investigation. PET is nowadays routinely used for clinical diagnosis worldwide; however, the widespread use of this technique is still limited by the need to operate a local cyclotron facility for the production of the short lived positron emitting radionuclides most commonly used, namely ^{11}C ($T_{1/2}$ = 20 min), ^{13}N (10 min), ^{15}O (2 min) and ^{18}F (110 min). The importance of these four basic radionuclides in PET is attributable to their suitability for labelling tracers to study biochemistry in vivo, as these elements are either found in organic compounds or, as in the case of ^{18}F, offer a substitute for hydrogen atoms or hydroxyl groups. Wider applications of PET would be facilitated with the availability of long lived positron emitters in locations that lack an in-house cyclotron for radionuclide production. That is one of the reasons that the demand for non-conventional PET radionuclides with longer half-lives, especially radiometals, has exponentially increased in recent years. The true power of PET molecular imaging in the clinical management of cancer patients

lies ahead, and the role of metallic radionuclides as versatile radiolabels has proved to be crucial in the task of developing PET agents capable of providing information about the physiological processes of cancer.

The copper transporter protein Ctr1, a 190 amino acid protein of 28 kDa with three transmembrane domains, is believed to be the main protein responsible for the uptake of copper in human cells [168]. It is expressed in many normal tissues, and most interestingly, it has been found that this copper transporter is overexpressed in a variety of cancer cells, converting it into a molecular target for tumours overexpressing Ctr1 [169] — a characteristic that has been employed for PET imaging with promising results in both preclinical applications in animal models and clinical applications in humans, using $^{64}CuCl_2$ as the substrate of Ctr1. As for the preclinical applications, a number of publications have provided strong experimental evidence of the increased uptake of $^{64}CuCl_2$ in different human tumour xenograft models, including models of PCa [156], neuroendocrine lung carcinoid, colorectal, head and neck, ovarian [170] and breast cancer [99], melanoma [171] and glioblastoma [172], which encouraged its evaluation in humans.

6.6. [^{64}Cu]$CuCl_2$ AS A THERANOSTIC AGENT

The goal of TRT is to deliver a tumoricidal dose for tumour ablation without compromising vital organs. To succeed in this goal, it is necessary to achieve a selective concentration and prolonged retention of the administered radiopharmaceutical within the tumour. Other important factors also to consider are the penetration range of the emitted radiation and cumulative radiation dose delivered to tumours. The latter will largely depend on the selected radionuclide, which has to emit particulate radiation, such as α, β and Auger electron emitters, as this kind of radiation is assumed to exhibit the highest therapeutic efficiency.

As stated before, ^{64}Cu possesses unique properties than can serve the dual role of diagnosis and therapy. In addition to the therapeutic potential of its beta decay (both negative and positive), the emission of Auger electrons, associated with the electron capture decay, can also considerably contribute to therapeutic effectiveness. Auger electrons are low energy atomic orbital electrons that are emitted as an alternative to X ray emission after electron capture. These low energy electrons have very short range biological effectiveness (<1 μm) and therefore are useful only if the source is attached to, or very close to, the cell nucleus. Auger electron emitters decaying in the neighbourhood of the DNA produce similar amounts of reactive chemical radical species as α emitters, which are regarded as the classical form of high linear energy transfer radiation. Thus, the therapeutic potential of ^{64}Cu could lie on its capability for internalization

into the cell nucleus where the emitted Auger electrons can further contribute to enhance the DNA damage. Thus, ^{64}Cu may be described as the archetypal 'theranostic' radionuclide, producing excellent PET molecular imaging at low administered doses without major dosimetric or radiobiological concerns and having potential for radionuclide therapy at high doses, with radionuclide distribution and accurate dosimetry possible using PET imaging during therapy.

There exists experimental evidence on the internalization of $^{64}CuCl_2$ into the cell nucleus of neoplastic cells. Guerreiro et al. [173] evaluated the nuclear uptake of this tracer in selected PCa cell lines, including castration resistance (22RV1 and PC3) PCa, hormone naive (LNCaP) PCa and a non-tumorigenic cell line (RWPE-1). They found that taking into account the overall cellular uptake, the highest nuclear uptake of $^{64}CuCl_2$ after 3 h of exposure was observed in the 22RV1 and LNCaP cell lines, reaching values of 35.9% and 35.3% of nucleus associated radioactivity normalized to the amount of protein, respectively, while the cell lines PC3 and RWPE-1 reached values of 9.4% and 9.6%, respectively. The nuclear uptake of $^{64}CuCl_2$ by the non-tumorigenic cell line seems high when considering the purposes of TRT, where the goal is to deliver the maximum dose to tumours, minimizing the dose to normal tissues. However, efflux experiments performed in the same study showed a continuous and moderate washout for all cell lines throughout time, but slightly more pronounced for normal cells (RWPE-1) compared to PCa cell lines. The results showed that $^{64}CuCl_2$ was taken up preferentially by PCa cells compared to normal cells, while no significant differences in cellular retention were observed among them.

In the light of the above discussion, there is evidence to support the potential of $^{64}CuCl_2$ as a theranostic agent. In fact, there are preclinical studies that have evaluated this potential in animal models. Preclinical studies using $^{64}CuCl_2$ as a theranostic agent in selected cancer xenograft models in mice demonstrated its potential as a therapeutic agent. Qin et al. first demonstrated the potential of $^{64}CuCl_2$ as a theranostic agent in malignant melanoma [171]. Mice bearing B16F10 and A375M tumours were systematically administered a therapeutic dose of $^{64}CuCl_2$ (~74 MBq) and tumour sizes were monitored over time. Results showed that the tumour growth in both models was slower than that of the placebo group treated with phosphate buffered saline (PBS). Results also showed that animals treated with $^{64}CuCl_2$ had significantly improved overall survival compared to mice treated with PBS, demonstrating the potential of $^{64}CuCl_2$ as a theranostic agent. In another study, Ferrari et al. evaluated the potential of $^{64}CuCl_2$ for the treatment of glioblastoma (U-87MG) in nude mice [172]. Ninety animals were equally divided into three groups: non-treated (control group), treated with a single administration of 333 MBq (single-dose group (SDG)) and treated with a multiple dose of 55.5 MBq on six consecutive days (multiple-dose group (MDG)). MicroPET imaging was used to monitor the tumour volume by

direct calculation of the volume of interest. A good response to both single and multiple doses was observed in almost all cases. Both treated groups showed a significant reduction in tumour size (68–94% for the SDG and 64–92% for the MDG), with complete tumour disappearance observed in two animals in the SDG and four animals in the MDG. Survival results were also encouraging; all the mice in the control group died within eight weeks, whereas by the end of the twentieth week the survival rates in the SDG and MDG were 73% and 70%, respectively.

To date, no clinical trials have been performed in humans to evaluate the potential of $^{64}CuCl_2$ as a theranostic agent, and only case reports have been described. Valentini et al. reported in 2014 the cases of two patients, one with metastatic prostate cancer and another with uterine cancer, who received a therapeutic dose of $^{64}CuCl_2$ [174]. They observed a significant reduction in volume of lesions and an improvement in overall condition following a single cycle treatment with 3700 MBq of $^{64}CuCl_2$. The same group reported in 2015 the case of a 71 year old patient with difficult gait, no fluent speech and severe epilepsy after a cerebral craniotomy for glioblastoma [175]. After complete radiation therapy and a partial chemotherapy treatment, the patient underwent a multidose treatment with 4 × 2.96 GBq of $^{64}CuCl_2$ every three months. PET–CT scans showed a marked volume reduction of tumour and the authors reported that the patient's life expectancy had been extended to 15 months after tumour diagnosis, with enhanced quality of life, improved walking, chewing and swallowing, and decreased, shorter and milder epilepsy crises. Those are promising results; however, there is still a need for a clinical trial to fully demonstrate the potential of $^{64}CuCl_2$ as a theranostic agent.

6.7. TRUE THERANOSTIC PAIRS OF COPPER

The theranostic approach in nuclear medicine applications consists of the use of specific molecular targets or biological pathways, to which specific radiopharmaceuticals are directed in order to acquire diagnostic images and also to deliver a therapeutic dose of radiation to a tumour, provided that the used radiopharmaceutical is labelled with the appropriate radionuclide. For diagnostic purposes, gamma and/or positron emitter radionuclides are required, whereas for therapeutic applications alpha or beta emitters are necessary.

The most common pair of radionuclides used for theranostic applications is $^{68}Ga/^{177}Lu$ for diagnostic/therapeutic purposes, respectively. However, it is desirable that the radionuclides used to label the radiopharmaceuticals for imaging and therapy are the same, or that radioisotopes of the same element are used, in order to ensure the same biodistribution and pharmacodynamics. In this regard, copper has a unique set of radioisotopes with potential applications not

TABLE 8. PHYSICAL PROPERTIES OF COPPER RADIONUCLIDES, INCLUDING THEIR SOURCE AND APPLICATION

Radionuclide	$T_{1/2}$	Decay (%)	E_γ [keV] (I_γ [%])	Source	Application
Cu-60	23.4 min	β^+ (93) EC (7)	511 1332 (87.9)	Cyclotron	Imaging
Cu-61	3.4 h	β^+ (62) EC (38)	511 283 (13.2)	Cyclotron	Imaging
Cu-62	9.7 min	β^+ (97.8) EC (2.2)	511 1173 (0.4)	Generator	Imaging
Cu-64	12.7 h	β^+ (17.4) EC (43.6) β^- (39.0)	511 1346 (0.6)	Cyclotron/ reactor	Imaging/ therapy
Cu-67	62 h	β^- (100)	185 (48)	Cyclotron/ reactor	Therapy

Note: E_γ: gamma energy; I_γ: relative gamma intensity.

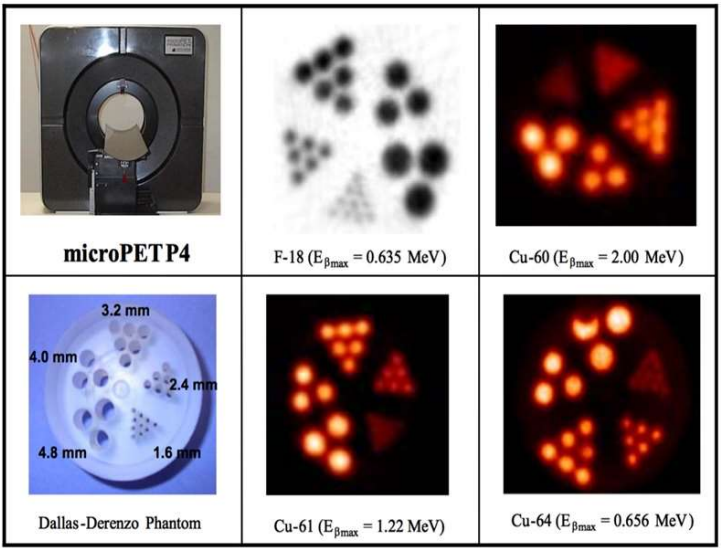

FIG. 31. Miniature hot-rod Derenzo Phantom filled with different radionuclides of copper and imaged on a P4 Concorde microPET scanner (University of Wisconsin-Madison). An image obtained with ^{18}F is included for comparison. Note that the spatial resolution obtained with ^{18}F and ^{64}Cu is similar (courtesy of M.A. Avila-Rodriguez, National Autonomous University of Mexico).

only for diagnostic imaging but also for TRT, as listed in Table 8. As already discussed, the half-life and decay scheme of ^{64}Cu make it the most versatile of the copper radionuclides, and the ideal pair for theranostic applications would be ^{64}Cu/^{64}Cu. However, there are other possibilities for true pairs (or isotopic pairs), such as ^{61}Cu/^{64}Cu, ^{61}Cu/^{67}Cu and ^{64}Cu/^{67}Cu. The radioisotopes ^{60}Cu, ^{62}Cu and ^{66}Cu are discarded because of their short half-lives. Note that from Fig. 31, the PET image quality obtained with ^{64}Cu is very similar to that obtained with ^{18}F, while images obtained with ^{61}Cu and ^{60}Cu are more degraded in spatial resolution, but still acceptable for clinical applications.

7. CLINICAL APPLICATIONS OF COPPER-64 RADIOPHARMACEUTICALS

7.1. INTRODUCTION

Several copper isotopes are available for cancer imaging and therapy, among which the cyclotron produced ^{64}Cu is considered one of the most versatile radionuclides with theranostic potential [176]. The intermediate half-life of ^{64}Cu of 12.7 h makes it a suitable radionuclide for both tracers with rapid pharmacokinetics, such as small molecules and peptides, and slow pharmacokinetic agents, such as mAbs and stem cell tracking. In addition, the positron (β^+) emission of ^{64}Cu with a relatively low dose reduces dosimetry concerns and patients' burdens. Its half-life of 12.7 h provides a suitable timeframe to allow for both high resolution PET imaging and therapeutic applications, through the combined emission of beta particles (β^-) and Auger electrons [176].

Furthermore, copper chemistry is advantageous for different clinical applications, since using well designed macrocyclic chelators enables stable attachment to various targeting molecules (e.g. mAbs, peptides, antibody). Copper plays an important role in many biological processes, and copper homeostasis in the cell is a tightly regulated process that is mainly dependent on the major high affinity copper influx transporter in mammalian cells, human copper transporter 1 (hCtr1) [177]. Disturbances of cellular copper homeostasis are known to be associated with various pathological conditions, including cancer, inflammation and copper metabolism related disease, where copper has been shown to play a critical role in cell proliferation, angiogenesis and tumour growth [178]. Considering that the identification of new biomarkers is a major area of ongoing research, copper metabolism emerges as an interesting potential

imaging biomarker of cancer, which can be explored using different copper isotopes currently available. The first ^{64}Cu based clinically evaluated peptide was the well known SST ligand DOTATATE for NETs — as will be discussed later in this section — and the potential application of ^{64}Cu-SARTATE in the diagnosis and pretherapeutic dosimetry of NETs has also been investigated.

More recently, immunoPET has been shown to provide valuable information about tumour location, phenotype, susceptibility to therapy and treatment response, especially to targeted radioimmunotherapy. An anti-colorectal carcinoma mAb (MAb 1A3) labelled with ^{64}Cu, using bromo-acetamidobenzyl-TETA as a bifunctional agent, was evaluated in patients with suspected advanced primary or metastatic colorectal cancer and studied with FDG as a standard. It was suggested that immunoPET using ^{64}Cu MAb 1A3 has important applications in clinical oncology, particularly for detecting smaller colorectal tumour foci in the abdomen or pelvis and for determining accurate dosimetry [179]. In vivo anti-epidermal growth factor receptor expression levels and its biodistribution have been evaluated via immunoPET imaging of [^{64}Cu] cetuximab. [^{64}Cu] cetuximab immunoPET presented epidermal growth factor receptor expression levels in oesophageal squamous cell carcinoma, and as a further step, [^{177}Lu] cetuximab radioimmunotherapy effectively inhibited the tumour growth. The study demonstrated the theranostic convergence of the radiopharmaceutical pair ^{64}Cu-/^{177}Lu-PCTA-cetuximab, which may be a useful diagnostic tool in restaging and patient selection, as well as a potent radioimmunotherapy agent in epidermal growth factor receptor positive oesophageal squamous cell carcinoma [180].

The most widely explored ^{64}Cu based compound so far is ^{64}Cu-diacetyl-bis N4-methylthiosemicarbazone (ATSM), which has shown promise in clinical trials as a hypoxia selective tracer and as an indicator of response to treatment and tumour recurrence [181].

Recent studies have also suggested that the simplest form of ^{64}Cu, $^{64}CuCl_2$, has unique advantages over other ^{64}Cu labelled compounds [181]. Preclinical studies in cellular and animal models have demonstrated that $^{64}CuCl_2$ has potential as a theranostic agent in several human malignancies, including PCa, glioblastoma and melanoma [156, 171, 172, 182]. In addition, hCtr1 expressing tumour cell lines and xenografts were found to exhibit increased $^{64}CuCl_2$ uptake, suggesting that this compound has potential for the treatment of tumours expressing high levels of hCtr1 [156, 183]. Based on the potential of copper as an imaging biomarker, small scale human studies have since revealed promising results for restaging of PCa and diagnosis of recurrent disease using $^{64}CuCl_2$ PET–CT, without adverse pharmacological effects reported in the participating subjects [158, 159]. The aim of this section is to highlight the most relevant clinical applications of ^{64}Cu based radiopharmaceuticals in PCa and NETs.

7.2. [^{64}Cu]$CuCl_2$ IN ONCOLOGICAL APPLICATIONS

It has been shown that Cu concentration is elevated in various cancer cells. This fact led to the possible application of copper radionuclides in the differentiation of healthy cells from pathologically transformed cells. As the first simple copper cation source, $^{64}CuCl_2$ was applied in diagnostic PET–CT studies in the restaging of PCa recurrent disease detection. Natural copper protein transports in serum carry copper into the liver, leading to high hepatic radioactivity concentration, so it is a challenge to use $^{64}CuCl_2$ PET–CT in clinics. Nevertheless, in a recent $^{64}CuCl_2$ study on Hodgkin lymphoma, two patients affected by progressive Hodgkin lymphoma post radiochemotherapy and transplantation underwent a diagnostic FDG PET–CT scan in two weeks. All the FDG positive lesions showed high $^{64}CuCl_2$ concentration in both patients. One of the hypermetabolic skeletal lesions on FDG PET–CT was not visualized on the corresponding $^{64}CuCl_2$ study. Further evaluation of this lesion was performed with MRI, which confirmed the benign nature of the lesion [184]. These data suggest the feasibility of $^{64}CuCl_2$ dichloride PET–CT scanning in patients with progressive Hodgkin lymphoma and its potential for personalized radionuclide therapy [158, 184, 185].

A recent study reported high uptake of $^{64}CuCl_2$ in metastatic PCa involving regional lymph node lesions [158]. The incidence of PCa is reportedly highest amongst the male population of the United States of America, as well as in the northern and western countries of the European Union, and it is the second highest cause of cancer related male mortality in these countries [186, 187]. When diagnosed at an early stage, PCa is a manageable disease, but the advanced progressive metastatic and castration resistant stage of the illness remains largely incurable [188]. Some authors have proposed MRI as a triage test for candidates for biopsy to increase detection of aggressive cancers. Currently, both CT and MRI demonstrate an equally poor performance in the detection of lymph node metastases from PCa [189].

The determination of serum prostate specific antigen (PSA) is a standard procedure for the screening and early detection of prostate carcinoma, but in some cases its diagnostic value is limited [190–192]. Despite local therapy, such as radical prostatectomy and external radiation therapy, up to 30% of patients eventually experience biochemical recurrence of disease according to PSA monitoring [193]. In these patients, localization of the site of cancer recurrence and that of the extent of metastatic disease may allow individualized treatment planning associated with relatively fewer side effects, and potentially, higher survival rates. Therefore, improvements in the early detection of prostate adenocarcinoma by methods that complement PSA determination are a subject of research [194]. Although choline based PET–CT has been widely used for

this purpose, numerous clinical studies have reported the low sensitivity and specificity of this technique, especially at low PSA levels and high Gleason score. Additionally, ^{11}C or ^{18}F choline are flow limited and higher uptake may be present in benign prostatic hyperplasia [193].

Conversely, ^{68}Ga labelled prostate specific membrane antigen targeted radiopharmaceuticals (^{68}Ga-PSMA), which are designed to recognize a membrane glycoprotein that is highly expressed in human PCa cells, have also emerged with tremendous potential for the detection and restaging of PCa following biochemical recurrence, offering superior contrast and sensitivity to [^{18}F] choline in patients with early PSA failure, and impact on the choice of potentially curative salvage treatments [195, 196].

Copper, as already mentioned, is required for the normal function of the signal transduction pathway regulating cell proliferation. Thus, increased copper uptake by PCa cells may reflect the increased demand for more copper ions due to oxidative stress related to uncontrolled growth of cancer cells. Altered copper metabolism holds potential as an imaging biomarker for metabolic imaging, and therefore, personalized therapy for PCa using radioactive copper is a possibility [197]. Preclinical in vivo studies have demonstrated human PCa xenografts with increased tracer uptake visualized by $^{64}CuCl_2$-PET [156, 157]. While ^{68}Ga-PSMA is now the standard of care in Europe, certain clinical studies evaluated the potential of $^{64}CuCl_2$ PET–CT in the staging of patients with PCa [158] or in the detection of PCa recurrence [159, 161]. Capasso et al. performed first-in-human studies with $^{64}CuCl_2$ PET–CT in the staging of patients with PCa [158], where metastatic lesions specifically in the pelvic area could be easily delineated, primarily owing to the absence of urinary excretion of the tracer, and their study indicated the advantage of this tracer for the diagnosis of recurrent PCa, as well as for potential therapeutic purposes [158]. $^{64}CuCl_2$ uptake was higher in primary tumours of patients without androgen deprivation therapy than in patients under bicalutamide therapy. This study showed a high uptake of $^{64}CuCl_2$ in PCa involving regional lymph nodes, indicating the great potential of $^{64}CuCl_2$ PET–CT even for primary staging of patients with metastatic PCa [158].

Despite its known potential as a therapeutic agent, there remains a lack of sufficient experience on the application of $^{64}CuCl_2$ as a therapeutic radiopharmaceutical. None of the previous studies addressed the potential of $^{64}CuCl_2$ for targeted therapy of PCa and focused primarily on its use for imaging purposes. Moreover, the cellular effects resulting from exposure to ^{64}Cu, which have important clinical implications for both tumoural and healthy tissues, remain largely unknown. A recent study evaluated, for the first time, the radiobiological effects resulting from exposure to $^{64}CuCl_2$ in prostate cells and assessed the potential of this compound for PCa theranostics. A systematic comparison of $^{64}CuCl_2$ uptake in a panel of PCa cell lines and in an immortalized epithelial

cell line used to study benign hyperplasia [173] revealed that PCa cells exhibited higher ^{64}Cu uptake than non-tumoural cells. This finding corresponds to the observation that $^{64}CuCl_2$ provides images with a very good contrast between malignant lesions and the adjacent non-tumour background [158, 161].

Several studies have shown that increased $^{64}CuCl_2$ uptake in different tumours, such as melanoma [171], breast [183] and prostate [156, 157] cancers, is dependent on Ctr1 overexpression. However, in another recent study, no such correlation could be found, leading to the conclusion that Ctr1 expression may not be universally increased in cancers [173]. Further investigation is required to establish whether Ctr1 overexpression indeed underlies increased uptake of $^{64}CuCl_2$ in cancerous tissues, and whether hCtr1 could be used as an appropriate biomarker to predict this compound's efficacy and monitor therapy in a clinical setting [173].

Recently, the European Medicines Agency published important $^{64}CuCl_2$ dosimetry data[1]. As expected from the copper physiology, the data indicate that the liver is the major critical organ. Hepatic tissue demonstrated the highest normalized cumulative activity (6.18 MBq h/MBq) and significant absorbed dose (2.94×10^{-1} mSv/MBq) [161], suggesting that research into preventing radiation induced hepatotoxicity and finding adequate provisions to reduce the inappropriate irradiation of the liver is needed. Further studies are required to evaluate the critical organ dosimetry. On the other hand, these dosimetric studies in humans reported that the dose absorbed by PCa lesions is low, hypothesizing that the therapeutic potential of $^{64}CuCl_2$ is largely dependent on the cytotoxic effects of the Auger electrons, rather than on the beta particles emitted [161]. Thus, from a therapeutic point of view, in order to be effective the $^{64}CuCl_2$ has to reach the nucleus, since the cytotoxic ability of Auger emitters has been shown to be dependent on the emitters' proximity to the DNA [198, 199].

Another group demonstrated that $^{64}CuCl_2$ was able to reach the cellular compartment and induce significant genotoxicity and cytotoxicity in PCa cells, targeting both castration resistance (22RV1 and PC3) and hormone naive (LNCaP) PCa cell lines [173]. In response to the DNA damage caused by $^{64}CuCl_2$, DNA repair mechanisms are induced by the cell, and therefore $^{64}CuCl_2$ might be presented as a therapeutic alternative to treat tumours that have DNA repair deficiencies. Additionally, the observation that non-tumoural cells can repair their damaged DNA supports the use of this radiopharmaceutical in a multidose regimen. Such a fractionated treatment has already been used successfully in a preclinical study with an animal model of glioblastoma, which demonstrated that the single and multiple dose administration was equally effective in terms

[1] See https://www.ema.europa.eu/en/documents/product-information/cuprymina-epar-product-information_en.pdf.

of tumour volume reduction and that the fractionated treatment was the one that displayed no symptoms of radiation associated toxicity. In summary, the study with different PCa cell lines was the first proof of concept cellular report showing high potential of $^{64}CuCl_2$ for theranostics of PCa with minimal possible secondary adverse effects to healthy tissues [173].

In another preliminary study using $^{64}CuCl_2$ in patients with glioma, a $^{64}CuCl_2$ PET scan showed a high uptake in the meningioma, where the patient was treated with intravenous application of 3300 and 2590 MBq of $^{64}CuCl_2$ [184]. Radionuclide treatment with $^{64}CuCl_2$ was very well tolerated and the tumour showed significant regression. Thus, $^{64}CuCl_2$ could be of potential benefit in malignant glioma patients with progressive disease despite standard treatment [184].

7.3. ^{64}Cu-PSMA LIGANDS

As mentioned before, several radiotracers for PET imaging have been evaluated in the imaging of PCa, including FDG as an indicator of glucose metabolism, ^{11}C- and ^{18}F-choline (^{18}F-FCH) and ^{18}F-fluoroethylcholine for phospholipids synthesis, ^{68}Ga/^{64}Cu-DOTA conjugates for SSTR density expression, ^{68}Ga-PSMA ligands for PET of upregulated folate hydrolase, ^{11}C-acetate for lipid synthesis, ^{18}F-fluoro-β-d-arabinofuranosyluracil for DNA synthesis, ^{11}C-methionine and ^{64}Cu-L-asparagine for protein synthesis and ^{64}Cu-dichloride for copper metabolism. As PCa shows no or mild FDG uptake because of its low glucose metabolism [200, 201], FDG is inferior to other tracers for primary staging. ^{18}F-choline PET has been used with a very high number of patients, but it has been clearly shown that its sensitivity and specificity is much lower than for PET with PSMA ligands [202]. Thus, in most centres ^{18}F-choline has been replaced by PSMA PET. While choline derivates are incorporated into the cell membrane, the PSMA ligands are bound to the extracellular part of the PSMA, which is overexpressed in most PCa types. However, the PSMA ligands do not always have the same structure and are labelled with different radio isotopes, such as ^{68}Ga, ^{64}Cu and, more recently, ^{18}F [203–205].

For the detection of recurrent disease, ^{68}Ga-PSMA PET–CT is currently the method of choice [206]. Recent studies have shown the potential of ^{68}Ga-PSMA-11 PET/MRI even at a very low PSA level of <0.5 ng/ml, additionally reporting up to 25% extra pelvic tumour manifestations with low PSA levels [207].

The clinical use of different isotopes is based on logistics and radiopharmaceutical availability. Since ^{68}Ga has a relatively short half-life of 68 minutes, an on-site generator is required, rendering its supply to satellite centres more difficult than for ^{18}F or ^{64}Cu. Furthermore, the longer half-life of ^{64}Cu

enables clinical studies with delayed image acquisition, with the potential for pre-therapy dosimetry calculations [201].

PSMA is a highly attractive target for the diagnosis of metastatic disease [208] and subsequent therapeutic application following the concept of theranostics [209–211]. The introduction of PET imaging with ^{68}Ga labelled urea based PSMA ligands was a significant step forward in the diagnosis of recurrent PCa, as the outstanding feature is the detection of lesions even at very low PSA values, which can significantly influence further clinical management strategies. However, because of its short half-life, the application of ^{68}Ga-PSMA is limited to PET centres with an on-site radiopharmacy. In this regard, it would be of interest to use a PET radionuclide with a longer half-life. Copper-64 is an excellent candidate, as it decays with a half-life of 12.7 h and emits positrons of favourably low energy ($E_{\beta+av}$ = 278 keV), like ^{18}F ($E_{\beta+av}$ = 250 keV). Therefore, the image resolution is expected to be significantly better than that of ^{68}Ga, which emits positrons of a higher energy ($E_{\beta+av}$ = 830 keV) [176]. Another interesting option is to use ^{18}F-PSMA [212].

PSMA ligands have the potential to have a high impact on the management of patients with PCa [200–203]. PET imaging with ^{68}Ga-PSMA-HBED-CC has demonstrated great promise for the detection of small PCa lesions. PSMA ligands have also showed great promise for TRT owing to the overexpression of PSMA in tumour tissue and low uptake in normal tissue [210].

Grubmüller et al. reported the first-in-human application of a urea based PSMA ligand labelled with ^{64}Cu, combining the advantages of a small PSMA targeting agent and a longer lived positron emitter with excellent image quality, resulting in high image contrast. The study was simultaneously performed at two different centres in Austria and Germany [201]. The images obtained with ^{64}Cu-PSMA-617 showed a high lesion to background contrast, as shown in Fig. 32, with a reasonable effective dose. Metastases were frequently detected in pelvic lymph nodes and in the skeleton. The authors further postulated the concept of its use in theranostics, since ^{64}Cu-PSMA could be used to select patients for ^{177}Lu PSMA radioligand therapy [201].

Similar results were achieved by Cantiello et al. in their study to evaluate the diagnostic performance of ^{64}Cu-PSMA-617 PET-CT for restaging of PCa after biochemical recurrence in comparison with ^{18}F-choline PET–CT in a per patient analysis. They clearly demonstrated the superiority of ^{64}Cu-PSMA-617 PET–CT, especially in patients with low PSA values [213].

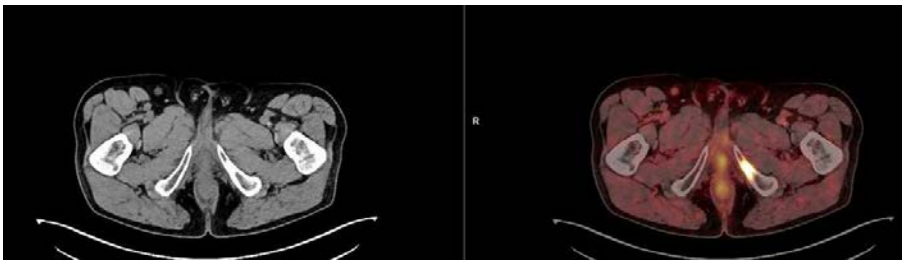

FIG. 32. Images obtained using ^{64}Cu-PSMA-617 PET-CT for a male aged 73 y with prostate neoplasm, 1 h p.i., showing pathological uptake in the left inferior pubis, indicating an osseous metastasis (right image), with corresponding sclerotic lesion on CT (left image). A remarkable lesion to background contrast is observed (maximum standardized uptake value SUVmax: lesion = 11.2, background (gluteal) = 1.3) (courtesy of S. Mirzaei, Wilhelminenspital).

7.4. ^{64}Cu SOMATOSTATIN RECEPTORS

Neuroendocrine neoplasms (NENs) originate from neuroendocrine (enterochromaffin) cells, including gastroenteropancreatic and lung NENs, as well as other neoplasms originating from neuroendocrine cells such as pheochromocytoma, paraganglioma, neuroblastoma and medullary thyroid cancer [214]. NENs are characterized by the immunohistochemical expression of specific markers, such as chromogranin A (CgA), synaptophysin and CD53 protein. Depending on their ability to produce clinical symptoms or their indolent nature, they are classified as functional or non-functional, respectively. Several functional NENs are named according to their clinical syndromes, such as insulinoma, glucagonoma, gastrinoma and VIPoma. The prognosis of NEN depends primarily on the grade and stage of the tumour. The WHO 2010 classification of NENs divides them by mitotic index or Ki-67 index into well differentiated tumours, such as NET G1 (maximum intensity MI < 2, Ki-67 ≤ 2%) and NET G2 (MI = 3–20, Ki-67 = 3–20%), and poorly differentiated cancers, such as neuroendocrine cancer neuroendocrine carcinoma (MI > 20%, Ki-67 > 20%) and mixed adenoneuroendocrine cancers [215]. However, the updated WHO 2017 classification pertaining to pancreatic NENs introduced the novel well differentiated NET of high grade (NET G3). A sharp distinction between NETs and poorly differentiated neuroendocrine carcinoma is emphasized to highlight substantial biological differences. Further changes comprise the definition of mixed neuroendocrine non-neuroendocrine neoplasm to accommodate all grades of both neoplasm components [216]. The characteristic pattern of well differentiated NETs is the overexpression of

specific SST receptors on their cell surface, which can be visualized by targeted molecular imaging modalities. There are five subtypes of SST receptor, so-called SSTR1–5 [217], among which SSTR2 and SSTR5 are mostly overexpressed on NEN cells [218, 219]. The distribution of SSTR in NENs differs depending on the type of the tumour and degree of its differentiation, and furthermore may also differ in the same patient within the metastatic spread of the disease.

Naturally occurring SST has a very low metabolic stability in vivo (<2 min), therefore synthetic SST analogues (SSAs) with a significantly longer biological half-life have been developed for imaging and therapy with varying affinity to the SSTR subtypes [220]. Interestingly, tumours other than NENs, such as small cell lung cancer, breast and ovary cancers, malignant lymphomas, gliomas and meningiomas, can overexpress SSTR [214]. ^{111}In-diethylenetriaminepentaacetic acid-D-Phe1-octreotide ([^{111}In]In-DTPA-OC) was one of the first compounds used for imaging patients with NENs. Other SSTR agonists labelled with ^{99m}Tc have been developed, such as ^{99m}Tc-EDDA-hydrazinonicotinyl-Tyr^3-octreotate (^{99m}Tc-HYNIC-TATE) and ^{99m}Tc-EDDA-hydrazinonicotinyl-Tyr^3-octreotide (^{99m}Tc-EDDA/HYNIC-TOC) [221].

Given the significantly higher spatial resolution of PET imaging, further SSAs labelled with positron emitters have been developed with different affinities to SSTR subtypes. All of them have high affinity to SSTR2, while ^{68}Ga-DOTA-NOC also binds to SSTR3 and SSTR5, and ^{68}Ga-DOTA-TOC to SSTR5 [222]. SSTR imaging facilitates patient management, including staging, detection of new sites of disease in patients with treated NEN (restaging), diagnosis of patients with suspected NEN on the basis of biochemical or clinical findings, localization of the primary tumour in case of initially disseminated disease, and selection of candidates for cold SSA or peptide receptor radionuclide therapy [223, 224].

Generally, well differentiated tumours are detectable with SSTR imaging with higher sensitivity than high grade tumours, which are usually found to be hypermetabolic on FDG PET–CT. Metastases from NENs are predominantly found in the liver, lymph nodes and/or bones, affecting the grading of the disease. However, with the use of more sensitive SSTR PET–CT, it has been shown that skeletal involvement is higher than estimated by conventional radiological techniques [100, 225].

The role of SSTR imaging with radiolabelled SSA is well established in clinical practice, and ^{68}Ga-DOTATATE has also been approved by the US Food & Drug Administration as well as the European Medicines Agency for clinical imaging of gastroenteropancreatic neuroendocrine neoplasms. However, uncertainties regarding optimum imaging persists, including and not limited to the selection of the most suitable peptide or the evolving role of SSTR antagonist imaging. Use of different radionuclides and radiolabelling strategies influences

the peptide's affinity for SSTR and changes the radiopharmaceutical properties of the compound. Alternatively, ^{18}F-SSTR tracers have also been synthesized, but they did not succeed as tracers radiolabelled with, for example, ^{64}Cu, such as ^{64}Cu-DOTATATE, ^{64}Cu-TETA-TOC [100, 224, 226] or ^{64}Cu-DOTATOC [227], as shown in Fig. 33.

There are some advantages of using ^{64}Cu compared to ^{68}Ga. First, ^{64}Cu has a much longer half-life (>12 h), whereas that of ^{68}Ga is only about 1 h. Therefore, delayed imaging is possible with ^{64}Cu. The first-in-human study using ^{64}Cu-DOTATATE revealed that imaging after 3 h was better than 1 h, since most of the renal activity was cleared at the later time point [228]. The authors of this study discussed the finding that because of differences in its physical properties, the detection of smaller foci was better achieved by ^{64}Cu.

In another study, a head to head comparison with [^{111}In]In-DTPA-OC was performed, and it could be shown that in 6 out of 14 patients, additional lesions were found with ^{64}Cu-DOTATATE compared with [^{111}In]In-DTPA-OC [100]. Later on, the same group presented data from the first 100 patients, showing that they found a sensitivity of 91% for detecting NENs with ^{64}Cu-DOTATATE PET. Thirty-five patients demonstrated lesions in organs localized on ^{64}Cu-DOTATATE PET that were not identified with [^{111}In]In-DTPA-OC scintigraphy [100]. The authors concluded that PET imaging with ^{64}Cu-DOTATATE, compared to [^{111}In] In-DTPA-OC scintigraphy, had great potential for clinical use [100, 229].

Further practical advantages of ^{64}Cu-DOTATATE include the possibility to produce the tracer in a central location and to distribute it to satellite PET centres. The positron energy of ^{64}Cu is also much lower than that of ^{68}Ga, and

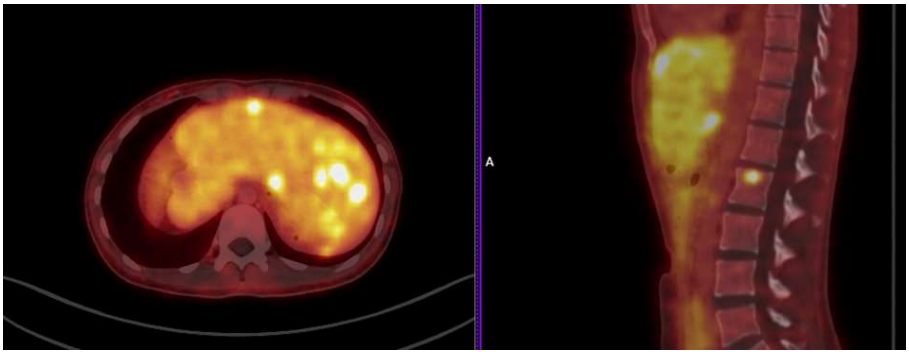

FIG. 33. Images obtained using ^{64}Cu-DOTA-TOC PET–CT for a female aged 31 y with pancreatic NEN post-pancreatectomy and partial hepatectomy, 1 h p.i., demonstrating multiple hepatic metastases within the residual liver (left image) and a solitary bone metastasis in L2 (right image) (courtesy of S. Mirzaei, Wilhelminenspital).

therefore will ideally translate into better spatial resolution. ^{64}Cu-DOTATATE is also a better biochemical match for the commonly used therapy ligand ^{177}Lu-DOTATATE, enabling accurate diagnostic imaging of the organs treated with ^{177}Lu-DOTATATE [224]. Data from the first-in-human study of 14 patients demonstrated that imaging was feasible using an activity of 200 MBq, with a favourable dose of only 6.3 mSv [100].

Hicks et al. performed a first-in-human trial of ^{64}Cu-SARTATE to assess its safety and ability to localize disease at early and late imaging time points [101]. They prospectively studied ten patients with known NENs and positive ^{68}Ga-DOTA-octreotate at variable time points (30 min, 1, 4 and 24 h) following the intravenous administration of ^{64}Cu-SARTATE. Diagnostic, safety and dosimetry analysis demonstrated that ^{64}Cu-SARTATE was mostly well tolerated during the study, showing high lesion uptake and retention in the tumours, with the highest lesion to liver contrast at 24 h. Comparative PET–CT images obtained with ^{64}Cu-SARTATE at 4 h and ^{68}GaDOTA-TATE at 1 h showed comparable or superior lesion detection in all patients, especially in the liver, thereby indicating its suitability for diagnostic studies as well as for prospective dosimetry for ^{67}Cu-SARTATE peptide receptor radionuclide therapy [101].

7.5. [^{64}Cu]$CuCl_2$ APPLICATIONS IN METABOLIC DISEASES

Copper-64 presents the opportunity to use PET to study in vivo copper transport and its alteration during various pathological states. This approach will ideally yield insight into the biological handling of this essential element, and may also yield useful applications of ^{64}Cu imaging. The ^{64}Cu clinical imaging potential has not been fully explored. However, certain studies on animal tumour models [230], Alzheimer's disease [231–233], Niemann–Pick disease [234], Menkes disease [235] and Wilson's disease [231] have reported changes in copper distribution, assumed to be related to activity of the Cu transporter Ctr1. Most of these studies involved ^{64}Cu-dichloride or acetate intravenous injection; however, this behaviour does not mimic the normal copper biological route, which is oral. In order to understand biological copper transportation completely, ^{64}Cu intravenous administration (in ionic form) is not adequate. It is believed that alternative routes of administration (especially oral), as well as other copper biological forms such as copper bound to albumin, amino acids and ceruloplasmin, among others, will ideally also be studied.

CONCLUSIONS

The suitability of ^{64}Cu radiometal for use as a tracer radionuclide for the molecular imaging of human cancers is due to a combination of its availability, ideal physical half-life, ideal PET decay characteristics and routine radiolabelling strategies. Advances in the discovery of new chelating agents and labelling chemistries, and ultimately, the inherent in vivo stability of new targeting vectors based on ^{64}Cu macrocyclic complexes clearly demonstrate the usefulness and necessity of this unique PET imaging radionuclide. In addition, for nearly two decades, the field of nuclear medicine has been investigating the usage of radiolabelled peptides for molecular targeting of receptors highly expressed on specific human tumours. The ability to target specific receptors expressed in very high numbers on the surfaces of human cancer cells creates the opportunity to use [^{64}Cu] radiolabelled peptides as site directed diagnostic probes, as a highly selective treatment regimen for tumour targeting or as a mechanism for this strategy to complement traditional, clinically useful chemotherapeutic regimens of treatment. On the other hand, antibody based molecular imaging agents, including ^{64}Cu radiolabelled antibodies, have also gained considerable interest in both the scientific and medical communities.

Radiopharmaceuticals labelled with ^{64}Cu, such as [^{64}Cu] PSMA and [^{64}Cu] SST analogues (^{64}Cu-SARTATE, ^{64}Cu-DOTATOC), have proved to be useful imaging tools in the detection of residual disease in patients with recurrent disease or primary progressive PCa and in patients with NETs. The long half-life of ^{64}Cu allows distribution of the tracer to PET centres as a satellite concept that do not have access to ^{68}Ga generators.

Additionally, ^{64}Cu in ionic form has been identified as a potential agent for PET imaging and radionuclide therapy using the copper transporter Ctr1 as molecular target. Ctr1 is overexpressed in a variety of cancer cells, a characteristic that has been employed for PET imaging with promising results in both preclinical applications in animal models and clinical applications in humans. TRT is rapidly growing in nuclear medicine, with the aim of enabling tailored therapy for individual patients. Several factors need to be considered to choose the appropriate radioisotope for therapeutic applications, such as physical half-life, energy of particle emission, type of particle emission, specific tumour activity, and the cost and availability of the radioisotope. Preliminary results with therapeutic application of $^{64}CuCl_2$ in selected trials have demonstrated the therapeutic potential of this radionuclide in patients with PCa and recurrent therapy resistant glioblastoma.

In summary, the future appears to be very bright for radiopharmaceutical development based on the ^{64}Cu radionuclide, whether it is used as a radioactive probe attached to specific ligands for the molecular targeting of receptors, or even in its most simple chemical form of ^{64}Cu dichloride.

REFERENCES

[1] CONRY, R.R., "Copper: inorganic & coordination chemistry", Encyclopedia of Inorganic Chemistry, Vol. 43, Wiley, Hoboken, NJ (2006).

[2] BOKHARI, T.H., MUSHTAQ, A., KHAN, I.U., Production of low and high specific activity ^{64}Cu in a reactor, J. Radioanal. Nucl. Chem. **284** (2010) 265.

[3] VIMALNATH, K.V., et al., Studies on the production feasibility of ^{64}Cu by (*n, p*) reactions on Zn targets in Dhruva research reactor, J. Radioanal. Nucl. Chem. **294** (2012) 43.

[4] ZINN, K.R., CHAUDHURI, T.R., CHENG, T.P., MORRIS, J.S., MEYER, W.A.J., Production of no-carrier-added ^{64}Cu from zinc metal irradiated under boron shielding, Cancer **73** S3 Suppl. (1994) 774.

[5] ABBASI, I., ZAIDI, J., ARIF, M., SUBHANI, M., Measurement of fission neutron spectrum averaged cross sections of some threshold reactions on zinc: Small-scale production of no-carrier-added ^{64}Cu in a nuclear reactor, Radiochim. Acta **94** (2006) 63.

[6] ZWEIT, J., SMITH, A.M., DOWNEY, S., SHARMA, H.L., Excitation functions for deuteron induced reactions in natural nickel: Production of no-carrier-added ^{64}Cu from enriched ^{64}Ni targets for positron emission tomography, Int. J. Radiat. Appl. Instrum. **42** 2 (1991) 193.

[7] TÁRKÁNYI, F., et al., Excitation functions of deuteron induced nuclear reactions on natural zinc up to 50 MeV, Nucl. Instrum. Methods Phys. Res. B **217** 4 (2004) 531.

[8] BONARDI, M.L., et al., Thin-target excitation functions and optimization of simultaneous production of NCA copper-64 and gallium-66,67 by deuteron induced nuclear reactions on a natural zinc target, J. Radioanal. Nucl. Chem. **257** (2003) 229.

[9] GROPPI, F., et al., Thin-target excitation functions and optimisation of NCA ^{64}Cu and ^{66,67}Ga production by deuteron induced nuclear reactions on natural zinc target, for radiometabolic therapy and for PET, Nucl. Instrum. Methods Phys. Res. Sect. B **213** (2004) 373.

[10] NEIRINCKX, R.D.D., Simultaneous production of ^{67}Cu, ^{64}Cu and ^{67}Ga and labelling of bleomycin with ^{67}Cu or ^{64}Cu, Int. J. Appl. Radiat. Isot. **28** 9 (1977) 802.

[11] WILLIAMS, D.C., IRVINE, J.W., Nuclear excitation functions and thick-target yields: Zn+*d* and Ar^{40}(*d*, *α*), Phys. Rev. **130** 1 (1963) 265.

[12] MAZIÈRE, B., STULZAFT, O., VERRET, J.M., COMAR, D., SYROTA, A., [^{55}Co]- and [^{64}Cu]DTPA: New radiopharmaceuticals for quantitative tomocisternography, Int. J. Appl. Radiat. Isot. **34** (1983) 595.

[13] HILGERS, K., STOLL, T., SKAKUN, Y., COENEN, H.H., QAIM, S.M., Cross-section measurements of the nuclear reactions ^{nat}Zn(d, *x*)^{64}Cu, ^{66}Zn(d, *α*)^{64}Cu and ^{68}Zn(p, *α*n)^{64}Cu for production of ^{64}Cu and technical developments for small-scale production of ^{67}Cu via the ^{70}Zn(p, *α*)^{67}Cu process, Appl. Radiat. Isot. **59** 5–6 (2003) 343.

[14] KOZEMPEL, J., et al., A novel method for n.c.a. ^{64}Cu production by the ^{64}Zn(*d*, 2*p*) ^{64}Cu reaction and dual ion-exchange column chromatography, Radiochim. Acta **95** (2007) 75.

[15] ABBAS, K., et al., Cyclotron production of ^{64}Cu by deuteron irradiation of ^{64}Zn, Appl. Radiat. Isot. **64** (2006) 1001.
[16] OMETÁKOVÁ, J., et al., Automated production of ^{64}Cu prepared by 18 MeV cyclotron, J. Radioanal. Nucl. Chem. **293** 1 (2012) 217.
[17] RAJEC, P., et al., Preparation and characterization of nickel targets for cyclotron production of ^{64}Cu, J. Radioanal. Nucl. Chem. **286** 3 (2010) 665.
[18] McCARTHY, D.W., et al., Efficient production of high specific activity ^{64}Cu using a biomedical cyclotron, Nucl. Med. Biol. **24** 1 (1997) 35.
[19] AL RAYYES, A.H., AILOUTI, Y., Production and quality control of ^{64}Cu from high current Ni target, World J. Nucl. Sci. Technol. **3** 2 (2013) 72.
[20] TANG, L., Radionuclide production and yields at Washington University School of Medicine, Q. J. Nucl. Med. Mol. Imaging **52** (2008) 121.
[21] SZELECSÉNYI, F., BLESSING, G., QAIM, S.M., Excitation functions of proton induced nuclear reactions on enriched ^{61}Ni and ^{64}Ni: Possibility of production of no-carrier-added ^{61}Cu and ^{64}Cu at a small cyclotron, Appl. Radiat. Isot. **44** 3 (1993) 575.
[22] OBATA, A., et al., Production of therapeutic quantities of ^{64}Cu using a 12 MeV cyclotron, Nucl. Med. Biol. **30** 5 (2003) 535.
[23] AVILA-RODRIGUEZ, M.A., NYE, J.A., NICKLES, R.J., Simultaneous production of high specific activity ^{64}Cu and ^{61}Co with 11.4 MeV protons on enriched ^{64}Ni nuclei, Appl. Radiat. Isot. **65** 10 (2007) 1115.
[24] SZELECSÉNYI, F., et al., Investigation of the ^{66}Zn(p,2pn)^{64}Cu and ^{68}Zn(p,x)^{64}Cu nuclear processes up to 100 MeV: Production of ^{64}Cu, Nucl. Instrum. Methods Phys. Res., Sect. B **240** 3 (2005) 625.
[25] SMITH, S.V., WATERS, D.J., DI BARTOLO, N., Separation of ^{64}Cu from ^{67}Ga waste products using anion exchange and low acid aqueous/organic mixtures, Radiochim. Acta **75** (1996) 65.
[26] FAZAELI, Y., et al., Production, quality control and imaging of ^{64}Cu-ATSM in healthy rabbits for clinical applications, Iran. J. Nucl. Med. **18** 2 (2010) 29.
[27] INTERNATIONAL ATOMIC ENERGY AGENCY, Manual for Reactor Produced Radioisotopes, IAEA-TECDOC-1340, IAEA, Vienna (2003).
[28] McCARTHY, D.W.W., et al., Efficient production of high specific activity ^{64}Cu using a biomedical cyclotron, Nucl. Med. Biol. **24** 1 (1997) 35.
[29] HOEHR, C., et al., "Production of Radiometals in a Liquid Target", Proc. 15th Int. Workshop on Targetry and Target Chemistry, 2015, HZDR, Dresden (2015).
[30] OEHLKE, E., et al., Production of Y-86 and other radiometals for research purposes using a solution target system, Nucl. Med. Biol. **42** (2015) 842.
[31] DO CARMO, S.J.C., ALVES, V.H.P., ALVES, F., ABRUNHOSA, A.J., Fast and cost-effective cyclotron production of ^{61}Cu using a ^{nat}Zn liquid target: An opportunity for radiopharmaceutical production and R&D, Dalton Trans. **46** 42 (2017) 14556.
[32] ALVES, F., et al., Production of copper-64 and gallium-68 with a medical cyclotron using liquid targets, Mod. Phys. Lett. A **32** 17 (2017) 1740013.
[33] DO CARMO, S.J.C., SCOTT, P.J.H., ALVES, F., Production of radiometals in liquid targets, EJNMMI Radiopharm. Chem. **5** (2020) 2.

[34] MORLEY, T.J., et al., An automated module for the separation and purification of cyclotron-produced $^{99m}TcO_4^-$, Nucl. Med. Biol. **39** 4 (2012) 551.
[35] XIE, Q., et al., Establishing reliable Cu-64 production process: From target plating to molecular specific tumor micro-PET imaging, Molecules **22** 4 (2017) 641.
[36] DARABAN, L., Production and Characterization of New Radionuclides Used for Medical Applications, PhD Thesis, Babes-Bolyai Univ. (2010).
[37] INTERNATIONAL ATOMIC ENERGY AGENCY, Cyclotron Produced Radionuclides: Emerging Positron Emitters for Medical Applications: ^{64}Cu and ^{124}I, IAEA Radioisotopes and Radiopharmaceuticals Reports No. 1, IAEA, Vienna (2016).
[38] LE, V.S., et al., Alternative method for ^{64}Cu radioisotope production, Appl. Radiat. Isot. **67** 7–8 (2009) 1324.
[39] AVILA-RODRIGUEZ, M.A., et al., A simple and efficient method to recover isotopically enriched Ni-64 from electrolytic solutions, Appl. Radiat. Isot. **145** (2019) 55–58.
[41] SCHAFFER, P., et al., Direct production of ^{99m}Tc via $^{100}Mo(p,2n)$ on small medical cyclotrons, Phys. Procedia **66** (2015) 383.
[42] VAN DER WALT, T.N., STRELOW, F.W.E., Quantitative separation of gallium from other elements by cation-exchange chromatography, Anal. Chem. **55** 2 (1983) 212.
[43] DIRKS, C., et al., Characterisation of a Cu selective resin and its application to the production of ^{64}Cu, J. Radioanal. Nucl. Chem. **286** 3 (2010) 671.
[44] VAN SO, L., PELLEGRINI, P., KATSIFIS, A., HOWSE, J., GREGURIC, I., Radiochemical separation and quality assessment for the ^{68}Zn target based ^{64}Cu radioisotope production, J. Radioanal. Nucl. Chem. **277** 2 (2008) 451.
[45] KUME, M., et al., A semi-automated system for the routine production of copper-64, Appl. Radiat. Isot. **70** 8 (2012) 1803.
[46] ALVES, V., DO CARMO, S., ALVES, F., ABRUNHOSA, A., Automated purification of radiometals produced by liquid targets, Instruments **2** 3 (2018) 17.
[47] RAKSHIT, A., KHATUA, K., SHANBHAG, V., COMBA, P., DATTA, A., Cu^{2+} selective chelators relieve copper-induced oxidative stress in vivo, Chem. Sci. **9** 41 (2018) 7916.
[48] ANDERSON, C.J., WADAS, T.J., WONG, E.H., WEISMAN, G.R., Cross-bridged macrocyclic chelators for stable complexation of copper radionuclides for PET imaging, Q. J. Nucl. Med. Mol. Imaging **52** (2008) 185–192.
[49] MUKAI, H., WADA, Y., WATANABE, Y., The synthesis of ^{64}Cu-chelated porphyrin photosensitizers and their tumor-targeting peptide conjugates for the evaluation of target cell uptake and PET image-based pharmacokinetics of targeted photodynamic therapy agents, Ann. Nucl. Med. **27** 7 (2013) 625.
[50] MA, M.T., KARAS, J.A., WHITE, J.M., SCANLON, D., DONNELLY, P.S., A new bifunctional chelator for copper radiopharmaceuticals: A cage amine ligand with a carboxylate functional group for conjugation to peptides, Chem. Commun. **14** (2009) 3237.
[51] BOSWELL, C.A., et al., Comparative in vivo stability of copper-64-labeled cross-bridged and conventional tetraazamacrocyclic complexes, J. Med. Chem. **47** 6 (2004) 1465.

[52] XIE, D., KING, T.L., BANERJEE, A., KOHLI, V., QUE, E.L., Exploiting copper redox for ^{19}F magnetic resonance-based detection of cellular hypoxia, J. Am. Chem. Soc. **138** 9 (2016) 2937.
[53] DEARLING, J.L.J., LEWIS, J.S., MULLEN, G.E.D., WELCH, M.J., BLOWER, P.J., Copper bis(thiosemicarbazone) complexes as hypoxia imaging agents: structure-activity relationships, J. Biol. Inorg. Chem. **7** 3 (2002) 249.
[54] BLOWER, P.J., et al., Structural trends in copper(II) bis(thiosemicarbazone) radiopharmaceuticals, Dalton Trans. **23** (2003) 4416.
[55] MAURER, R.I., et al., Studies on the mechanism of hypoxic selectivity in copper bis(thiosemicarbazone) radiopharmaceuticals, J. Med. Chem. **45** 7 (2002) 1420.
[56] JONES-WILSON, T.M., et al., The in vivo behavior of copper-64-labeled azamacrocyclic complexes, Nucl. Med. Biol. **25** 6 (1998) 523.
[57] REUBI, J.C., Peptide receptors as molecular targets for cancer diagnosis and therapy, Endocr. Rev. **24** (2003) 389.
[58] LANE, S.R., et al., $^{99m}Tc(CO)_3$-DTMA bombesin conjugates having high affinity for the GRP receptor, Nucl. Med. Biol. **35** 3 (2008) 263.
[59] PARRY, J.J., KELLY, T.S., ANDREWS, R., ROGERS, B.E., In vitro and in vivo evaluation of ^{64}Cu-labeled DOTA-linker-bombesin(7–14) analogues containing different amino acid linker moieties, Bioconjug. Chem. **18** 4 (2007) 1110.
[60] GARRISON, J.C., et al., In vivo evaluation and small-animal PET/CT of a prostate cancer mouse model using ^{64}Cu bombesin analogs: Side-by-side comparison of the CB-TE2A and DOTA chelation systems, J. Nucl. Med. **48** 8 (2007) 1327.
[61] PRASANPHANICH, A.F., et al., [^{64}Cu-NOTA-8-Aoc-BBN(7–14)NH_2] targeting vector for positron-emission tomography imaging of gastrin-releasing peptide receptor-expressing tissues, Proc. Natl. Acad. Sci. U.S.A. **104** 30 (2007) 12462.
[62] PRASANPHANICH, A.F., et al., The effects of linking substituents on the in vivo behavior of site-directed, peptide-based, diagnostic radiopharmaceuticals, In Vivo **21** 1 (2007) 1.
[63] PRASANPHANICH, A.F., et al., In vitro and in vivo analysis of [^{64}Cu-NO2A-8-Aoc-BBN(7–14)NH_2]: a site-directed radiopharmaceutical for positron-emission tomography imaging of T-47D human breast cancer tumors, Nucl. Med. Biol. **36** 2 (2009) 171.
[64] LANE, S.R., et al., Optimization, biological evaluation and microPET imaging of copper-64-labeled bombesin agonists, [^{64}Cu-NO2A-(X)-BBN(7–14)NH_2], in a prostate tumor xenografted mouse model, Nucl. Med. Biol. **37** 7 (2010) 751.
[65] NANDA, P.K., et al., Positron-emission tomography (PET) imaging agents for diagnosis of human prostate cancer: Agonist vs. antagonist ligands, In Vivo **26** 4 (2012) 583.
[66] MARKWALDER, R., REUBI, J.C., Gastrin-releasing peptide receptors in the human prostate: Relation to neoplastic transformation, Cancer Res. **59** 5 (1999) 1152.
[67] GOURNI, E., et al., N-terminal modifications improve the receptor affinity and pharmacokinetics of radiolabeled peptidic gastrin-releasing peptide receptor antagonists: Examples of ^{68}Ga-and ^{64}Cu-labeled peptides for PET imaging, J. Nucl. Med. **55** 10 (2014) 1719.

[68] TAKAHASHI, M., TAKAMOTO, S., The preparation of trivalent metal chelates with some N_3O_3-type ligands, Bull. Chem. Soc. Jpn **50** 12 (1977) 3413.
[69] KUBÍČEK, V., et al., NOTA complexes with copper(II) and divalent metal ions: kinetic and thermodynamic studies, Inorg. Chem. **57** 6 (2018) 3061.
[70] SUN, X., et al., In vivo behavior of copper-64-labeled methanephosphonate tetraaza macrocyclic ligands, J. Biol. Inorg. Chem. **8** 1–2 (2003) 217.
[71] ATKINS, T., RICHMAN, J., OETTLE, W., Macrocyclic polyamines-1, 4, 7, 10, 13, 16-hexaazacyclooctadecane, Org. Synth. **50** (1988) 652.
[72] STETTER, H., FRANK, W., Complex formation with tetraazacycloalkane-N,N′,N″,N‴-tetraacetic acids as a function of ring size, Angew. Chem., Int. Ed. Engl. **15** 11 (1976) 686.
[73] BAREFIELD, E.K., New synthesis of 1,4,8,11-tetraazacyclotetradecane (Cyclam) via the nickel(II) complex, Inorg. Chem. **11** 9 (1972) 2273.
[74] STIGERS, D.J., et al., A new phosphonate pendant-armed cross-bridged tetraamine chelator accelerates copper(II) binding for radiopharmaceutical applications, Dalton Trans. **39** 7 (2010) 1699.
[75] SARGESON, A.M., The potential for the cage complexes in biology, Coord. Chem. Rev. **151** (1996) 89.
[76] DI BARTOLO, N., SARGESON, A.M., SMITH, S.V., New ^{64}Cu PET imaging agents for personalised medicine and drug development using the hexa-aza cage, SarAr, Org. Biomol. Chem. **4** 17 (2006) 3350.
[77] MUME, E., et al., Synthesis of hexa aza cages, SarAr-NCS and AmBaSar and a study of their metal complexation, conjugation to nanomaterials and proteins for application in radioimaging and therapy, Dalton Trans. **42** 40 (2013) 14402.
[78] CAI, H., FISSEKIS, J., CONTI, P.S., Synthesis of a novel bifunctional chelator AmBaSar based on sarcophagine for peptide conjugation and ^{64}Cu radiolabelling, Dalton Trans. **27** (2009) 5395.
[79] AGUILAR-ORTÍZ, E., JALILIAN, A.R., ÁVILA-RODRÍGUEZ, M.A., Porphyrins as ligands for ^{64}copper: background and trends, MedChemComm **9** (2018) 1577.
[80] HARMATYS, K.M., et al., Tuning pharmacokinetics to improve tumor accumulation of a prostate-specific membrane antigen-targeted phototheranostic agent, Bioconjug. Chem. **29** 11 (2018) 3746.
[81] NANDA, P.K., LANE, S.R., RETZLOFF, L.B., PANDEY, U.S., SMITH, C.J., Radiolabeled regulatory peptides for imaging and therapy, Curr. Opin. Endocrinol. Diabetes Obes. **17** (2010) 69.
[82] REUBI, J.C., MAECKE, H.R., Peptide-based probes for cancer imaging, J. Nuclear Medicine **49** (2008) 1735.
[83] CUTLER, C.S., et al., Current and potential therapeutic uses of lanthanide radioisotopes, Cancer Biother. Radiopharmaceut. **15** (2000) 531.
[84] ANDERSON, C.J., WELCH, M.J., Radiometal-labeled agents (non-technetium) for diagnostic imaging, Chem. Rev. **99** 9 (1999) 2219.
[85] LEWIS, J., WANG, J., ANDERSON, C., McCARTHY, D., WELCH, M., Comparison of cell killing ability of copper-64 and copper-61, J. Label. Compd. Radiopharm. **42** (1999) S753.

[86] ANTUNES, P., et al., Are radiogallium-labelled DOTA-conjugated somatostatin analogues superior to those labelled with other radiometals? Eur. J. Nucl. Med. Mol. Imaging **34** 7 (2007) 982.
[87] DE JONG, M., et al., Therapy of neuroendocrine tumors with radiolabeled somatostatin-analogues, Q. J. Nucl. Med. **43** 4 (1999) 356.
[88] FANI, M., MAECKE, H.R., OKARVI, S.M., Radiolabeled peptides: valuable tools for the detection and treatment of cancer, Theranostics **2** (2012) 481.
[89] HOOSEIN, N.M., LOGOTHETIS, C.J., CHUNG, L.W.K., Differential effects of peptide hormones bombesin, vasoactive intestinal polypeptide and somatostatin analog RC-160 on the invasive capacity of human prostatic carcinoma cells, J. Urol. **149** 5 (1993) 1209.
[90] KRENNING, E.P., et al., Somatostatin receptor scintigraphy with [^{111}In-DTPA-D-Phe^{1}]- and [^{123}I-Tyr^{3}]-octreotide: The Rotterdam experience with more than 1000 patients, Eur. J. Nucl. Med. **20** 8 (1993) 716.
[91] KRENNING, E.P., et al., The role of radioactive somatostatin and its analogues in the control of tumor growth, Recent Results Cancer Res. **153** (2000) 1.
[92] DE JONG, M., et al., Tumour uptake of the radiolabelled somatostatin analogue [DOTA^{0},TYR^{3}]octreotide is dependent on the peptide amount, Eur. J. Nucl. Med. **26** 7 (1999) 693.
[93] KRENNING, E.P., et al., Radiolabelled somatostatin analogue(s) for peptide receptor scintigraphy and radionuclide therapy, Ann. Oncol. **10** (1999) S23.
[94] ANDERSON, C.J., et al., ^{64}Cu-TETA-octreotide as a PET imaging agent for patients with neuroendocrine tumors, J. Nucl. Med. **42** 2 (2001) 213.
[95] LEWIS, M.R., et al., Comparison of copper-64 radiopharmaceuticals for conventional and pretargeted radioimmunotherapy, J. Labelled Comp. Radiopharm. **42** Suppl. 1 (1999) S252.
[96] WADAS, T., WONG, E., WEISMAN, G., ANDERSON, C., Copper chelation chemistry and its role in copper radiopharmaceuticals, Curr. Pharm. Des. **13** (2006) 3.
[97] SPRAGUE, J.E., et al., Synthesis, characterization and in vivo studies of Cu(II)-64-labeled cross-bridged tetraazamacrocycle-amide complexes as models of peptide conjugate imaging agents, J. Med. Chem. **50** 10 (2007) 2527.
[98] SPRAGUE, J.E., et al., Preparation and biological evaluation of copper-64–labeled Tyr^{3}-octreotate using a cross-bridged macrocyclic chelator, Clin. Cancer Res. **10** 24 (2004) 8674.
[99] NEDROW, J.R., et al., Positron emission tomographic imaging of copper 64- and gallium 68-labeled chelator conjugates of the somatostatin agonist Tyr^{3}-octreotate, Mol. Imaging **13** 7 (2014).
[100] PFEIFER, A., et al., ^{64}Cu-DOTATATE PET for neuroendocrine tumors: A prospective head-to-head comparison with ^{111}In-DTPA-octreotide in 112 patients, J. Nucl. Med. **56** 6 (2015) 847.
[101] HICKS, R.J., et al., ^{64}Cu-SARTATE PET imaging of patients with neuroendocrine tumors demonstrates high tumor uptake and retention, potentially allowing prospective dosimetry for peptide receptor radionuclide therapy, J. Nucl. Med. **60** 6 (2019) 777.

[102] PATERSON, B.M., et al., PET imaging of tumours with a ^{64}Cu labeled macrobicyclic cage amine ligand tethered to Tyr^3-octreotate, Dalton Trans. **43** 3 (2014) 1386.
[103] WADAS, T.J., et al., Preparation and biological evaluation of ^{64}Cu-CB-TE2A-sst$_2$-ANT, a somatostatin antagonist for PET imaging of somatostatin receptor-positive tumors, J. Nucl. Med. **49** (2008) 1819.
[104] GUILLOU, A., et al., Methylthiazolyl tacn ligands for copper complexation and their bifunctional chelating agent derivatives for bioconjugation and copper-64 radiolabeling: An example with bombesin, Inorg. Chem. **58** 4 (2019) 2669.
[105] GOURNI, E., et al., Copper-64 labeled macrobicyclic sarcophagine coupled to a GRP receptor antagonist shows great promise for PET imaging of prostate cancer, Mol. Pharm. **12** 8 (2015) 2781.
[106] CHEN, J., GIBLIN, M.F., WANG, N., JURISSON, S.S., QUINN, T.P., In vivo evaluation of ^{99m}Tc/^{188}Re-labeled linear alpha-melanocyte stimulating hormone analogs for specific melanoma targeting, Nucl. Med. Biol. **26** 6 (1999) 687.
[107] GIBLIN, M.F., WANG, N., HOFFMAN, T.J., JURISSON, S.S., QUINN, T.P., Design and characterization of α-melanotropin peptide analogs cyclized through rhenium and technetium metal coordination, Proc. Natl. Acad. Sci. U.S.A. **95** 22 (1998).
[108] CHEN, J.Q., et al., Evaluation of an ^{111}In-DOTA-rhenium cyclized α-MSH analog: A novel cyclic-peptide analog with improved tumor-targeting properties, J. Nucl. Med. **42** 12 (2001) 1847.
[109] DURKAN, K., et al., A heterodimeric [RGD-Glu-[^{64}Cu-NO2A]-6-Ahx-RM2] $\alpha_v\beta_3$/GRPr-targeting antagonist radiotracer for PET imaging of prostate tumors, Nucl. Med. Biol. **41** 2 (2014) 133.
[110] MIAO, Y., BENWELL, K., QUINN, T.P., ^{99m}Tc- and ^{111}In-labeled α-melanocyte-stimulating hormone peptides as imaging probes for primary and pulmonary metastatic melanoma detection, J. Nucl. Med. **48** 1 (2007) 73.
[111] MIAO, Y., et al., ^{203}Pb-labeled α-melanocyte-stimulating hormone peptide as an imaging probe for melanoma detection, J. Nucl. Med. **49** 5 (2008) 823.
[112] MIAO, Y., QUINN, T.P., Peptide-targeted radionuclide therapy for melanoma, Crit. Rev. Oncol. Hematol. **67** (2008) 213.
[113] CANTORIAS, M.V., et al., Development of high-specific-activity ^{68}Ga-labeled DOTA-rhenium-cyclized α-MSH peptide analog to target MC1 receptors overexpressed by melanoma tumors, Nucl. Med. Biol. **36** 5 (2009) 505.
[114] CHEN, J.Q., CHENG, Z., HOFFMAN, T.J., JURISSON, S.S., QUINN, T.P., Melanoma-targeting properties of ^{99m}technetium-labeled cyclic α-melanocyte-stimulating hormone peptide analogues, Cancer Res. **60** 20 (2000) 5649.
[115] MIAO, Y., FISHER, D.R., QUINN, T.P., Reducing renal uptake of ^{90}Y- and ^{177}Lu-labeled alpha-melanocyte stimulating hormone peptide analogues, Nucl. Med. Biol. **33** 6 (2006) 723.
[116] GUO, H., MIAO, Y., Cu-64-labeled lactam bridge-cyclized α-MSH peptides for PET imaging of melanoma, Mol. Pharm. **9** 8 (2012) 2322.
[117] BEER, A.J., et al., Patterns of $\alpha_v\beta_3$ expression in primary and metastatic human breast cancer as shown by ^{18}F-galacto-RGD PET, J. Nucl. Med. **49** 2 (2008) 255.

[118] CHEN, X., et al., ^{18}F-labeled RGD peptide: Initial evaluation for imaging brain tumor angiogenesis, Nucl. Med. Biol. **31** 2 (2004) 179.
[119] JANSSEN, M., et al., Improved tumor targeting of radiolabeled RGD peptides using rapid dose fractionation, Cancer Biother. Radiopharm. **19** 4 (2004) 399.
[120] JANSSEN, M., et al., Comparison of a monomeric and dimeric radiolabeled RGD-peptide for tumor targeting, Cancer Biother. Radiopharm. **17** 6 (2002) 641.
[121] WU, Y., et al., microPET imaging of glioma integrin $\alpha_v\beta_3$ expression using ^{64}Cu-labeled tetrameric RGD peptide, J. Nucl. Med. **46** 10 (2005) 1707.
[122] DECRISTOFORO, C., et al., Comparison of in vitro and in vivo properties of [^{99m}Tc] cRGD peptides labeled using different novel Tc-cores, Q. J. Nucl. Med. Mol. Imaging **51** 1 (2007) 33.
[123] DIJKGRAAF, I., et al., $\alpha_v\beta_3$ integrin-targeting of intraperitoneally growing tumors with a radiolabeled RGD peptide, Int. J. Cancer **120** 3 (2007) 605.
[124] LIU, S., Radiolabeled multimeric cyclic RGD peptides as integrin $\alpha_v\beta_3$ targeted radiotracers for tumor imaging, Mol. Pharmaceut. **3** (2006) 472.
[125] LIU, S., Radiolabeled cyclic RGD peptides as integrin $\alpha_v\beta_3$-targeted radiotracers: Maximizing binding affinity via bivalency, Bioconjug. Chem. **20** (2009) 2199.
[126] LIU, S., et al., ^{18}F-labeled galacto and PEGylated RGD dimers for PET imaging of $\alpha_v\beta_3$ integrin expression, Mol. Imag. Biol. **12** (2010) 530.
[127] LUCIE, S., et al., Clustering and internalization of integrin $\alpha_v\beta_3$ with a tetrameric RGD-synthetic peptide, Mol. Ther. **17** 5 (2009) 837.
[128] CHEN, X., et al., MicroPET and autoradiographic imaging of GRP receptor expression with ^{64}Cu-DOTA-[Lys^3]bombesin in human prostate adenocarcinoma xenografts, J. Nucl. Med. **45** 8 (2004) 1390.
[129] CHEN, X., et al., MicroPET imaging of breast cancer α_v-integrin expression with ^{64}Cu-labeled dimeric RGD peptides, Mol. Imag. Biol. **6** 5 (2004) 350.
[130] CHEN, X., et al., Pegylated Arg-Gly-Asp peptide: ^{64}Cu labeling and PET imaging of brain tumor $\alpha_v\beta_3$-integrin expression, J. Nucl. Med. **45** 10 (2004) 1776.
[131] SPRAGUE, J.E., et al., Noninvasive imaging of osteoclasts in parathyroid hormone-induced osteolysis using a ^{64}Cu-labeled RGD peptide, J. Nucl. Med. **48** 2 (2007) 311.
[132] WEI, L., et al., ^{64}Cu-labeled CB-TE2A and diamsar-conjugated RGD peptide analogs for targeting angiogenesis: comparison of their biological activity, Nucl. Med. Biol. **36** 3 (2009) 277.
[133] CAI, H., LI, Z., HUANG, C.-W., PARK, R., CONTI, P.S., 64Cu labeled AmBaSar-RGD2 for micro-PET imaging of integrin αvβ3 expression, Curr. Radiopharm. **4** 1 (2011) 68.
[134] JIANG, M., FERDANI, R., SHOKEEN, M., ANDERSON, C.J., Comparison of two cross-bridged macrocyclic chelators for the evaluation of ^{64}Cu-labeled-LLP2A, a peptidomimetic ligand targeting VLA-4-positive tumors, Nucl. Med. Biol. **40** 2 (2013) 245.
[135] BANDARI, R.P., et al., Synthesis and biological evaluation of copper-64 radiolabeled [DUPA-6-Ahx-(NODAGA)-5-Ava-BBN(7–14)NH_2], a novel bivalent targeting vector having affinity for two distinct biomarkers (GRPr/PSMA) of prostate cancer, Nucl. Med. Biol. **41** 4 (2014) 355.

[136] JIANG, Z., et al., Molecular imaging investigations of a $^{67}Ga/^{64}Cu$ labeled bivalent ligand, [RGD-Glu-(DO3A)-6-Ahx-RM2], targeting GRPR/$\alpha_v\beta_3$ biomarkers: A comparative study, Radiochim. Acta **104** 7 (2016) 499.
[137] LIU, Z., NIU, G., WANG, F., CHEN, X., ^{68}Ga-labeled NOTA-RGD-BBN peptide for dual integrin and GRPR-targeted tumor imaging, Eur. J. Nucl. Med. Mol. Imaging **36** 9 (2009) 1483.
[138] SHALLAL, H.M., et al., Heterobivalent agents targeting PSMA and integrin-$\alpha_v\beta_3$, Bioconjug. Chem. **25** 2 (2014) 393.
[139] LIU, Z., et al., Small-animal PET of tumors with ^{64}Cu-labeled RGD-bombesin heterodimer, J. Nucl. Med. **50** 7 (2009) 1168.
[140] LIU, Z., YAN, Y., CHIN, F.T., WANG, F., CHEN, X., Dual integrin and gastrin-releasing peptide receptor targeted tumor imaging using ^{18}F-Labeled PEGylated RGD-bombesin heterodimer ^{18}F-FB-PEG 3-Glu-RGD-BBN, J. Med. Chem. **52** 2 (2009) 425.
[141] LIU, Z., YAN, Y., LIU, S., WANG, F., CHEN, X., ^{18}F, ^{64}Cu, and ^{68}Ga labeled RGD-bombesin heterodimeric peptides for PET imaging of breast cancer, Bioconjug. Chem. **20** 5 (2009) 1016.
[142] JACKSON, A.B., et al., ^{64}Cu-NO2A-RGD-Glu-6-Ahx-BBN(7–14)NH_2: A heterodimeric targeting vector for positron emission tomography imaging of prostate cancer, Nucl. Med. Biol. **39** 3 (2012) 377.
[143] CHANG, S.S., et al., Five different anti-prostate-specific membrane antigen (PSMA) antibodies confirm PSMA expression in tumor-associated neovasculature, Cancer Res. **59** 13 (1999) 3192.
[144] RAJASEKARAN, A.K., ANILKUMAR, G., CHRISTIANSEN, J.J., Is prostate-specific membrane antigen a multifunctional protein? Am. J. Physiol.: Cell Physiol. **288** (2005) C975.
[145] FOSS, C.A., et al., Radiolabeled small-molecule ligands for prostate-specific membrane antigen: In vivo imaging in experimental models of prostate cancer, Clin. Cancer Res. **11** 11 (2005) 4022.
[146] BANERJEE, S.R., et al., Synthesis and evaluation of technetium-99m- and rhenium-labeled inhibitors of the prostate-specific membrane antigen (PSMA), J. Med. Chem. **51** 15 (2008) 4504.
[147] CHEN, Y., et al., A low molecular weight PSMA-based fluorescent imaging agent for cancer, Biochem. Biophys. Res. Commun. **390** 3 (2009) 624.
[148] EDER, M., et al., ^{68}Ga-complex lipophilicity and the targeting property of a urea-based PSMA inhibitor for PET imaging, Bioconjug. Chem. **23** 4 (2012) 688.
[149] KULARATNE, S.A., WANG, K., SANTHAPURAM, H.K.R., LOW, P.S., Prostate-specific membrane antigen targeted imaging and therapy of prostate cancer using a PSMA inhibitor as a homing ligand, Mol. Pharm. **6** 3 (2009) 780.
[150] KULARATNE, S.A., ZHOU, Z., YANG, J., POST, C.B., LOW, P.S., Design, synthesis, and preclinical evaluation of prostate-specific membrane antigen targeted ^{99m}Tc-radioimaging agents, Mol. Pharm. **6** 3 (2009) 790.
[151] MA, M.T., et al., Macrobicyclic cage amine ligands for copper radiopharmaceuticals: A single bivalent cage amine containing two Lys^3-bombesin targeting peptides, Inorg. Chem. **50** 14 (2011).

[152] ANDERSON, C.J., et al., Copper-64-labeled antibodies for PET imaging, J. Nucl. Med. **33** (1992) 1685.
[153] ANDERSON, C.J., FERDANI, R., Copper-64 Radiopharmaceuticals for PET imaging of cancer: Advances in preclinical and clinical research, Cancer Biother. Radiopharm. **24** (2009) 379.
[154] CHEN, Y., Drug-to-antibody ratio (DAR) by UV/Vis spectroscopy, Methods Mol. Biol. **1045** (2013) 267.
[155] SHARMA, S.K., et al., A rapid bead-based radioligand binding assay for the determination of target-binding fraction and quality control of radiopharmaceuticals, Nucl. Med. Biol. **71** (2019) 32.
[156] PENG, F., LU, X., JANISSE, J., MUZIK, O., SHIELDS, A.F., PET of human prostate cancer xenografts in mice with increased uptake of $^{64}CuCl_2$, J. Nucl. Med. **47** 10 (2006) 1649.
[157] CAI, H., et al., Reduced ^{64}Cu uptake and tumor growth inhibition by knockdown of human copper transporter 1 in xenograft mouse model of prostate cancer, J. Nucl. Med. **55** 4 (2014) 622.
[158] CAPASSO, E., et al., Role of $^{64}CuCl_2$ PET/CT in staging of prostate cancer, Ann. Nucl. Med. **29** 6 (2015) 482.
[159] PICCARDO, A., et al., $^{64}CuCl_2$ PET/CT in prostate cancer relapse, J. Nucl. Med. **59** 3 (2018) 444.
[160] AVILA-RODRIGUEZ, M.A., et al., Biodistribution and radiation dosimetry of [^{64}Cu] copper dichloride: First-in-human study in healthy volunteers, EJNMMI Res. 7 (2017) 98.
[161] RIGHI, S., et al., Biokinetic and dosimetric aspects of $^{64}CuCl_2$ in human prostate cancer: Possible theranostic implications, EJNMMI Res. **8** (2018) 18.
[162] THIERENS, H.M., et al., Dosimetry from organ to cellular dimensions, Comput. Med. Imaging Graph. **25** 2 (2001) 187.
[163] SANTA CRUZ, G.A., Microdosimetry: Principles and applications, Reports Pract. Oncol. Radiother. **21** 2 (2016) 135.
[164] ROESKE, J.C., AYDOGAN, B., BARDIES, M., HUMM, J.L., Small-scale dosimetry: Challenges and future directions, Semin. Nucl. Med. **38** (2008) 367.
[165] CARRASCO-HERNÁNDEZ, J., et al., Monte Carlo track-structure for the radionuclide Copper-64: Characterization of S-values, nanodosimetry and quantification of direct damage to DNA, Phys. Med. Biol. **65** (2020) 155005.
[166] RABUS, H., NETTELBECK, H., Nanodosimetry: Bridging the gap to radiation biophysics, Radiat. Meas. **46** (2011) 1522.
[167] GROSSWENDT, B., PSZONA, S., BANTSAR, A., New descriptors of radiation quality based on nanodosimetry, a first approach, Radiat. Prot. Dosimetry **126** 1–4 (2007) 432.
[168] ZHOU, B., GITSCHIER, J., hCTR1: A human gene for copper uptake identified by complementation in yeast, Proc. Natl. Acad. Sci. U.S.A. **94** 14 (1997) 7481.
[169] HOLZER, A.K., et al., Expression of the human copper influx transporter 1 in normal and malignant human tissues, J. Histochem. Cytochem. **54** 9 (2006) 1041.
[170] JØRGENSEN, J.T., PERSSON, M., MADSEN, J., KJÆR, A., High tumor uptake of ^{64}Cu: Implications for molecular imaging of tumor characteristics with copper-based PET tracers, Nucl. Med. Biol. **40** 3 (2013) 345.

[171] QIN, C., et al., Theranostics of malignant melanoma with $^{64}CuCl_2$, J. Nucl. Med. **55** 5 (2014) 812.
[172] FERRARI, C., et al., Copper-64 dichloride as theranostic agent for glioblastoma multiforme: A preclinical study, Biomed. Res. Int. **2015** (2015) 129764.
[173] GUERREIRO, J.F., et al., Radiobiological characterization of $^{64}CuCl_2$ as a simple tool for prostate cancer theranostics, Molecules **23** 11 (2018) 2944.
[174] VALENTINI, G., PANICHELLI, P., VILLANO, C., PIGOTTI, G., MARTINI, D., $^{64}CuCl_2$: New theranostic agent, Nucl. Med. Biol. **41** (2014) 638.
[175] VILLANO, C., et al., Case report: Glioblastoma imaging and therapy with ^{64}Cu-asparigne, Eur. J. Nucl. Med. Mol. Imaging **39** Suppl. 2 (2012) S610.
[176] RAMOGIDA, C.F., ORVIG, C., Tumour targeting with radiometals for diagnosis and therapy, Chem. Commun. **49** 42 (2013) 4720.
[177] LEE, J., PEÑA, M.M.O., NOSE, Y., THIELE, D.J., Biochemical characterization of the human copper transporter Ctr1, J. Biol. Chem. **277** 6 (2002) 4380.
[178] ISHIDA, S., ANDREUX, P., POITRY-YAMATE, C., AUWERX, J., HANAHAN, D., Bioavailable copper modulates oxidative phosphorylation and growth of tumors, Proc. Natl. Acad. Sci. U.S.A. **110** 48 (2013).
[179] PHILPOTT, G.W., et al., RadioimmunoPET: Detection of colorectal carcinoma with positron-emitting copper-64-labeled monoclonal antibody, J. Nucl. Med. **36** 10 (1995) 1818.
[180] SONG, I.H., et al., Immuno-PET imaging and radioimmunotherapy of ^{64}Cu-/^{177}Lu-labeled anti-EGFR antibody in esophageal squamous cell carcinoma model, J. Nucl. Med. **57** 7 (2016) 1105.
[181] EVANGELISTA, L., LUIGI, M., CASCINI, G., New issues for copper-64: From precursor to innovative PET tracers in clinical oncology, Curr. Radiopharm. **6** 3 (2014) 117.
[182] CATALOGNA, G., et al., The SGK1 kinase inhibitor SI113 sensitizes theranostic effects of the $^{64}CuCl_2$ in human glioblastoma multiforme cells, Cell. Physiol. Biochem. **43** 1 (2017) 108.
[183] KIM, K.I., et al., Detection of increased ^{64}Cu uptake by human copper transporter 1 gene overexpression using PET with $^{64}CuCl_2$ in human breast cancer xenograft model, J. Nucl. Med. **55** 10 (2014) 1692.
[184] CAPASSO, E., VALENTINI, M.C., MIRZAEI, S., KNOLL, P., MELEDDU, C., Radionuclide treatment with 64Cu-Cl2 in patients with progressive malignant gliomas, Eur. J. Nucl. Med. Mol. Imaging **42** Suppl. 1 (2015) S12.
[185] JALILIAN, A.R., OSSO, J., The current status and future of theranostic copper-64 radiopharmaceuticals, Iranian J. Nucl. Med. **25** (2017) 1.
[186] BROGSITTER, C., ZÖPHEL, K., KOTZERKE, J., ^{18}F-Choline, ^{11}C-choline and ^{11}C-acetate PET/CT: Comparative analysis for imaging prostate cancer patients, Eur. J. Nucl. Med. Mol. Imaging **40** (2013).
[187] SIEGEL, R.L., MILLER, K.D., JEMAL, A., Cancer statistics, 2018, CA – Cancer J. Clin. **68** 1 (2018) 7.
[188] SUMANASURIYA, S., DE BONO, J., Treatment of advanced prostate cancer — A review of current therapies and future promise, Cold Spring Harb. Perspect. Med. **8** 6 (2018) a030635.

[189] HÖVELS, A.M., et al., The diagnostic accuracy of CT and MRI in the staging of pelvic lymph nodes in patients with prostate cancer: A meta-analysis, Clin. Radiol. **63** 4 (2008) 387.
[190] WIRTH, M., et al., Interdisziplinäre Leitlinie der Qualität S3 zur Früherkennung, Diagnose und Therapie der verschiedenen Stadien des Prostatakarzinoms, AWMF, Düsseldorf (2009).
[191] LILJA, H., et al., Prediction of significant prostate cancer diagnosed 20 to 30 years later with a single measure of prostate-specific antigen at or before age 50, Cancer **117** 6 (2011) 1210.
[192] RAAIJMAKERS, R., et al., Prostate-specific antigen change in the European Randomized Study of Screening for Prostate Cancer, section Rotterdam, Urology **63** 2 (2004) 316.
[193] SUTINEN, E., et al., Kinetics of [^{11}C]choline uptake in prostate cancer: A PET study, Eur. J. Nucl. Med. Mol. Imaging **31** 3 (2004) 317.
[194] BRATT, O., LILJA, H., Serum markers in prostate cancer detection, Curr. Opin. Urol. **25** 1 (2015) 59.
[195] BASHIR, U., et al., Impact of Ga-68-PSMA PET/CT on management in prostate cancer patients with very early biochemical recurrence after radical prostatectomy, Eur. J. Nucl. Med. Mol. Imaging **46** 4 (2019) 901.
[196] KITAJIMA, K., et al., Update on advances in molecular PET in urological oncology, Jpn. J. Radiol. **34** (2016) 470.
[197] SPARKS, R., PENG, F., Positron emission tomography of altered copper metabolism for metabolic imaging and personalized therapy of prostate cancer, J. Radiol. Radiat. Ther. **1** 3 (2013) 1015.
[198] PEREIRA, E., et al., Evaluation of acridine orange derivatives as DNA-targeted radiopharmaceuticals for auger therapy: Influence of the radionuclide and distance to DNA, Sci. Rep. **7** (2017) 42544.
[199] CORNELISSEN, B., A VALLIS, K., Targeting the nucleus: An overview of auger-electron radionuclide therapy, Curr. Drug Discov. Technol. **7** 4 (2010) 263.
[200] KHAWAR, A., et al., Sc-PSMA-617 biodistribution and dosimetry in patients with metastatic castration-resistant prostate carcinoma, Clin. Nucl. Med. **43** 5 (2018) 323.
[201] GRUBMÜLLER, B., et al., ^{64}Cu-PSMA-617 PET/CT imaging of prostate adenocarcinoma: First in-human studies, Cancer Biother. Radiopharm. **31** 8 (2016) 277.
[202] EIBER, M., et al., Evaluation of hybrid ^{68}Ga-PSMA ligand PET/CT in 248 patients with biochemical recurrence after radical prostatectomy, J. Nucl. Med. **56** 5 (2015) 668.
[203] MIRZAEI, S., KNOLL, P., ZANDIEH, S., Die Rolle der molekularen Bildgebung (PET-CT) in der Diagnostik und Therapie des Prostatakarzinoms, Wien. Med. Wochenschr. **169** 1 (2019) 12.
[204] GIESEL, F.L., et al., Detection efficacy of ^{18}F-PSMA-1007 PET/CT in 251 patients with biochemical recurrence of prostate cancer after radical prostatectomy, J. Nucl. Med. **60** 3 (2019) 362.
[205] BEHESHTI, M., et al., Optimal time-point for ^{68}Ga-PSMA-11 PET/CT imaging in assessment of prostate cancer: Feasibility of sterile cold-kit tracer preparation? Eur. J. Nucl. Med. Mol. Imaging **45** 7 (2018) 1188.

[206] EIBER, M., RÖTHKE, M.C., Diagnose und Ausbreitungsdiagnostik des Prostatakarzinoms, Forum **31** 2 (2016) 115.
[207] KRANZBÜHLER, B., et al., Clinical performance of ^{68}Ga-PSMA-11 PET/MRI for the detection of recurrent prostate cancer following radical prostatectomy, Eur. J. Nucl. Med. Mol. Imaging **45** 1 (2018) 20.
[208] BANERJEE, S.R., et al., ^{68}Ga-labeled inhibitors of prostate-specific membrane antigen (PSMA) for imaging prostate cancer, J. Med. Chem. **53** 14 (2010) 5333.
[209] WEINEISEN, M., et al., ^{68}Ga-and ^{177}Lu-labeled PSMA I&T: Optimization of a PSMA-targeted theranostic concept and first proof-of-concept human studies, J. Nucl. Med. **56** 8 (2015) 1169.
[210] BAUM, R.P., et al., ^{177}Lu-labeled prostate-specific membrane antigen radioligand therapy of metastatic castration-resistant prostate cancer: Safety and efficacy, J. Nucl. Med. **57** 7 (2016) 1006.
[211] KULKARNI, H., et al., First clinical results with Lu-^{177} PSMA-TUM1 for the treatment of castrate-resistant metastatic prostate cancer, J. Nucl. Med. **55** Suppl. 1 (2014) 10.
[212] ROBU, S., et al., Synthesis and preclinical evaluation of novel ^{18}F-labeled Glu-urea-Glu-based PSMA inhibitors for prostate cancer imaging: a comparison with ^{18}F-DCFPyl and ^{18}F-PSMA-1007, EJNMMI Res. **8** 1 (2018) 30.
[213] CANTIELLO, F., et al., Comparison between ^{64}Cu-PSMA-617 PET/CT and ^{18}F-choline PET/CT imaging in early diagnosis of prostate cancer biochemical recurrence, Clin. Genitourin. Cancer **16** 5 (2018) 385.
[214] REUBI, J.C., KVOLS, L., KRENNING, E., LAMBERTS, S.W.J., Distribution of somatostatin receptors in normal and tumor tissue, Metabolism **39** 9 Suppl. 2 (1990) 78.
[215] ÖBERG, K., CASTELLANO, D., Current knowledge on diagnosis and staging of neuroendocrine tumors, Cancer Metastasis Rev. **30** Suppl. 1 (2011) 3.
[216] INZANI, F., PETRONE, G., RINDI, G., The New World Health Organization classification for pancreatic neuroendocrine neoplasia, Endocrinol. Metab. Clin. North Am. **47** (2018) 463.
[217] REUBI, J.C., Peptide receptor expression in GEP-NET, Virchows Arch. **451** (2007) 47.
[218] RINKE, A., et al., Placebo-controlled, double-blind, prospective, randomized study on the effect of octreotide LAR in the control of tumor growth in patients with metastatic neuroendocrine midgut tumors: A report from the PROMID study group, J. Clin. Oncol. **27** 28 (2009) 4656.
[219] PEPE, G., MONCAYO, R., BOMBARDIERI, E., CHITI, A., Somatostatin receptor SPECT, Eur. J. Nucl. Med. Mol. Imaging **39** (2012) S41.
[220] JOHNBECK, C.B., KNIGGE, U., KJÆR, A., PET tracers for somatostatin receptor imaging of neuroendocrine tumors: current status and review of the literature, Future Oncol. **10** (2014) 2259.
[221] HUBALEWSKA-DYDEJCZYK, A., et al., ^{99m}Tc-EDDA/HYNIC-octreotate — A new radiotracer for detection and staging of NET. A case of metastatic duodenal carcinoid, Nucl. Med. Rev. **8** 2 (2005) 155.
[222] VIRGOLINI, I., et al., Procedure guidelines for PET/CT tumour imaging with ^{68}Ga-DOTA-conjugated peptides: ^{68}Ga-DOTA-TOC, ^{68}Ga-DOTA-NOC, ^{68}Ga-DOTA-TATE, Eur. J. Nucl. Med. Mol. Imaging **37** 10 (2010) 2004.

[223] AALBERSBERG, E.A., et al., Influence of lanreotide on uptake of ^{68}Ga-DOTATATE in patients with neuroendocrine tumours: A prospective intra-patient evaluation, Eur. J. Nucl. Med. Mol. Imaging **46** 3 (2019) 696.
[224] KJAER, A., KNIGGE, U., Use of radioactive substances in diagnosis and treatment of neuroendocrine tumors, Scand. J. Gastroenterol. **50** 6 (2015) 740.
[225] PAVEL, M., et al., ENETS consensus guidelines update for the management of distant metastatic disease of intestinal, pancreatic, bronchial neuroendocrine neoplasms (NEN) and NEN of unknown primary site, Neuroendocrinology **103** (2016) 172.
[226] HANAOKA, H., et al., Evaluation of ^{64}Cu-labeled DOTA-D-Phe^{1}-Tyr^{3}-octreotide (^{64}Cu-DOTA-TOC) for imaging somatostatin receptor-expressing tumors, Ann. Nucl. Med. **23** 6 (2009) 559.
[227] MIRZAEI, S., et al., ^{64}Cu-DOTATOC PET-CT in patients with neuroendocrine tumors, Oncol. Ther. **8** (2020) 125.
[228] PFEIFER, A., et al., Clinical PET of neuroendocrine tumors using ^{64}Cu-DOTATATE: First-in-humans study, J. Nucl. Med. **53** 8 (2012) 1207.
[229] JOHNBECK, C.B., et al., Head-to-head comparison of ^{64}Cu-DOTATATE and ^{68}Ga-DOTATOC PET/CT: A prospective study of 59 patients with neuroendocrine tumors, J. Nucl. Med. **58** 3 (2017) 451.
[230] HUETING, R., Radiocopper for the imaging of copper metabolism, J. Label. Compd. Radiopharm. **57** (2014) 231.
[231] BANDMANN, O., WEISS, K.H., KALER, S.G., Wilson's Disease and other neurological copper disorders, Lancet Neurol. **14** (2015) 103.
[232] FODERO-TAVOLETTI, M.T., et al., Bis (thiosemicarbazonato) Cu-64 complexes for positron emission tomography imaging of Alzheimer's disease, J. Alzheimer's Dis. **20** 1 (2010) 49.
[233] PAL, A., SIOTTO, M., PRASAD, R., SQUITTI, R., Towards a unified vision of copper involvement in Alzheimer's disease: A review connecting basic, experimental, and clinical research, J. Alzheimer's Dis. **44** (2015) 343.
[234] ÁLVAREZ-HERNÁNDEZ, J., et al., Prevalencia y costes de la malnutrición en pacientes hospitalizados; estudio PREDyCES®, Nutr. Hosp. **27** 4 (2012) 1049.
[235] SMPOKOU, P., et al., Menkes disease in affected females: The clinical disease spectrum, Am. J. Med. Genet. A **167** 2 (2015) 417.

Annex I

COPPER IN LIFE

I–1. OXIDATION AND SPIN STATES

Copper occurs in four oxidation states: 0, +1, +2, +3 and +4. The latter two become increasingly unstable as the ionization potentials increase from 745 kJ/mol for Cu^{+} to 5682 kJ/mol for Cu^{4+} [I–1] and the electronic orbitals contract in response to the increased effective nuclear charge. The oxidation state +4 is exceedingly rare, best represented by Cs_2CuF_6 [I–2]. The oxidation state +3 is also uncommon, as the Cu^{3+} ion is a potent oxidant in aqueous solutions. This oxidation state can lead to both diamagnetic ($KCuO_2$) and paramagnetic species (K_3CuF_6) [I–3]. The Cu^{2+} (cuprous) and Cu^{+} (cupric) states are the main oxidation states of copper, and their relative stabilities are reflective of their respective redox potentials, E' (see Eqs (I–1) and (I–2)). As a consequence, Cu^{+} quickly (<1 s) disproportionates in aqueous solution according to the equilibrium (see Eq. (I–3) and Ref. [I–4]). This equilibrium, however, can be easily driven in either direction. The relative stability of Cu^{+} versus Cu^{2+} depends on the presence and nature of anions, the ligand, the solvent and the E_h (a measure of the redox state) of the solution. While water is a much better ligand for Cu^{2+}, moving the equilibrium in favour of Cu^{2+}, acetonitrile efficiently solvates Cu^{+} so that $[Cu(CH_3CN)_4]^{+}$ can be isolated [I–5]. The stabilization of Cu^{+} can be achieved by the formation of low solubility compounds, such as CuCl and CuCN. The case in point is the Earth's crust, where chalcocite, Cu_2S, is more abundant than covellite, CuS, and cuprite, Cu_2O, is more abundant than tenorite, CuO. The Cu^{+} ion has a d^{10} configuration and therefore is diamagnetic and colourless. The Cu^{2+} is a d^9 ion and is paramagnetic and coloured. The paramagnetism of Cu^{2+} is the reason the corresponding organometallic complexes and chelates are generally not amenable to NMR structural elucidation but can be analysed using electron paramagnetic resonance [I–6]. Both stable isotopes of copper are NMR active (nuclear spin $I = 3/2$) and despite strong quadruple interactions, the $^{63}Cu/^{65}Cu$ NMR is gaining acceptance in solid state research [I–7]. While Cu^{+} and Cu^{2+} heavily dominate copper oxidation states, zero valent copper was found to exist in aqueous solution only in the form of metal nanoparticles.

$$Cu^{+} + e^{-} \longrightarrow Cu \qquad E^{0} = 0.52\ V \qquad \text{(I–1)}$$

$$Cu^{+} \longrightarrow Cu^{2+} + e^{-} \qquad E^{0} = -0.53\ V \qquad \text{(I–2)}$$

$$2Cu^{+} \longrightarrow Cu + Cu^{2+} \qquad E^{0} = 0.367\ V \quad (K \approx 10^{6}) \qquad \text{(I–3)}$$

where K is the reaction constant.

I–2. COORDINATION GEOMETRY

The orange-red Cs_2CuF_6 is one of the few Cu^{4+} compounds that has been characterized by X ray crystallography. It reveals a paramagnetic ($\mu = 1.76\mu_B$; μ_B is the Bohr magneton) d^7 Cu^{4+} centre in a distorted octahedral environment. The examples of Cu^{3+} compounds are more numerous. The d^8 Cu^{3+} configuration is expected to form predominantly diamagnetic, square-planar complexes, and this tendency is reinforced by high field ligands such as fluoride in $CsCuF_4$. An octahedral paramagnetic structure is also possible, as exemplified by Cs_2KCuF_6 ($\mu = 2.0\mu_B$). A one electron reduction of Cu^{3+} gives rise to Cu^{2+}, which has a d^9 configuration and possesses a pair of degenerate orbitals. As such, it is subject to Jahn–Teller distortion, which lowers the overall symmetry of the complex. As a consequence, the Cu^{2+} hexa-aqua cation is not octahedral, but rather five coordinated, with the sixth water ligand further distant and easily dissociating. In general, the copper–water exchange rate in the first coordination sphere is extremely high and ligand substitution is very fast. Coordination numbers 6, 5 and 4 are the most common for Cu^{2+} (see Fig. I–1 images (4) to (8)). The radius of Cu^{2+} increases as its coordination number increases, from 57 pm for four coordinate to 73 pm for six coordinate. From a hard and soft (Lewis) acids and bases perspective, Cu^{2+} can be considered as a borderline Lewis acid, allowing it to form complexes with both hard and soft ligands. Cu^{+}, on the other hand, is a soft cation, which prefers soft Lewis bases, such as S and C based ligands. Cu^{+} demonstrates significant coordination flexibility, its coordination numbers spanning the range from 5 to 2 (see Fig. I–1 images (4) to (8)). Copper with varying oxidation states and associated stereochemistry determined by X ray crystallography is also shown in Fig. I–1.

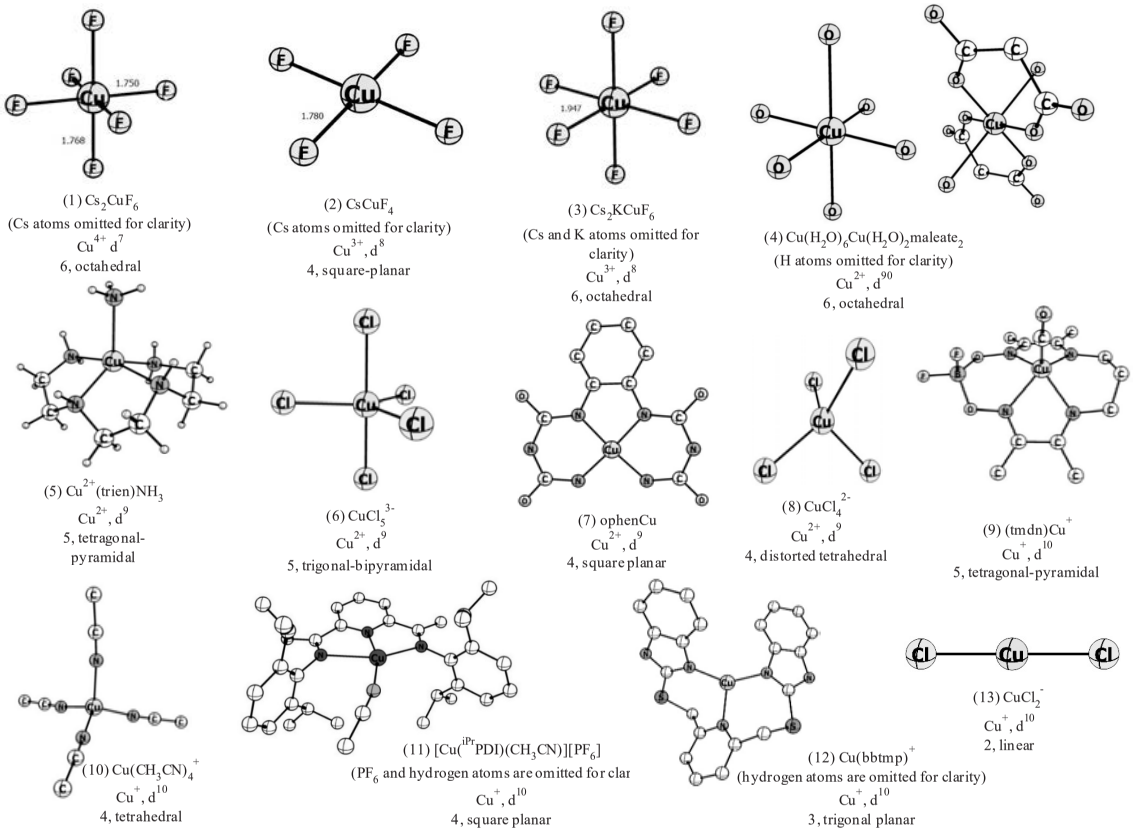

FIG. I–1. A schematic overview of the coordination geometry of copper complexes. Data from: (1) [I–8], (2), (3) [I–9], (4) [I–10], (5) [I–11], (6) [I–12], (7) [I–13], (8) [I–14], (9) [I–15], (10) [I–16], (11) [I–17], (12) [I–18], (13) [I–19].

REFERENCES TO ANNEX I

[I–1] LEVASON, W., SPICER, M.D., The chemistry of copper and silver in their higher oxidation states, Coord. Chem. Rev. **76** C (1987) 45.

[I–2] MÜLLER, B.G., Fluorides of copper, silver, gold, and palladium, Angew. Chemie Int. Ed. **26** (1987) 1081.

[I–3] POPOVA, T.V., AKSENOVA, N.V., Complexes of copper in unstable oxidation states, Russ. J. Coord. Chem. **29** (2003) 743.

[I–4] COTTON, F.A., WILKINSON, G., MURILLO, C.A., BOCHMANN, M., Advanced Inorganic Chemistry, 6th edn, Wiley-Interscience, New York (1999).

[I–5] GILL, D.S., SINGH, R., RANA, D.S., WAGLER, J., KROKE, E., Preparation, characterization, X-ray structure determination and solution properties of some novel copper(I) bisulfate and sulfate salts and their stable derivatives, Z. Naturforsch. B **66** 10 (2011) 1042.

[I–6] HITCHMAN, M.A., SIMMONS, C.J., STRATEMEIER, H., EPR of two Cu^{2+} complexes showing dynamic Jahn–Teller effects, Appl. Magn. Reson. **19** 1 (2000) 121.

[I–7] TANG, J.A., et al., Solid-state ^{63}Cu and ^{65}Cu NMR spectroscopy of inorganic and organometallic copper(I) complexes, J. Am. Chem. Soc. **129** 43 (2007) 13049.

[I–8] VILLARS, P., CENZUAL, K. (Eds), $Cs_2[CuF_6]$ (Cs_2CuF_6) Crystal Structure, Dataset sd_1706578, PAULING FILE Multinaries Edition — 2012, Springer Materials, Springer, Heidelberg, https://materials.springer.com/isp/crystallographic/docs/sd_1706578.

[I–9] JAIN, A., et al., Commentary: The Materials Project: a materials genome approach to accelerating materials innovation, APL Mater. **1** (2013) 011002.

[I–10] PROUT, C.K., CARRUTHERS, J.R., ROSSOTTI, F.J.C., Structure and stability of carboxylate complexes. Part VIII. Crystal and molecular structures of copper(II) hydrogen maleate tetrahydrate and copper(II) maleate hydrate, J. Chem. Soc. A **1971** (1971) 3342.

[I–11] BRYLEV, K.A., NAUMOV, N.G., PERIS, G., LLUSAR, R., FEDOROV, V.E., Novel inorganic ionic compounds based on Re_6 chalcocyanide cluster complexes: synthesis and crystal structures of $[CuNH_3(trien)]_2[Re_6S_8(CN)_6]\cdot 7H_2O$, $[CuNH_3(trien)]_2[Re_6Se_8(CN)_6]$ and $[CuNH_3(trien)]_2[Re_6Te_8(CN)_6]\cdot H_2O$, Polyhedron **22** 25–26 (2003) 3383.

[I–12] RAYMOND, K.N., MEEK, D.W., IBERS, J.A., The structure of hexaamminechromium(III) pentachlorocuprate(II), $[Cr(NH_3)_6][CuCl_5]$, Inorg. Chem. **7** 6 (1968) 1111.

[I–13] BARBIER, J.P., EL BIYYADH, A., KAPPENSTEIN, C., DONGUI MABIALA, N., HUGEL, R.P., Square-planar complexes of copper(II), nickel(II), and cobalt(II) with deprotonated biuret derivatives. Crystalline and molecular structures of sodium (o-phenylenebis(biuretato))- and (propylenebis(biuretato))cuprate(II)-dimethyl sulfoxide complexes, Inorg. Chem. **24** 22 (1985) 3615.

[I–14] BHATTACHARYA, R., et al., Synthesis, crystal structure and thermochromism of benzimidazolium tetrachlorocuprate: $(C_7H_7N_2)_2[CuC_{l4}]$, Polyhedron **21** 25–26 (2002) 2561.

[I–15] GAGNE, R.R., ALLISON, J.L., GALL, R.S., KOVAL, C.A., Models for copper-containing proteins: structure and properties of novel five-coordinate copper(I) complexes, J. Am. Chem. Soc. **99** 22 (1977) 7170.

[I–16] JONES, P.G., CRESPO, O., Tetrakis(acetonitrile-N)copper(I) tetrafluoroborate, Acta Crystallogr. C **54** 1 (1998) 18.

[I–17] CHEUNG, P.M., BERGER, R.F., ZAKHAROV, L.N., GILBERTSON, J.D., Square planar Cu(ı) stabilized by a pyridinediimine ligand, Chem. Commun. **52** 22 (2016) 4156.

[I–18] BALAMURUGAN, R., PALANIANDAVAR, M., SRINIVASA GOPALAN, R., Trigonal planar copper(I) complex: Synthesis, structure, and spectra of a redox pair of novel copper(II/I) complexes of tridentate bis(benzimidazol-2′-yl) ligand framework as models for electron-transfer copper proteins, Inorg. Chem. **40** 10 (2001) 2246.

[I–19] MARGRAF, G., LERNER, H.W., WAGNER, M., BOLTE, M., The absolute structure of tetrakis(trimethylphosphine)copper(I) dichlorocopper(I), Acta Crystallogr. E **60** 2 (2004).

Annex II

COPPER BIOLOGY

This annex describes the copper in biosystems, namely copper proteins and copper interactions with biomolecules and human diseases. Copper transport and metabolic diseases can be diagnosed or followed up in the future using $CuCl_2$ radiopharmaceutical in human clinical trials. Although most of the copper proteins covered in this annex are important and active in non-human biological systems, the significant role of copper in organisms can also be investigated by the application of the ^{64}Cu radionuclide for basic biological and biochemical research.

II–1. COPPER PROTEINS

II–1.1. Evolution of copper proteins

Redox function is central to copper proteins, where they function either as electron or dioxygen carriers. In evolutionary terms, copper became bioavailable approximately one billion years ago, when the Earth's atmosphere became oxygenated enough to allow for the oxidation of insoluble Cu_2S into soluble Cu^{2+}. This allowed newly formed copper enzymes to find their unique place in rapidly expanding aerobic life forms and even compete with already existing iron enzymes, replacing them or augmenting their function. For example, cyanobacteria use Cu-containing plastocyanin together with Fe-containing cytochrome c for photosynthesis, and adjust the levels of these enzymes depending on the amount of bioavailable iron and copper [II–1]. From an evolutionary standpoint, it is likely that some cupredoxin 9 proteins initially formed in a metal free state [II–1, II–2]. By incorporating copper, the new complexes had structural stability and new enzymatic functions. Conversely, coagulation factors CF5 and CF8 were created from the precursor of the copper protein ceruloplasmin, which lost its copper and catalytic activity.

Proteins with copper metal centres are usually classified into four types, depending on the coordination structure of the metal.

II–1.2. Blue copper proteins: Copper proteins containing type 1 sites

Found in archaea, bacteria and eukarya, blue copper proteins are ubiquitous in nature. Known as cupredoxins [II–2], a large family of small (10–20 kDa), freely diffusible proteins containing a single copper type 1 site associated with a

domain with typical protein folding (Fig. II–1, left) belongs to the first class of blue copper proteins and includes azurin, pseudoazurin, amicyanin, rusticyanin (all from bacteria) and plastocyanin and stellacyanin (from plants and algae). Other blue copper proteins contain multiple domains of the typical protein folding and are called multidomain cupredoxins (2 domain, e.g. nitrite reductase; 3 domain, e.g. laccase, ascorbate oxidase; and 6 domain, e.g. ceruloplasmin, hephaestin). The main function of blue copper proteins containing a type 1 site is to mediate electron transfer. As the name suggests, they are characterized by an intense blue colour due to the S(Cys) Sπ → Cu^{2+} charge transfer and by a small hyperfine coupling in the electron paramagnetic resonance spectrum. The structural hallmark of the type 1 binding site is the coordination of copper by two histidines (His) and a cysteine (Cis) residue, leading to a trigonal planar environment found in some laccases (vide infra). In most cases, however, a fourth ligand, often methionine (Met), is complexed, creating a distorted tetrahedral environment around the metal (Fig. II–1, centre). In some proteins, such as azurin, additional side chain coordination leads to a trigonal bipyramid geometry (Fig. II–1, right). Functioning primarily as mediators of electron transfer, the key to the cupredoxin active site is the flexible coordination environment and mixture of hard and soft ligands (His versus Cys) able to accommodate both Cu^{+} and Cu^{2+} oxidation states. This leads to a certain 'metal promiscuity' of cupredoxins, exhibiting Cu transchelation by Zn^{2+}, Hg^{2+}, Cd^{2+}, Co^{2+} and Ni^{2+}. The composition and the variable geometry of the copper type 1 site is also responsible for a variable redox potential, ranging from +183 mV in halocyanin to +680 mV in rusticyanin (compare to +153 mV for aqueous Cu^{2+}/Cu^{+}).

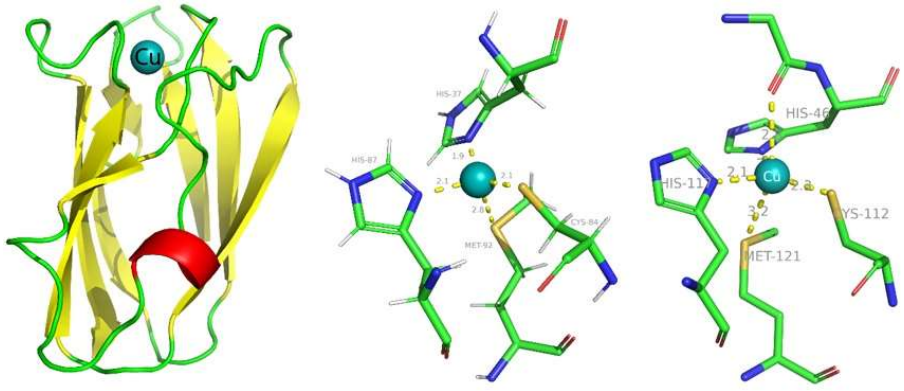

FIG. II–1. Left: crystal structure of plastocyanin (PDB:1PLC); centre: crystal structure of active site of plastocynin (1PLC) [II–3]; right: crystal structure of active site of azurin (PDB:4AZU) [II–4] (reproduced with permission from Refs [II–3, II–4]).

II–1.3. Copper protein containing type 2 sites

In contrast to copper type 1, type 2 binding sites are very heterogeneous in terms of ligand composition, stereochemistries around the metal and reactivity. On the one hand, the type 2 copper binding site lacks Cys-Cu coordination, and as a consequence shows no significant visible absorption. On the other hand, the electron paramagnetic resonance spectrum of the copper type 2 site is characterized by a large hyperfine coupling ($A_{\|}$ = 160–200 × 10^{-4} cm^{-1}). Functionally, type 2 copper proteins are involved in oxygen metabolism and include oxidase, oxygenase and superoxide dismutase subfamilies. One of the most studied members of this family is Cu,Zn superoxide dismutase (Cu,Zn-SOD). Cu,Zn-SOD is found in all eukaryotic tissues and is a critical component of cellular defence against oxidative stress, converting two superoxide radical anions ($\cdot O_2^-$) to dioxygen and H_2O_2. In Cu,Zn-SOD, the Cu and Zn are situated at the bottom of the active site and are coordinated to the same His-61 residue. In the resting state, the Cu^{2+} centre is additionally bound to three other His residues. Upon electron transfer from O_2^- to Cu^{2+}, the copper dissociates from the bridging His-61, which is protonated, while the superoxide is oxidized to O_2. The reduced Cu^+ becomes three coordinated and can act as a reductant for the next superoxide, which is converted into H_2O_2. The trigonal planar geometry of the reduced Cu^+ was elucidated from single crystal structure refinement (Fig. II–2, left) [II–5]. Although it is the copper, and not the zinc, that is essential for catalytic activity, the mutated Zn deficient SOD proteins show decreased stability and have been implicated in the development of familial amyotrophic lateral sclerosis.

Dopamine-β-hydroxylase, another type 2 copper protein, converts dopamine into norepinephrine, constituting one of the crucial neurotransmitter regulators. Its crystal structure is a protein dimer with each chain consisting of four domains and two copper sites, Cu_H and Cu_M. It has been suggested that an

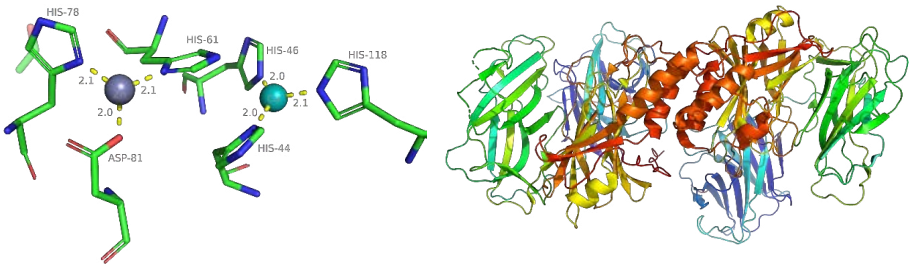

FIG. II–2. Left: coordination structure of the active site of the reduced form of Cu,Zn-SOD (PDB:1Q0E) [II–5]; right: crystal structure of the dopamine-β-hydroxylase (PDB:4ZEL) [II–6] (reproduced with permission from Refs [II–5, II–6]).

initial reduction of the Cu^{2+} centres by two molecules of ascorbic acid leads to the dioxygen and substrate binding, hydroxylation and electron transfer from Cu_H and Cu_M [II–6]. The other copper type 2 family includes amine and galactose and lysyl oxidases, quercetinase and peptidylglycine α-amidating monooxygenase.

II–1.4. Copper proteins containing type 3 sites

Type 3 copper proteins contain two copper atoms (CuA and CuB) in a binuclear centre, where each copper is coordinated to three His residues in a distorted trigonal geometry. Optically, copper type 3 proteins often show a strong absorption at 330 nm, owing to a ligand–metal charge transfer. When oxidized, they absorb in the visible region. Because of antiferromagnetic coupling, the copper type 3 proteins are electron paramagnetic resonance silent. All type 3 copper proteins reversibly bind dioxygen. Functionally, they perform dioxygen transport (haemocyanins), oxidation of diphenols (catechol oxidase) and o-hydroxylation of monophenols (phenol oxidase, tyrosinase). Haemocyanins are large multimeric proteins found in the haemolymph of arthropods and molluscs. The oxygen carrier function of haemocyanins is structurally imposed by a narrow and deep tunnel that leads from the globular protein surface to the binuclear active site (Fig. II–3) [II–7], allowing oxygen to enter and bind to both coppers ions μ–η^2:η^2. Remarkably, when haemocyanins are partially denatured, they start to display phenoloxidase activity, owing to protein unfolding and easier access to organic substrates at the active site. This indicates evolutionary relationships between haemocyanins and phenol oxidases.

Tyrosinase and catechol oxidase are ubiquitous in all three kingdoms of life, participating in immune response, wound healing and pigmentation. Chemically,

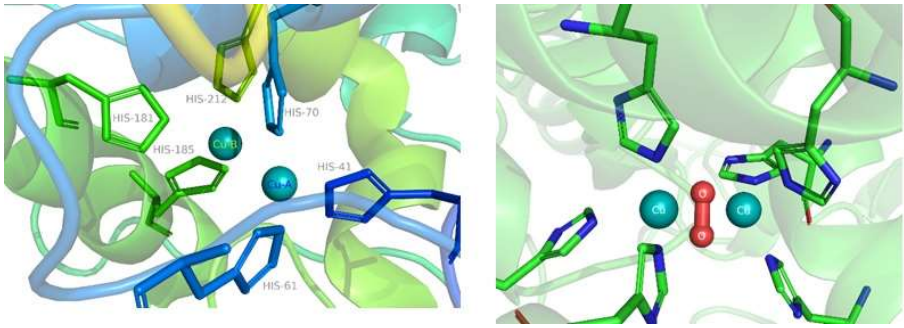

FIG. II–3. Crystal structures of oxygen free (PDB:1LNL, left) [II–7] and oxygenated (PDB:1NOL, right) [II–8] type 3 active sites of haemocyanin (reproduced with permission from Refs [II–7, II–8]).

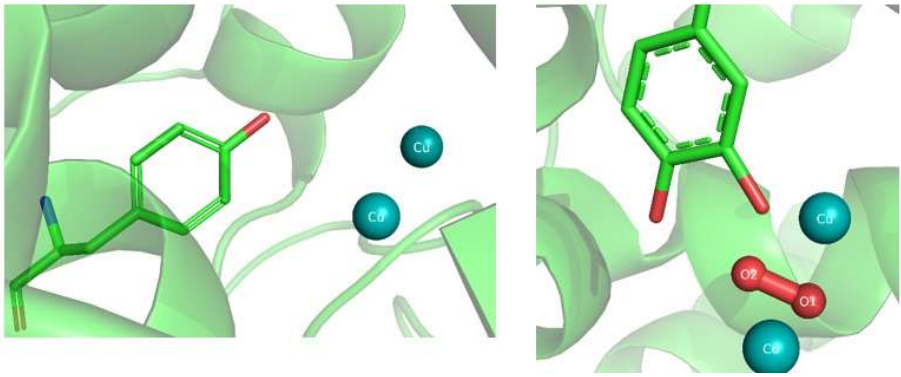

FIG. II–4. Crystal structures of oxygen free (PDB:5Z0D, left) and oxygenated (PDB:5Z0H, right) type 3 active site of tyrosinase, with the substrate and the ortho substituted product highlighted.

they hydroxylate phenols at the ortho position and oxidize the resulting catechols into o-quinones. A recent study caught tyrosinase in action and delineated its oxidation mechanism by providing the crystal structures of the substrate and the oxidized product directly at the active site of the enzyme (Fig. II–4) [II–9].

II–1.5. Blue multicopper oxidases

Blue multicopper oxidases are a unique class of enzymes that contain all three types of copper site in a single enzyme. The presence of four Cu atoms is required for catalytic activity, which includes a 4e oxidation of four 1e donor substrates. Mechanistically, the substrate is bound at the type 1 site, where the copper extracts electrons and transfers them along the 13 Å Cys-His pathway towards the trinuclear (T2, T3, T3′) copper cluster, which binds one molecule of dioxygen (Fig. II–5, left) [II–10]. As a result of a poorly understood process that includes multiple electrons and proton transfers, the substrate undergoes a 1e oxidation, while one molecule of dioxygen is reduced to two molecules of water: $4S + O_2 \rightarrow 2H_2O$ (S: 1e donor substrate). A crystal structure (Fig. II–5, right) of recombinant melanocarpus albomyces laccase (rMaL) captures the essential features of the multicopper oxidase functional site (Fig. II–5, left), including a T2-T3-T3′-bound O_2 [II–10]. The MCO family includes laccase, ascorbate oxidase, ceruloplasmin (Cp), Fet3p[1] and CueO[2],

[1] Fet3p is a multicopper-containing glycoprotein that catalyses the oxidation of Fe(II) to Fe(III).

[2] CueO is a periplasmic protein involved in the Cu efflux system.

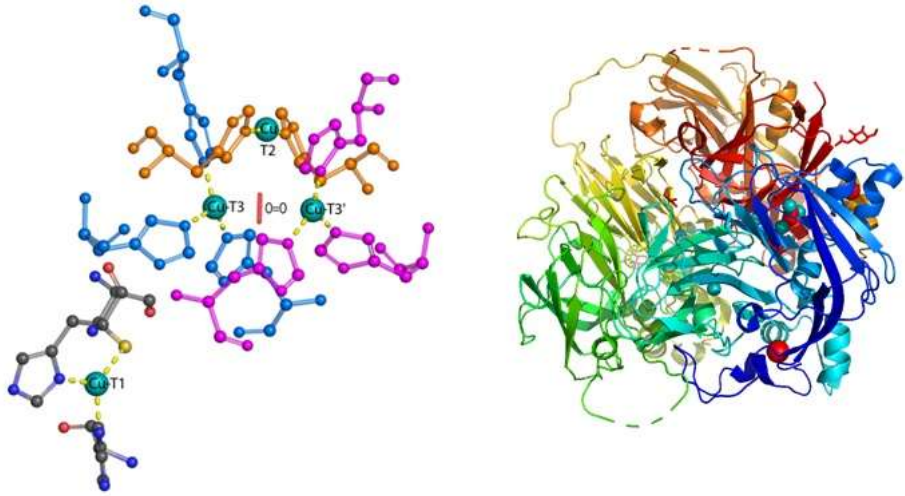

FIG. II–5. Left: crystal structure showing the functional site of rMaL, laccase featuring T1, T2, T3 binding sites and a coordinated O_2 molecule (PDB:2Q9O). Right: crystal structure of human ceruloplasmin (reproduced from Ref. [II–11] with permission).

which oxidizes a variety of phenols and amines, as well as some metal ions, such as Fe^{2+}, Cu^{+} and Mn^{2+}.

Remarkably, copper, which is mainly found in blood plasma, functions not only as an oxidase, but also as a copper transport protein.

II–2. COPPER HOMEOSTASIS, COPPER TRANSPORTERS AND COPPER RELATED GENETIC DISORDERS

Free copper ions are toxic for living organisms [II–12]. Therefore, copper inventory is strictly regulated by copper homeostasis (Fig. II–6) [II–13].

While the number of copper atoms in a cell is of the order of 10^5, there are no free copper ions in either extra- or intracellular domains [II–14]. Normally, dietary copper is absorbed through the small intestine by the duodenal enterocytes, which need to reduce Cu^{2+} to Cu^{+} to transport copper across the cell membrane [II–15]. Upon entering the bloodstream, copper is momentarily scavenged by serum albumin (SA) and transcuprein. Copper-64 labelling studies showed that copper bound to SA (dissociation constant $K_d = 10^{-12}$M) and transcuprein is exchangeable. In SA, Cu^{2+} is complexed to the R–NH_2 terminal and two deprotonated peptide nitrogens (NH of Ala-2 and NH of His-3) as well as to the imidazole nitrogen of His-3 [II–16].

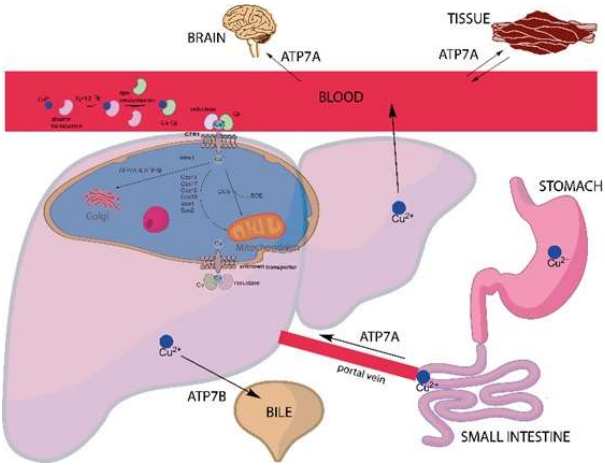

FIG. II–6. Schematic diagram of copper homeostasis (courtesy of F. Zhuravlev, Technical University of Denmark).

Through the portal vein, SA-Cu travels to the liver, where hepatocytes synthesize apo-ceruloplasmin (apo-Cp). There, apo-Cp is loaded with Cu^{2+} and the resulting Cp-Cu does not exchange copper in solution, as shown by the radiolabelled [^{64}Cu]Cu-Cp. Nevertheless, Cp-Cu is the key participant in delivering copper across the cell membrane via Ctr1, a Cu^{+} selective high affinity copper transmembrane transport protein [II–17]. A recent crystal structure of Ctr1 reveals an ion channel-like trimeric structure with two Cu^{+} binding sites [II–18]. The ion channel is gated by 2 × 3 Met residues (Fig. II–7) [II–18]. The Cu^{+} transport might be driven by an electrostatic potential gradient [II–17]. Upon entry in the intercellular domain, Cu^{+} binds to several copper chaperones and delivers them to various organelles, most importantly to mitochondria and the Golgi apparatus. The copper chaperone for SOD (CCS) picks up Cu^{+} in the cytosol and activates SOD1 by directly transferring copper from CCS to SOD1. Despite the simple linear, two coordinate geometry of the CCS binding site (Fig. II–8) [II–19], the binding is extremely tight, as evidenced by bathocuproine sulphonate (BCS) competition. This chelator reacts rapidly with, and has a high affinity for, aqueous Cu^{+} ions (dissociation constant $K_d = 10^{-20}$M]. Thus, CCS effectively prevents the presence of any free copper in the cytosol.

ATP7A regulates Cu^{+} absorption from intestines into the blood. The ATP7B protein is located in the Golgi network of the liver and brain and balances the copper level in the body by excreting excess copper into bile and plasma.

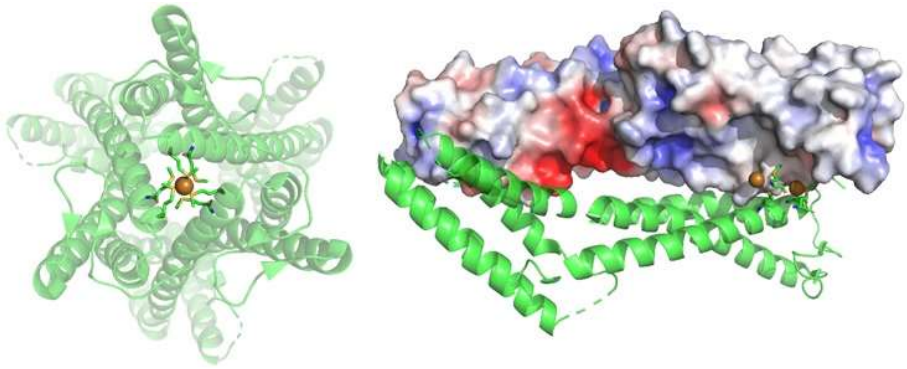

FIG. II–7. Left: crystal structure of Ctr1 showing a trimeric structure forming a Met-gated Cu^{+} ion channel (PDB:6M98). Right: cross-sectional view showing the electrostatic potential surface of chain 2 in the Ctr1 ion channel (red: −5 kT*/e; white: neutral; blue: +5* kT*/e;* k *is the Boltzmann constant,* T *is the temperature and e is the elementary charge). Chain 1 is hidden for clarity (courtesy of F. Zhuravlev, Technical University of Denmark).*

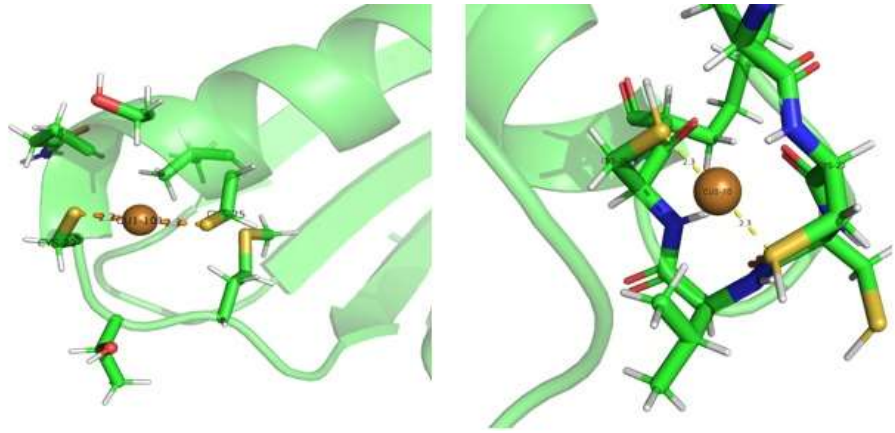

FIG. II–8. Left: crystal structure of the active site of the CCS (PDB:2RSQ). Right: crystal structure of the active site of COX17.

Dysfunctional ATP7A leads to severe copper deficiency (Menkes disease) and is fatal, whereas dysfunctional ATP7B leads to excessive copper accumulation (Wilson's disease) and can be mitigated by treatment with copper chelators (vide infra).

Another copper dependent organelle is the mitochondrion. Six chaperones, cyclooxygenase (COX) 11, COX17, COX19, COX23, SCO1[3] and SCO2, are responsible for delivering copper to the cytochrome c oxidase (Fig. II–8). The active site structure of COX17, which in turn delivers copper to the mononuclear and dinuclear centres in SCO1 and COX11, is shown in Fig. II–8 (right). The X ray analysis reveals a striking similarity between COX17 and CCS copper containing sites: both proteins coordinate copper in a two coordinate, linear arrangement with two Cys residues acting as ligands with a formation constant of ~10^6M–10^7M [II–19].

II–3. NATURAL COPPER CHELATORS

The 8-hydroxyquinoline structure is an important structural motif for chelation of divalent metals such as Cu, Fe and Zn [II–20] (Fig. II–9) [II–21]. Clioquinol (CQ), earlier used to treat human intestinal amoebiasis, has produced promising effects in early clinical trials on Alzheimer's disease patients. CQ forms a 2:1 complex with Cu^{2+} with conditioned stability constant measured in Barth's buffer (mimicking extracellular brain ionic composition) equal to $12 \times 10^9 M^{-2}$ [II–22]. PBT2 was developed as a second generation CQ, showing better solubility and ability to cross the blood brain barrier [II–20].

1,10-Phenanthroline is an iconic organic chelator efficiently ligating the first row transition metals [II–23]. Bathocuproine (BC) is a functionalized phenantroline based chelator that binds tightly to Cu^+ in preference to Cu^{2+} [II–24], with a dissociation constant estimated at 10^{-20}M [II–14]. A crystal structure with two BC ligands complexed to a Cu^+ centre in a tetrahedral fashion is obtained (Fig. II–10) [II–25]. Although Cu^{2+} does not bind as strongly as Cu^+, it still forms isolable tetrahedral complexes with BC. The water soluble version of BC, BCS, is often used as an efficient Cu^+ scavenger in aqueous media.

Penicillamine (D-Pen), found in urine as a metabolite after penicillin administration, has a remarkable capacity to remove copper [II–27]. In solution (in vitro), the interaction of Cu^{2+} with D-Pen leads to a purple $[Cu_4Pen_2Cl]^{5-}$ cluster, which contains both Cu^{2+} and Cu^+ centres (Fig. II–11, part B) [II–9].

---

[3] SCO1 is the name of the gene encoding for the cytochrome c oxidase assembly protein.

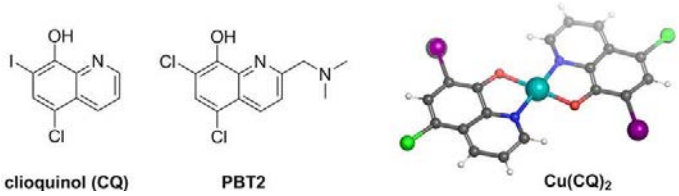

FIG. II–9. Left: 8-hydroxyquinoline based chelators CQ and PBT2 (courtesy of F. Zhuravlev, Technical University of Denmark); right: the crystal structure of $Cu(CQ)_2$.

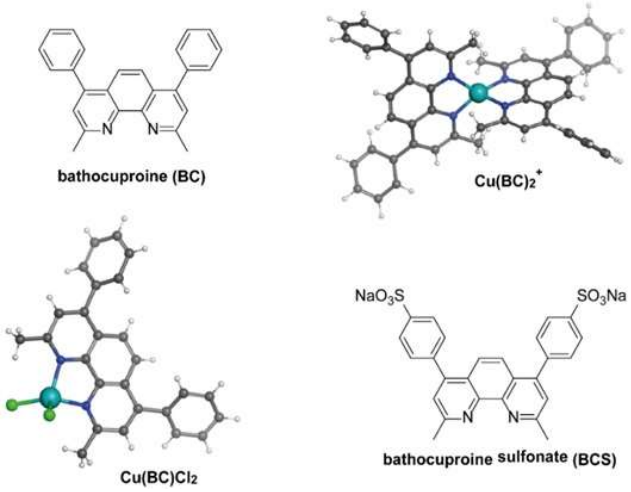

FIG. II–10. 1,10-Phenanthroline based chelators BC and BCS (courtesy of F. Zhuravlev, Technical University of Denmark) and the crystal structures of the corresponding copper complexes (reproduced with permission from Refs [II–25, II–26]).

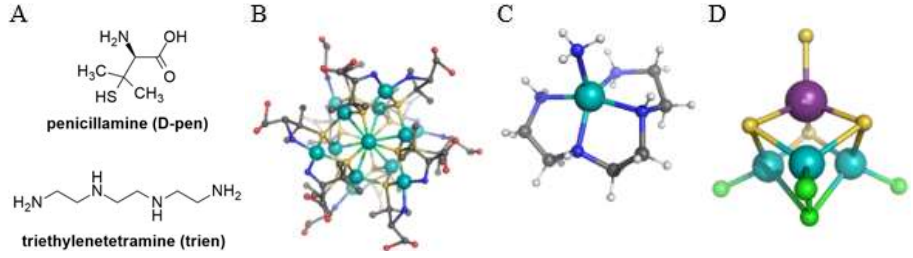

FIG. II–11. (A) The structures of penicillamine (D-Pen) and triethylenetetramine (trien) (courtesy of F. Zhuravlev, Technical University of Denmark). The crystal structures of (B) $[Cu_4Pen_2Cl]^{5-}$; (C) Cu(II)-triethylenetetramine complex; and (D) multicopper tetrahedral tetrathiomolybdate complex.

It is likely that the first step in the reaction of Cu^{2+} with D-Pen in aqueous solution involves the reduction of Cu^{2+} to Cu^{+} and the oxidation of D-Pen to penicillamine disulphide. Although the mobilization of copper by D-Pen in Wilson's disease is complete within 24 h of drug administration, it is unlikely that this reaction takes place in vivo, since neither D-Pen nor its disulphide are able to transchelate the copper bound to albumin, and the cluster has not yet been found in vivo [II–28]. The mechanism of copper removal with D-Pen is still unclear.

Triethylenetetramine (trien) is another efficient Cu^{2+} chelator, approved for the treatment of Wilson's disease by the United States Food & Drug Administration in 1985. Trien is better tolerated than D-Pen and its *p*Cu constant (defined as –log[*M*] and measured keeping [*M*] = 1 μM, [*L*] = 10 μM at pH7.4; *p*Cu: copper potential; [*M*]: molar concentration of metal; [*L*]: molar concentration of ligand) [II–29] was determined to be 17.1 [II–30]. The compound features a penta-ligated copper centre with pyramidal geometry (Fig. II–11, part C) [II–31].

Earlier studies linked excess dietary molybdate (MoO_4^{2-}) uptake with cattle disorders known as 'teart' pastures syndrome and 'swayback' in sheep. It was found that both disorders can be traced to Mo induced copper deficiency induced by tetrathiomolybdate (MoS_4^{2-}), which forms in the digestive tract and readily reacts with copper. Since then, ammonium tetrathiomolybdate has become an important medically relevant Cu chelator. Tetrathiomolybdate inhibits a number of copper chaperones and copper enzymes, including ceruloplasmin, ascorbate oxidase, cytochrome oxidase, superoxide dismutase, tyrosinase and ATPase [II–32]. The crystal structure in Fig. II–11, part D shows how one tetrahedral anion of tetrathiomolybdate can bind several copper ions [II–33].

REFERENCES TO ANNEX II

[II–1] ABOLMAALI, B., TAYLOR, H.V., WESER, U., "Evolutionary aspects of copper binding centers in copper proteins", Bioinorganic Chemistry (CLARKE, M.J., et al., Eds), Springer-Verlag, Berlin (2007) 91–190.

[II–2] CHOI, M., DAVIDSON, V.L., Cupredoxins — a study of how proteins may evolve to use metals for bioenergetic processes, Metallomics **3** 2 (2011) 140.

[II–3] GUSS, J.M., BARTUNIK, H.D., FREEMAN, H.C., Accuracy and precision in protein structure analysis: Restrained least-squares refinement of the structure of poplar plastocyanin at 1.33 Å resolution, Acta Crystallogr. B **48** 6 (1992) 790.

[II–4] NAR, H., MESSERSCHMIDT, A., HUBER, R., VAN DE KAMP, M., CANTERS, G.W., Crystal structure analysis of oxidized Pseudomonas aeruginosa azurin at pH 5.5 and pH 9.0: A pH-induced conformational transition involves a peptide bond flip, J. Mol. Biol. **221** 3 (1991) 765.

[II–5] HOUGH, M.A., HASNAIN, S.S., Structure of fully reduced bovine copper zinc superoxide dismutase at 1.15 Å, Structure **11** 8 (2003) 937.

[II–6] VENDELBOE, T.V., et al., The crystal structure of human dopamine β-hydroxylase at 2.9 Å resolution, Sci. Adv. **2** (2016) e1500980.
[II–7] PERBANDT, M., et al., The structure of a functional unit from the wall of a gastropod hemocyanin offers a possible mechanism for cooperativity, Biochemistry **42** 21 (2003) 6341.
[II–8] HAZES, B., et al., Crystal structure of deoxygenated limulus polyphemus subunit II hemocyanin at 2.18 Å resolution: Clues for a mechanism for allosteric regulation, Protein Sci. **2** 4 (1993) 597.
[II–9] BIRKER, P.J.M.W.L., FREEMAN, H.C., Structure, properties, and function of a copper(I)-copper(II) complex of D-penicillamine: pentathallium(I) μ_8-chloro-dodeca (D-penicillaminato)-octacuprate(I)hexacuprate(II) *n*-hydrate, J. Am. Chem. Soc. **99** 21 (1977) 6890.
[II–10] HAKULINEN, N., et al., A near atomic resolution structure of a *Melanocarpus albomyces* laccase, J. Struct. Biol. **162** 1 (2008) 29.
[II–11] SAMYGINA, V.R., et al., Ceruloplasmin: macromolecular assemblies with iron-containing acute phase proteins, PLoS One **8** 7 (2013) e67145.
[II–12] STAUBER, J.L., FLORENCE, T.M., Mechanism of toxicity of ionic copper and copper complexes to algae, Mar. Biol. **94** 4 (1987) 511.
[II–13] LUTSENKO, S., Human copper homeostasis: A network of interconnected pathways, Curr. Opin. Chem. Biol. **14** (2010) 211.
[II–14] RAE, T.D., SCHMIDT, P.J., PUFAHL, R.A., CULOTTA, V.C., O'HALLORAN, T.V., Undetectable intracellular free copper: the requirement of a copper chaperone for superoxide dismutase, Science **284** 5415 (1999) 805.
[II–15] COLLINS, J.F., PROHASKA, J.R., KNUTSON, M.D., Metabolic crossroads of iron and copper, Nutr. Rev. **68** (2010) 133.
[II–16] VALKO, M., et al., High-affinity binding site for copper(II) in human and dog serum albumins (an EPR study), J. Phys. Chem. B **103** 26 (1999) 5591.
[II–17] RAMOS, D., et al., Mechanism of copper uptake from blood plasma ceruloplasmin by mammalian cells, PLoS One **11** 3 (2016) e0149516.
[II–18] REN, F., et al., X-ray structures of the high-affinity copper transporter Ctr1, Nat. Commun. **10** 1 (2019) 1–9.
[II–19] ABAJIAN, C., YATSUNYK, L.A., RAMIREZ, B.E., ROSENZWEIG, A.C., Yeast Cox17 solution structure and copper(I) binding, J. Biol. Chem. **279** 51 (2004) 53584.
[II–20] PRACHAYASITTIKUL, V., PRACHAYASITTIKUL, S., RUCHIRAWAT, S., PRACHAYASITTIKUL, V., 8-Hydroxyquinolines: A review of their metal chelating properties and medicinal applications, Drug Des. Devel. Ther. **7** (2013) 1157.
[II–21] DI VAIRA, M., et al., Clioquinol, a drug for Alzheimer's disease specifically interfering with brain metal metabolism: Structural characterization of its zinc(II) and copper(II) complexes, Inorg. Chem. **43** 13 (2004) 3795.
[II–22] FERRADA, E., et al., Stoichiometry and conditional stability constants of Cu(II) or Zn(II) clioquinol complexes; implications for Alzheimer's and Huntington's disease therapy, Neurotoxicology **28** 3 (2007) 445.
[II–23] BENCINI, A., LIPPOLIS, V., 1,10-Phenanthroline: A versatile building block for the construction of ligands for various purposes, Coord. Chem. Rev. **254** (2010) 2096.

[II–24] MOFFETT, J.W., ZIKA, R.G., PETASNE, R.G., Evaluation of bathocuproine for the spectro-photometric determination of copper(I) in copper redox studies with applications in studies of natural waters, Anal. Chim. Acta **175** C (1985) 171.

[II–25] KLEMENS, F.K., FANWICK, P.E., BIBLER, J.K., McMILLIN, D.R., Crystal and molecular structure of $[Cu(bcp)_2]BF_4 \cdot CH_3OH$ (bcp = 2,9-dimethyl-4,7-diphenyl-1,10-phenanthroline), Inorg. Chem. **28** (1989) 3076.

[II–26] WALL, M., LINKLETTER, B., WILLIAMS, D., HYNES, R.C., CHIN, J., Rapid hydrolysis of 2',3'-cAMP with a Cu(II) complex: Effect of intramolecular hydrogen bonding on the basicity and reactivity of a metal-bound hydroxide, J. Am. Chem. Soc. **121** 19 (1999) 4710.

[II–27] TEGONI, M., VALENSIN, D., TOSO, L., REMELLI, M., Copper chelators: Chemical properties and bio-medical applications, Curr. Med. Chem. **21** 33 (2014) 3785.

[II–28] LAURIE, S.H., PRIME, D.M., The formation and nature of the mixed valence copper-D-penicillamine-chloride cluster in aqueous solution and its relevance to the treatment of Wilson's disease, J. Inorg. Biochem. **11** 3 (1979) 229.

[II–29] HARRIS, W.R., RAYMOND, K.N., WEITL, F.L., Ferric ion sequestering agents; 6; The spectrophotometric and potentiometric evaluation of sulfonated tricatecholate ligands, J. Am. Chem. Soc. **103** 10 (1981) 2667.

[II–30] NURCHI, V.M., et al., Complex formation equilibria of Cu^{II} and Zn^{II} with triethylenetetramine and its mono- and di-acetyl metabolites, Dalton Trans. **42** 17 (2013) 6161.

[II–31] BRYLEV, K.A., NAUMOV, N.G., PERIS, G., LLUSAR, R., FEDOROV, V.E., Novel inorganic ionic compounds based on Re_6 chalcocyanide cluster complexes: Synthesis and crystal structures, Polyhedron **22** 25–26 (2003) 3383.

[II–32] ALVAREZ, H.M., et al., Tetrathiomolybdate inhibits copper trafficking proteins through metal cluster formation, Science **327** 5963 (2010) 331.

[II–33] SHIN, B.K., HAN, J., Structure and physical properties of copper thiomolybdate complex, $({}^nBu_4N)_3[MoS_4Cu_3Cl_4]$, Bull. Korean Chem. Soc. **29** 11 (2008) 2299.

Annex III

DETAILED PROCEDURE FOR THE DEVELOPMENT OF A ^{64}Cu-NOTA-mAb FOR PET APPLICATIONS

In this annex, a generic protocol for ^{64}Cu labelling and quality control of a monoclonal antibody (mAb) (an immunoglobulin G model) is described in detail [III–1]. Figure III–1 demonstrates the schematic process for the development of the product. In short, ^{64}Cu-NOTA-mAb is prepared with the following steps:

— Conjugation of mAb with *p*-SCN-Bn-NOTA as a bifunctional chelator and for purification;
— Determination of the average number of NOTA conjugated per mAb;
— Immunoconjugate labelling with ^{64}Cu in chloride form;
— Immunoreactivity determination;
— Stability determination studies;
— Internalization of the radiolabelled antibody in target cells.

III–1. PROCEDURES

III–1.1. Radionuclide

Although the best source of ^{64}Cu is production via ^{64}Ni(p, n), with the highest purity and quality specificity for peptide radiopharmaceutical production, radiolabelling of mAbs using copper produced by the ^{68}Zn(p, αn) method has also been successfully reported [III–2, III–3]. In this case, ^{64}Cu chloride was obtained from a commercial source producing ^{64}Cu via the ^{68}Zn(p, αn)^{64}Cu reaction with a proton energy from 20 to 35 MeV, which is usually enough for preparing diagnostic scales of ^{64}Cu mAbs (radionuclidic purity >99.8%; chemical purity: Cu <0.5 ppm, Zn <0.5 ppm; radiochemical purity >99.9% instant thin layer chromatography (iTLC)).

III–1.2. Preparation of mAb

mAbs are usually prepared from a specific hybridoma cell line or purchased as ready to use injections (commercially available or developed in house). In the latter case, a preliminary purification using a size exclusion method is necessary to remove the excipients before reconstitution in a suitable buffer for

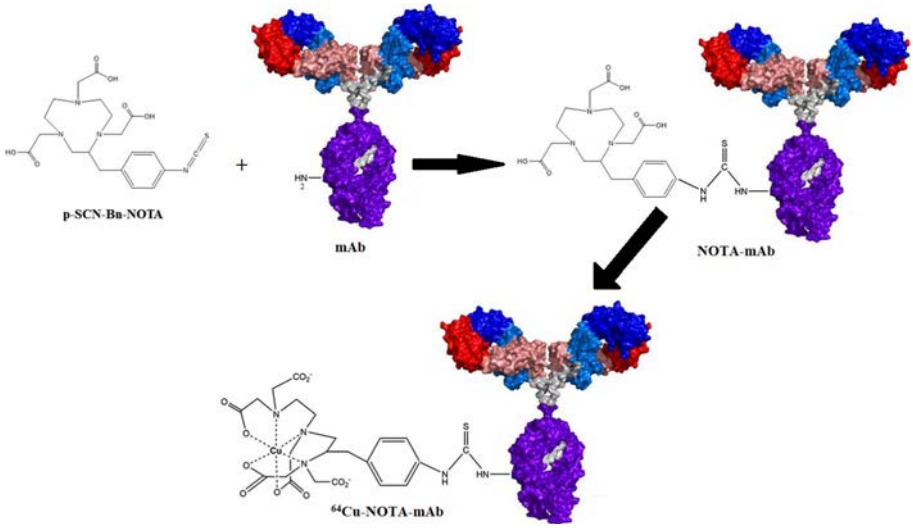

FIG. III–1. Schematic route to the preparation of ^{64}Cu-NOTA-mAb (adapted, with permission, from an original figure produced by B. Alirezapour).

the conjugation step. In the first case, the cells are usually cultured in RPMI 1 640 medium, supplemented with 10% foetal calf serum (heat inactivated), 2 mM glutamine, 100 µg/ml streptomycin and 100 IU/ml penicillin. The supernatant of the cell culture medium is collected and mAb is concentrated by ultrafiltration and salting out methods. The final purification is performed by affinity chromatography (protein A coupled to CNBr activated sepharose). Furthermore, the procedure has also been performed on a large scale using a cell line 1000 bioreactor (Integra Bioscience).

III–1.3. Reactivity of mAb towards antigen expressing cells by the enzyme linked immunosorbent assay method

The recombinant mAb is purified by an antibody sepharose affinity (immunoaffinity) column, which is explained in Ref. [III–4]. Purified mAb is coated onto the wells of microtiter plates (0.6 µg per well) at 37°C overnight. Bovine serum albumin (BSA) is used as negative control. The contents of the wells are emptied, washed and blocked with a 4% solution of skimmed milk in PBS (10 mM, pH7.2) for 1 h at 37°C. At the end of the incubation time, the wells are washed, before dilutions of mAb are added and incubated at 37°C for 2 h. Next, the wells are emptied and washed, and the required dilution of rabbit anti-mouse conjugated to horseradish peroxidase is added and incubated at 37°C for 1 h. Finally, the wells are washed, 50 µl of substrate tetramethylbenzidine

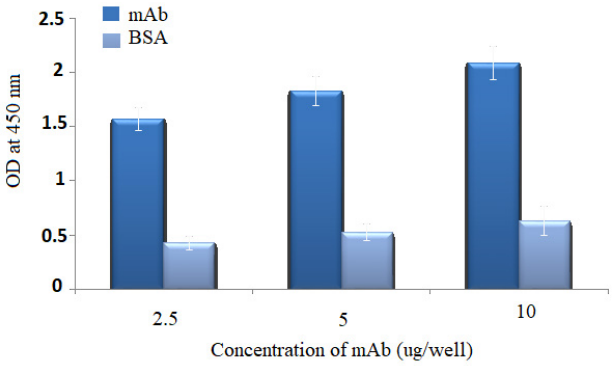

FIG. III–2. Reactivity of mAb (2.5, 5 and 10 µg per well) towards cancerous mAb (0.6 µg per well) and BSA (0.6 µg per well). Assays were performed in duplicate (adapted, with permission, from an original figure produced by B. Alirezapour).

(Roche Diagnostics) is added and the contents are incubated for 10 min. The reaction is stopped by adding 50 µl of 1M H_2SO_4 per well and the results are read at 450 nm in the enzyme linked immunosorbent assay (ELISA) autoreader. Figure III–2 demonstrates the results of mAb reactivity towards antigen expressing cells by ELISA.

III–1.4. Conjugation of *p*-SCN-Bn-NOTA with mAb

The conjugation process is performed as demonstrated in Fig. III–1. The purified antibody concentration is measured using a biophotometer (Eppendorf) at optical density OD = 280 nm, and then mAb (3.3 mg in 1 ml bicarbonate buffer; 0.2M Na_2CO_3, pH9.2) is added to a 50-fold molar excess of NOTA bifunctional agent (in this case, *p*-SCN-Bn-NOTA) (850 ng in 400 µl bicarbonate buffer (0.2M, pH9.2) in a borosilicate vial and mixed gently 20 times by pipetting. The mixture is gently shaken and incubated at room temperature for 12 h. The mixture is then transferred on a Vivaspin-2 cutoff filter (30 kDa) and centrifuged at 2.684*g* for 15 min. In order to terminate the conjugation step and provide the suitable radiolabelling pH, the upper filter fraction is washed thoroughly using ammonium acetate buffer (0.2M, pH5.5) three times in order to remove excess NOTA. At this stage, ammonium acetate buffer (1 ml) is added to the upper filter fraction and the mixture is pipetted 10–20 times for immunoconjugate dissolution. The filter is then centrifuged upside down at 2.684*g* for 5 min. The antibody conjugate concentration is measured using a biophotometer (Eppendorf) at OD = 280 nm.

III–1.5. Determination of the average chelate:antibody ratio

The spectrophotometric method for quantity measurement of micromolar concentrations of bifunctional NOTA ligand in NOTA–mAb conjugates is performed according to the method reported in Ref. [III–5]. Briefly, the optical density of arsenazo yttrium (III) complex (2:1, 1 ml), prepared in 5.0 µM AAIII, 1.6 µM Y(III), 0.15M sodium acetate buffer, pH4.0, is measured at 652 nm. A standard curve is then plotted by the addition of multiple (eight) 15 µl NOTA standard solutions (NOTA dissolved in 0.15M sodium acetate buffer, pH4.0) to the above mixture. In the second step, the optical density of 1:2 yttrium(III) complex of arsenazo (1 ml) is measured at 652 nm in the presence of conjugation product in order to determine NOTA antibody attachments (Fig. III–3).

III–1.6. Radiolabelling of the antibody conjugate with copper-64

Typically, 37.5 to 58 MBq of [^{64}Cu]$CuCl_2$ (in 0.2M HCl) is added to a conical vial and dried under a flow of nitrogen. Acetate buffer (500 µl, pH5.5) is added to the copper containing vial and the vial is vortexed for 10 min. The conjugate containing fraction (250 µg) in acetate buffer with the measured protein content is added to the vial and mixed gently for 5 min using pipetting (10–20 times). The mixture is then incubated at 38°C for 30 min, followed by testing the radiochemical purity by iTLC using a radio TLC scanner (Whatman No. 2, 1 mM diethylenetriaminepentaacetic acid (DTPA)). Finally, ETDA solution (5–10 µl, 10 mM) is added to the labelling mixture and incubated for 10 min to scavenge

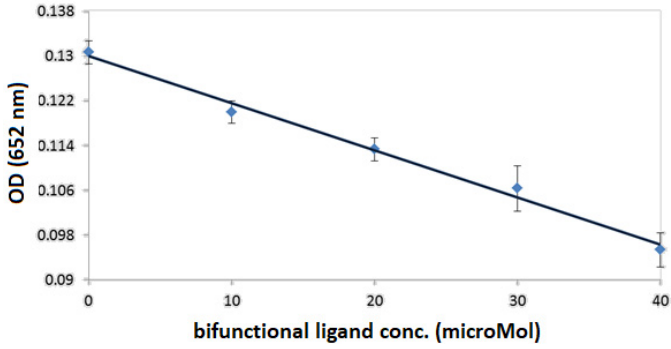

FIG. III–3. The absorption of Arsenazo III and yttrium(III) complex versus the concentration of p-SCN-Bn-NOTA at 652 nm; error bars represent standard error of the mean (adapted, with permission, from an original figure produced by B. Alirezapour).

the unlabelled Cu cation. Table III–1 demonstrates the retention factors of various possible radiochemical species found in the reaction mixture.

Using the above mentioned retention conditions, evaluation of various conjugation aliquots with different chelate:antibody ratios was performed, and the radiochemical purities of the reaction mixtures are listed in Table III–2.

To show the timeframe of the radiolabelling process at the optimized conditions, such as temperature, conjugate content and chelate ratio, Fig. III–4 demonstrates the labelling process, showing that after 30 min the best complexation ratio is obtained.

A better overview of the radiochromatogram is given in Fig. III–5, which demonstrates the peaks for the free copper cation as well as the radiolabelling mixture. To show the molecular integrity of the mAb during the conjugation and radiolabelling gel electrophoresis of the initial mAb, the conjugates mixture as well as the final radiolabelled antibody are shown in Fig. III–6. All samples showed a molecular mass related to the whole IgG of 150 kDa, compared with the standard molecular weight marker.

TABLE III–1. RETENTION FACTORS OF CHEMICAL IMPURITIES AND NOTA CONJUGATES

Chromatography system	Chemical species	Mobile phase	Stationary phase	Rf
1	^{64}Cu-NOTA-mAb	10% ammonium acetate:methanol (1:1)	Silica gel	0.0
	$^{64}Cu^{2+}$	n.a.	n.a.	0.0
	^{64}Cu-NOTA	n.a.	n.a.	0.3
2	^{64}Cu-NOTA-mAb	1 mM DTPA (pH5)	Whatman No. 2	0.0
	$^{64}Cu^{2+}$	n.a.	n.a.	0.9
	^{64}Cu-NOTA	n.a.	n.a.	0.0

Note: n.a.: not applicable.

TABLE III–2. MEAN VALUES OF CHELATOR:ANTIBODY RATIOS AND RADIOCHEMICAL PURITY FOR NOTA-mAb RADIOIMMUNOCONJUGATES (400 μg) AFTER 1 h AT pH5.5

Molar excess of chelator added to the conjugation reaction	Average chelator:mAb	Radiochemical purity (%)
50	3.3 ± 0.3	92.1 ± 1.5
80	5.9 ± 0.8	97.7 ± 1.4
120	10.8 ± 0.5	98.9 ± 0.8

Note: $p < 0.05$ ($n = 2$).

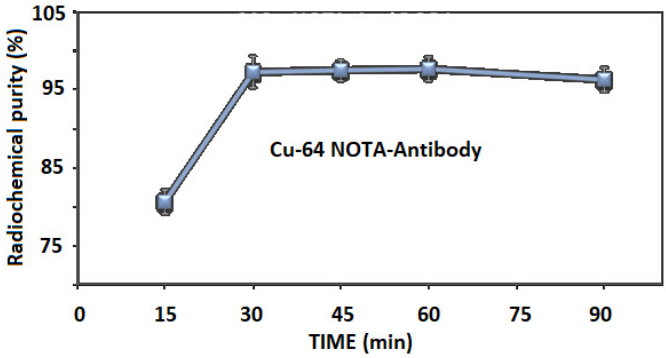

FIG. III–4. Radiochemical purities of ^{64}Cu-NOTA-mAb labelling mixture versus time (adapted, with permission, from an original figure produced by B. Alirezapour).

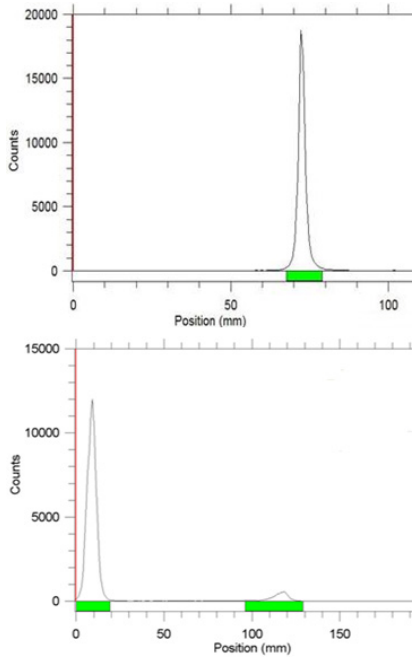

FIG. III–5. iTLC chromatograms of $^{64}CuCl_2$ solution (top) and final ^{64}Cu-NOTA-mAb solution (bottom) on Whatman No. 2 paper using 1 mM DTPA solution (pH5) (adapted, with permission, from an original figure produced by B. Alirezapour).

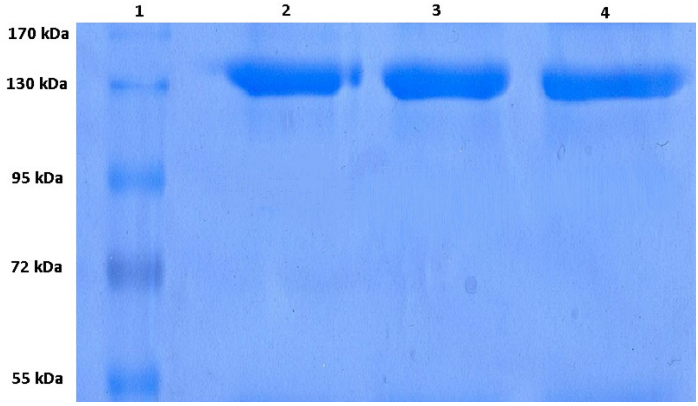

FIG. III–6. SDS-PAGE of the ^{64}Cu-NOTA-mAb (lane 2), conjugated NOTA-mAb (lane 3), purified initial cold mAb (lane 4) and standard high molecular mass protein marker (molecular weights: 170, 130, 95, 72 and 55 kDa) (lane 1) (adapted, with permission, from an original figure produced by B. Alirezapour).

III–1.7. Stability testing of the ^{64}Cu-NOTA-mAb in the presence of human serum and PBS

iTLC was performed to assess the in vitro stability of ^{64}Cu-NOTA-mAb in human serum. 200 µl (300 µCi) of the ^{64}Cu-NOTA-mAb complex was added to 1 ml of fresh human serum and 1 ml PBS separately, and was incubated at 37°C for different times (6 h, 12 h, 24 h and 48 h). 1 cm × 10.5 cm strips of Whatman No. 2 paper were used for checking each sample at different times. Five microlitres of ^{64}Cu-NOTA-mAb and serum containing this complex were applied to each strip at 1 cm from the bottom (origin) and the solvent (1 mM DTPA) front could rise to 10 cm from the bottom of the strip. Finally, each strip was read by a radio TLC scanner. Table III–3 demonstrates the conditions and stability data of ^{64}Cu-NOTA-mAb.

III–1.8. Reactivity of ^{64}Cu-NOTA-mAb towards the antigen by radioimmunoassay

After labelling of mAb with ^{64}Cu, the reactivity of ^{64}Cu-NOTA-mAb towards the antigen is usually considered by radioimmunoassay. Purified antigen is coated onto the wells of microtiter plates (0.2 µg per well) at 37°C overnight, and the same concentration of BSA is used as negative control. The contents of the wells are emptied, washed and blocked with a 4% solution of skimmed milk for 1 h at 37°C. Finally, the wells are washed and 30 000 cpm (counts per minute) of ^{64}Cu-NOTA-mAb

TABLE III–3. STABILITY OF ^{64}Cu-NOTA-mAb IN FRESH HUMAN SERUM AND PBS AT DIFFERENT TIMES (0, 6, 12, 24 AND 48 h).

Time after labelling (h)	PBS (4°C)	Human serum (37°C)
0	97.7 ± 1.45	97.7 ± 1.45
6	97.1 ± 1.84	96.2 ± 1.23
12	96.2 ± 1.34	92.6 ± 1.14
24	94.0 ± 2.03	88.1 ± 1.19
48	92.1 ± 1.01	81.5 ± 2.65

Note: Error bars represent the standard error of the mean for duplicates.

is added before incubation at 37°C for 2 h. The content of the wells is then emptied, the wells are washed again, and the radioactivity of the wells is measured by a gamma counter. The reactivity of a model mAb is usually compared to a non-specific protein such as BSA, as can be seen in Fig. III–7.

III–1.9. Immunoreactivity of ^{64}Cu-NOTA-mAb towards antigen expressing and non-expressing cell lines

The immunoreactivity of ^{64}Cu-NOTA-mAb towards antigen expressing and non-expressing cell lines is usually determined using a double inverse of the binding data, which may be considered a modification of the Lineweaver–Burk plot, as follows. Different quantities (5×10^6, 2.5×10^6, 1.25×10^6, 0.62×10^6, 0.31×10^6 and 0.15×10^6) of two different cells are added to the tubes, before 30 000 cpm of ^{64}Cu-NOTA-mAb is added and the mixture is incubated for 3 h at 4°C. After incubation, the radioactivity of the tubes is read by a gamma counter. Next, the tubes are centrifuged at 3000*g*, the supernatant is discarded and the radioactivity of the cells in the precipitate is read by a gamma counter. The immunoreactivity is determined using a Lineweaver–Burk plot and the data is analysed by the Lindmo method [III–6]. Figure III–8 demonstrates the specific binding of the mAb against the inverse of the cell concentration.

III–1.10. Internalization assays

Internalization studies were performed using acid dissociation of ^{64}Cu-NOTA-mAb [III–7]. Separate antigen expressing and non-expressing cell lines were harvested and resuspended in medium at 1×10^5 cells per 200 µl

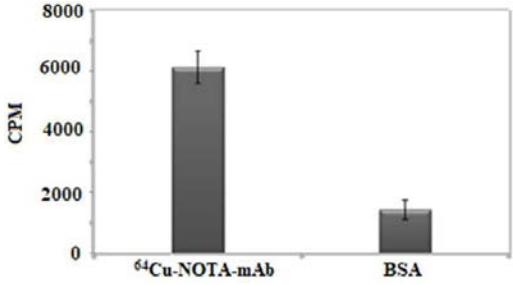

FIG. III–7. Reactivity of ^{64}Cu-NOTA-mAb (5 µg per well) towards specific antigen (0.2 µg per well) and BSA (0.2 µg per well). All assays were performed in duplicate (adapted, with permission, from an original figure produced by B. Alirezapour).

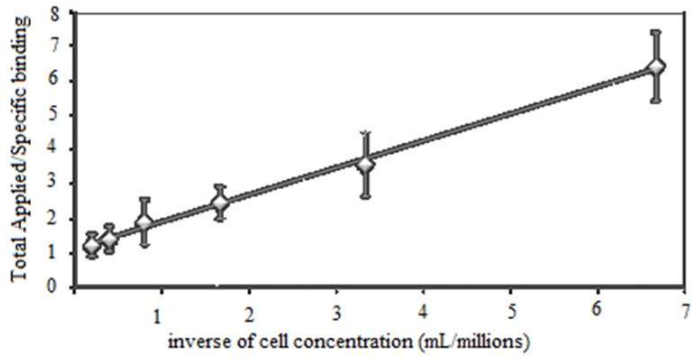

FIG. III–8. Immunoreactivity of ^{64}Cu-NOTA-mAb (total applied to specific binding) towards the antigen positive cell line at different cell concentrations (5×10^6, 2.5×10^6, 1.25×10^6, 0.62×10^6, 0.31×10^6 and 0.15×10^6) (adapted, with permission, from an original figure produced by B. Alirezapour).

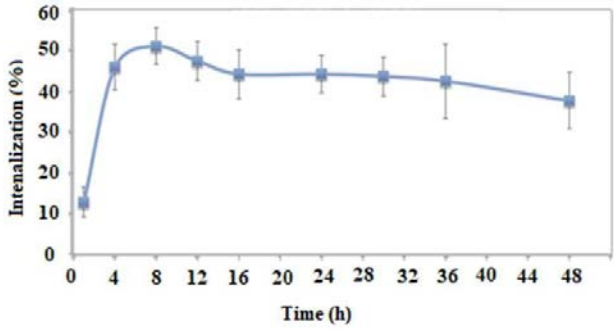

FIG. III–9. Internalization study of ^{64}Cu-NOTA-mAb by the MDA-MB-231 cell line at different times (1, 4, 8, 12, 16, 24, 30, 36 and 48 h) (adapted, with permission, from an original figure produced by B. Alirezapour).

and cultured in 24 well plates. After 24 h, 30 000 cpm of ^{64}Cu-NOTA-mAb was added to each well and incubated at 37°C. At various times (4, 8, 12, 16, 24, 30 and 36 h), the RPMI medium in the wells was removed from the cells, and half of the wells were then exposed to a 1 ml solution of 0.1M NaOH while the other half were exposed to a 1 ml solution of 0.1M acetic acid pH4.0. After 15 min, the radioactivity content of the supernatant was measured by a gamma counter. The NaOH solution destroyed cell lines and the solutions were considered as the whole activity (internalized, bound and dissociated ^{64}Cu-NOTA-mAb). The acetic

acid dissociated the interaction between ^{64}Cu-NOTA-mAb and the antigen in the surface of antigen expressing and non-expressing (in the case of non-specific binding) cell lines, and the radioactivity of this solution was considered as the bound and dissociated ^{64}Cu-NOTA-mAb. The difference between the two activities was considered as the activity of the internalized labelled compound, as shown in Fig. III–9.

REFERENCES TO ANNEX III

[III–1] ALIREZAPOUR, B., Production and Quality Control of Diagnostic Positron Emitter Radioimmunoconjugates (^{64}Cu-PR81 and ^{64}Cu-Trastuzumab) for Mouse Breast Tumor Imaging Using Dual Head SPECT, PhD Thesis, NSTRI (2013) (in Persian).

[III–2] ALIREZAPOUR, B., et al., Development of [^{64}Cu]-DOTA-PR81 radioimmunoconjugate for MUC-1 positive PET imaging, Nucl. Med. Biol. **43** 1 (2016) 73.

[III–3] ALIREZAPOUR, B., et al., Optimized preparation and preliminary evaluation of [^{64}Cu]–DOTA–trastuzumab for targeting ErbB2/Neu expression, J. Radioanal. Nucl. Chem. **295** 2 (2013) 1261.

[III–4] MOHAMMADNEJAD, J., et al., A new competitive enzyme linked immunosorbent assay (MRP83-CA15-3) for MUC1 measurement in breast cancer, J. Immunoassay Immunochem. **27** 2 (2006) 139.

[III–5] PIPPIN, C.G., PARKER, T.A., McMURRY, T.J., BRECHBIEL, M.W., Spectrophotometric method for the determination of a bifunctional DTPA ligand in DTPA-monoclonal antibody conjugates, Bioconjugate Chem. **3** 4 (1992) 342.

[III–6] LINDMO, T., BOVEN, E., CUTTITTA, F., FEDORKO, J., BUNN P.A., Jr, Determination of the immunoreactive function of radiolabeled monoclonal antibodies by linear extrapolation to binding at infinite antigen excess, J. Immunol. Methods **72** 1 (1984) 77.

[III–7] MATZKU, S., et al., Antibody transport and internalization into tumours, Br. J. Cancer Suppl. **10** (1990) 1.

ABBREVIATIONS

BBN	bombesin peptide
BC	bathocuproine
BCS	bathocuproine sulphonate
BSA	bovine serum albumin
CCS	copper chaperone for superoxide dismutase
COX	cyclooxygenase
CT	computed tomography
Ctr1	copper transport protein
FDG	^{18}F-fluorodeoxyglucose
GMP	good manufacturing practice
GRP	gastrin releasing peptide
HPLC	high performance liquid chromatography
iTLC	instant thin layer chromatography
LNCaP	lymph node carcinoma of the prostate
mAb	monoclonal antibody
microPET	micro-positron emission tomography
MIRD	medical internal radiation dose
MRI	magnetic resonance imaging
NEN	neuroendocrine neoplasm
NET	neuroendocrine tumour
NMR	nuclear magnetic resonance
p.i.	post-injection
PBS	phosphate buffered saline
PCa	prostate cancer
PET	positron emission tomography
PSA	prostate-specific antigen
PSMA	prostate-specific membrane antigen
SA	serum albumin
SCID	severe combined immunodeficient
SEC-HPLC	size exclusion high performance liquid chromatography
SSA	synthetic somatostatin analogue
SST	somatostatin
TLC	thin layer chromatography
TRT	targeted radionuclide therapy

CONTRIBUTORS TO DRAFTING AND REVIEW

Alirezapour, B.	Nuclear Science and Technology Research Institute, Islamic Republic of Iran
Alves, F.	University of Coimbra, Portugal
Avila-Rodriguez, M.A.	National Autonomous University of Mexico, Mexico
Cutler, C.S.	Brookhaven National Laboratory, United States of America
Denecke, M.	International Atomic Energy Agency
Giammarile, F.	International Atomic Energy Agency
Gutfilen, B.	Universidade Federal do Rio de Janeiro, Brazil
Jalilian, A.	International Atomic Energy Agency
Lyashchenko, S.K.	Memorial Sloan Kettering Cancer Center, United States of America
Mirzaei, S.	Wilhelminenspital, Austria
Singh, A.	Zentralklinik Bad Berka, Germany
Smith, J.	University of Missouri, United States of America
Zhuravlev, F.	Technical University of Denmark, Denmark

Consultants Meeting

Vienna, Austria: 26–29 August 2019

IAEA
International Atomic Energy Agency

No. 26

ORDERING LOCALLY

IAEA priced publications may be purchased from the sources listed below or from major local booksellers.

Orders for unpriced publications should be made directly to the IAEA. The contact details are given at the end of this list.

NORTH AMERICA

Bernan / Rowman & Littlefield
15250 NBN Way, Blue Ridge Summit, PA 17214, USA
Telephone: +1 800 462 6420 • Fax: +1 800 338 4550
Email: orders@rowman.com • Web site: www.rowman.com/bernan

REST OF WORLD

Please contact your preferred local supplier, or our lead distributor:

Eurospan Group
Gray's Inn House
127 Clerkenwell Road
London EC1R 5DB
United Kingdom

Trade orders and enquiries:
Telephone: +44 (0)176 760 4972 • Fax: +44 (0)176 760 1640
Email: eurospan@turpin-distribution.com

Individual orders:
www.eurospanbookstore.com/iaea

For further information:
Telephone: +44 (0)207 240 0856 • Fax: +44 (0)207 379 0609
Email: info@eurospangroup.com • Web site: www.eurospangroup.com

Orders for both priced and unpriced publications may be addressed directly to:

Marketing and Sales Unit
International Atomic Energy Agency
Vienna International Centre, PO Box 100, 1400 Vienna, Austria
Telephone: +43 1 2600 22529 or 22530 • Fax: +43 1 26007 22529
Email: sales.publications@iaea.org • Web site: www.iaea.org/publications

ALTERNATIVE RADIONUCLIDE PRODUCTION WITH A CYCLOTRON
IAEA Radioisotopes and Radiopharmaceuticals Reports No. 4
STI/PUB/1937 (69 pp.; 2021)
ISBN 978-92-0-103021-4 Price: €40

PRODUCTION AND QUALITY CONTROL OF FLUORINE-18 LABELLED RADIOPHARMACEUTICALS
IAEA-TECDOC-1968 (166 pp.; 2021)
ISBN 978-92-0-122721-8 Price: €18

PRODUCTION, QUALITY CONTROL AND CLINICAL APPLICATIONS OF RADIOSYNOVECTOMY AGENTS
IAEA Radioisotopes and Radiopharmaceuticals Reports No. 3
STI/PUB/1915 (69 pp.; 2021)
ISBN 978-92-0-118520-4 Price: €42

THERAPEUTIC RADIOPHARMACEUTICALS LABELLED WITH COPPER-67, RHENIUM-186 AND SCANDIUM-47
IAEA-TECDOC-1945 (56 pp.; 2021)
ISBN 978-92-0-127222-5 Price: €18

PRODUCTION OF EMERGING RADIONUCLIDES TOWARDS THERANOSTIC APPLICATIONS: COPPER-61, SCANDIUM-43 AND -44, AND YTTRIUM-86
IAEA-TECDOC-1955 (70 pp.; 2021)
ISBN 978-92-0-107321-1 Price: €18

QUALITY CONTROL IN THE PRODUCTION OF RADIOPHARMACEUTICALS
IAEA-TECDOC-1856 (148 pp.; 2018)
ISBN 978-92-0-107918-3 Price: €18

CYCLOTRON BASED PRODUCTION OF TECHNETIUM-99m
IAEA Radioisotopes and Radiopharmaceuticals Reports No. 2
STI/PUB/1743 (59 pp.; 2017)
ISBN 978-92-0-102916-4 Price: €33

CYCLOTRON PRODUCED RADIONUCLIDES: EMERGING POSITRON EMITTERS FOR MEDICAL APPLICATIONS: ^{64}Cu AND ^{124}I
IAEA Radioisotopes and Radiopharmaceuticals Reports No. 1
STI/PUB/1717 (63 pp.; 2016)
ISBN 978-92-0-109615-9 Price: €38

Positron emission tomography is an important clinical tool and copper-64, with its longer half-life, has several unique attributes that make it a multipurpose radionuclide with many potential applications. Additionally, copper as a trace element plays a pivotal role in several human metabolic and pathologic diseases and is involved in malignant cell biochemistry pathways. This offers the opportunity for scientists to explore the theranostic capabilities of copper-64. This publication, arising from an IAEA Coordinated Research Project, describes the biochemical and radiopharmaceutical aspects of copper-64, as well as its clinical applications, with specific guidelines and methods for the production of copper-64 chloride, peptide and monoclonal antibody radiopharmaceuticals. It is expected to be of use to all professionals involved in the field by specifying ideal production, formulation and quality control methods.

INTERNATIONAL ATOMIC ENERGY AGENCY
VIENNA